Spring 5-15-2019

Molecular Mechanisms Responsible for Functional Cortical Plasticity During Development and after Focal Ischemic Brain Injury

Andrew Wiggen Kraft
Washington University in St. Louis

WASHINGTON UNIVERSITY IN ST. LOUIS

Division of Biology and Biomedical Sciences
Neurosciences

Dissertation Examination Committee:
Jin-Moo Lee, Chair
Joseph Culver
Nico Dosenbach
Marcus Raichle
Bradley Schlaggar
Abraham Snyder

Molecular Mechanisms Responsible for Functional Cortical Plasticity During Development and after Focal Ischemic Brain Injury

by
Andrew Wiggen Kraft

A dissertation presented to
The Graduate School
of Washington University
in partial fulfillment
of the requirements for the degree
of Doctor of Philosophy

May 2019
St. Louis, Missouri

Table of Contents

List of Figures

Chapter 2

Chapter 3

Chapter 4

Acknowledgements

Over the last five years, I have received tremendous support and encouragement from a great number of mentors. Jin-Moo Lee has been a mentor and friend since my early exposure to science as an undergraduate student. Jin-Moo has provided unending guidance, support, patience, and encouragement for almost a decade. Any chance I have for scientific success is owed to him.

I would like to thank the member of my thesis committee which consists of Joseph Culver, Bradley Schlaggar, Marcus Raichle, Nico Dosenbach, and Abraham Snyder. All of these individuals have gone above and beyond in offering their time and intellect to further my scientific development.

In addition to these formal mentors, I have benefited greatly from time spent with close collaborators. In particular, Adam Bauer and Anish Mitra have played crucial roles in my scientific development. Furthermore, all members of the Jin-Moo Lee laboratory have played critical roles in my scientific development.

Friends and family have also played a critical role in helping me get to this point. I thank my parents, Stephen Kraft and Linda Wiggen, and brother, Adam Kraft, for their unwavering support. In addition, I cannot thank Lucy Liu enough for enduring the many failures and celebrating the few successes that have come with me over the last five years.

Finally, I would like to thank the American Heart Association and National Institute of Neurological Disorders and Stroke for the financial support provided to this dissertation (AHA 14PRE18410013, NIH F31 NS089135-02).

Andrew Wiggen Kraft

Washington University in St. Louis

May 2019

ABSTRACT OF THE DISSERTATION

Molecular Mechanisms Responsible for Functional Cortical Plasticity During Development and after Focal Ischemic Brain Injury

by

Andrew W. Kraft

Doctor of Philosophy in Biology and Biomedical Sciences

Neurosciences

Washington University in St. Louis, 2019

Professor Jin-Moo Lee, Chair

The cerebral cortex is organized into functional representations, or maps, defined by increased activity during specific tasks. In addition, the brain exhibits robust spontaneous activity with spatiotemporal organization that defines the brain's functional architecture (termed functional connectivity). Task-evoked representations and functional connectivity demonstrate experience-dependent plasticity, and this plasticity may be important in neurological development and disease. An important case of this is in focal ischemic injury, which results in destruction of the involved representations and disruption of functional connectivity relationships. Behavioral recovery correlates with representation remapping and functional connectivity normalization, suggesting functional organization is critical for recovery and a potentially valuable therapeutic target. However, the cellular and molecular mechanisms that drive this systems-level plasticity are unknown, making it difficult to approach therapeutic modulation of functional brain organization. Using cortical neuroimaging in mice, this dissertation explores the role of specific genes in sensory deprivation induced functional brain map plasticity during development and after

focal ischemic injury. In the three contained chapters, I demonstrate the following: 1) Arc, an excitatory neuron synaptic-plasticity gene, is required for representation remapping and behavioral recovery after focal cortical ischemia. Further, perilesional sensory deprivation can direct remapping and improve behavioral recovery. 2) Early visual experience modulates functional connectivity within and outside of the visual cortex through an Arc-dependent mechanism. 3) Electrically coupled inhibitory interneuron networks limit spontaneous activity syncrhony between distant cortical regions. This work starts to define the molecular basis for plasticity in functional brain organization and may help develop approaches for therapeutic modulation of functional brain organization.

Chapter 1

Introduction and Perspective

Recovery after ischemic stroke

With over 5.8 million survivors, stroke is the leading cause of adult disability in the United States (*1*). The nature of neurologic deficits can encompass several cognitive domains (motor, sensory, attention, language), depending on infarction location. The acute deficits caused by the ischemic event are followed by spontaneous recovery that occurs in the subsequent weeks to months. This recovery, however, is often incomplete leaving patients in a state of chronic disability (*2*). Nonetheless, the fact that recovery occurs suggests that endogenous repair mechanisms exist, and these mechanisms might be potentiated in order to improve recovery after an ischemic stroke.

Current approaches to stroke rehabilitative therapy

Current approaches to therapy are limited. In the case of upper limb motor deficits, rehabilitative therapy aims to force use of the disabled arm by preventing use of the unaffected arm. This strategy, termed constraint-induced movement therapy (CIMT) has demonstrated limited, but significant benefit for stroke patients (*3*). Importantly, CIMT's success suggests that activity-dependent plasticity within the injured system appears central to recovery after brain injury.

Given the need for better therapies to alleviate disability, other approaches to influencing activity-dependent cerebral physiology are being examined with great interest. Common approaches include various pharmacologic manipulations and cortical stimulation approaches (*4-6*). Non-invasive stimulation approaches (using transcranial direct current stimulation and transcranial magnetic stimulation) have been used extensively. Although select small studies have demonstrated benefits with these techniques (*7-9*), the benefits were not reproduced in larger randomized controlled trials (*5, 6*).

These limitations highlight our poor understanding of the biology responsible for recovery after stroke. In order to develop better therapeutic approaches, the mechanisms involved in recovery after focal ischemic injury must be better understood.

Animal models of recovery after ischemic injury

Pre-clinical animal models offer an important platform to investigate the mechanisms involved in recovery after stroke. Many different animal models exist, and they vary in species and how ischemia is induced. The most commonly used species include monkeys, rats, and mice. Common approaches to induce ischemia include mechanical vessel ligation (permanent or temporary), endovascular vessel occlusion, exogenous emboli infusion, and photochemically induced thrombosis. These choices can be tailored to generate a model with features suited for the specific scientific question (*10, 11*).

Some models enable a reproducible infarction and behavioral deficits that are followed by consistent behavioral recovery profiles following injury. Long-term recovery models have been developed for non-human primates, rats, and mice, and these models are especially valuable for experimental determination of factors influencing behavioral recovery. Non-human primates and rats offer superior assays for neurologic behavior assays, whereas the advanced molecular biology tools readily available in the mouse have made mice valuable for mechanistic investigation in recovery after injury (*11*).

Recovery studies in animal models after focal ischemia have characterized some of the cellular and physiologic changes which occur in association with behavioral recovery. For example, proteins involved in axonal growth and synaptogenesis are upregulated in peri-lesional areas after stroke, including neuronal growth promoting factors (BDNF, Insulin growth factors, fibroblast growth factors), axonal guidance cues (Nogo, SDF-1, ephrins, GDF10), and synaptogenic molecules (*12*). These processes may be critical for restoration, or novel formation, of connections required to restore neural communication.

In addition to structural repair, changes in signaling physiology may also be important for recovery. Brain tissue in the perilesional area becomes hypoexcitable due to a decrease in extracellular γ-aminobutyric acid (GABA) uptake by activated astrocytes, resulting in increased

tonic neuronal inhibition (*13*). Blocking this tonic GABA signaling pharmacologically or by genetic manipulation accelerates motor recovery in mice (*13*). Moreover, AMPA receptor potentiation enhances limb recovery in this same animal model (*14*). This suggests that altering the balance between excitatory and inhibitory signaling may be a critical target for improving recovery after ischemic injury.

These mechanistic discoveries offer insight into cellular processes that play a role in brain repair. However, synaptic branching and signaling both occur at the microscopic scale whereas behavioral performance involves large-scale integration of brain systems. Given the complex architecture of the brain, understanding the systems-level physiology involved in brain repair after ischemic injury will be critical.

Systems-level plasticity in recovery after focal ischemic injury

Indeed, animal models have suggested some systems-level phenomena that may be important for recovery after ischemic injury. Work in monkeys demonstrated that ablation of motor cortex representations was followed by a reappearance of lost representations in nearby motor cortex (*15*). Termed “cortical remapping,” it was also shown that this processes required physical use of the affected limb and occurred in conjunction with motor behavior recovery (*15*). This landmark discovery established functional cortex reorganization as an important component of recovery after cortical infarction.

In addition to plasticity in cortical maps defined by task, more recent work has found a robust correlation in correlated spontaneous activity and recovery after focal ischemia (for more on correlated spontaneous activity, see below). Taken together this suggests that plasticity in the cortex’s functional organization is a critical substrate in recovery after injury.

Indeed, modulating functional cortex organization might be a valuable therapeutic approach for patients with chronic disability due to an ischemic stroke. Unfortunately, there is no evidence for

specific mechanisms that drive these processes and it is unclear how they might be manipulated for therapeutic gain.

Overview of functional brain mapping

The anatomical basis for mental performance has been at the center of our fascination for centuries. The earliest “brain mapping” can be traced to ancient Egyptian hieroglyphs that recognized a relationship between head injury and altered mental status, resulting in the realization that the brain is the seat of consciousness (*16*). In the same vein, neurologic syndromes clinical correlation with neuroanatomical lesions has provided insight into certain aspect of function brain maps (*17, 18*).

Fortunately, brain activity involves precise physiologic alterations in ion conductance, cerebrovascular flow, blood oxygenation, and glucose metabolism (*19*). Although complex, and not entirely understood, these changes provide a robust platform to measure brain activity that can be measured by various non-invasive techniques (*19*). This technology has paired well with the neurosciences to determine how systems-scale changes in brain activity correspond to specific behaviors.

The hemodynamic response is an especially reliable component of brain activity. Blood-flow radioisotopes for positron emission topography (PET) imaging enabled landmark functional mapping work (*19*), and functional neuroimaging using hemoglobin-based contrasts have been especially important. Hemoglobin-based imaging via magnetic and optical platforms is made possible by its distinct magnetic and spectral properties that have made blood oxygen level dependent (BOLD) magnetic resonance imaging (MRI) and optical intrinsic signal (OIS) imaging neuroscience workhorses.

Cortical maps defined by activity increases during task

Intraoperative cortical microstimulation produced sensory and motor maps with beautiful detail (*20*). However, neuroimaging (both PET and MRI) enabled study of functional representations in a safer, less restricted setting. Not only could activation locations be determined non-invasively, but higher-order influences on sensory responses were demonstrated. Key findings include anticipatory responses to painful stimuli (*21*) and emotional modulation of sensory response amplitude (*22*). These examples, and others, revealed that task-evoked activity increases involve dynamic interaction with other components of the brain.

Furthermore, by sampling the entire brain volume, neuroimaging has enabled mapping beyond the sensorimotor system. Moreover, neuroimaging platforms are compatible with experimental paradigms that involve more complex cognitive tasks. Certain tasks were shown to activate a collection of separate brain regions, which were collectively termed a network. Key examples include networks activated during word processing and attention tasks (*23-27*). These experiments also revealed a set of cortical regions, termed the default mode network, with activity decreases during attention demanding tasks (*28-30*).

Cortical networks defined by spontaneous activity

BOLD data from task-evoked neuroimaging experiments revealed a high degree of signal variance even outside of active tasks (*31*). At first this was considered physiologic “noise” and that was actively removed by averaging. However, it was eventually realized that this intrinsic actively is precisely organized between distinct brain regions (*32-37*). Thus, these spontaneous activity relationships may reflect higher-level integration of information across distinct brain systems and be a critical aspect in forming complex behaviors.

Anti-correlations in spontaneous brain activity led to some of the earliest descriptions of spontaneous activity network organization (*32, 38*). Anti-correlations are especially interesting because they separate areas that have respective increases and decreases in activity during focused tasks (*22, 27, 32, 38-41*). The best demonstration of this is seen in the dorsal attention

networks and default mode networks in humans (*32*). Activity in the default mode network decreases during attention demanding tasks, and this is thought to be driven by the brain pivoting from self-referential activity to task-directed activity requiring focused attention (*28, 32, 42*).

In addition to the default mode and dorsal attention networks, additional analysis has shown robust correlation relationships for the executive control, salience, sensorimotor, visual, and auditory systems (*31*). Each of these networks involve strong homotopic correlation and variable anterior-posterior correlation in a manner that largely reflects task-evoked responses (*31*). Several studies have demonstrated a strong correlation between neurologic disease and functional connectivity (*43-45*), suggesting these spontaneous activity relationships are critical in brain function.

Although often studied separately, it is clear that spontaneous activity influences task-evoked responses. Animal studies have demonstrated that spontaneous fluctuations modulate sensory evoked responses (*46-48*). Human fMRI has revealed this also occurs within motor cortex for motor activity evoked somatomotor responses (*49*), and these fluctuations also correlate with the output motor force (*50*). This argues that the brain undergoes a constant, intrinsic conversation that interacts with stimulus, and it is not simply a set of cells that passively waits for input to determine output decisions.

Importantly, even though much effort towards understanding “brain connectivity” continues to focus on anatomically based connectivity, much of these functional relationships are not constrained by anatomy (*51, 52*). Thus, functional brain maps may represent a level of brain organization rooted in neural activity that is hierarchically above anatomy and provides the substrate for complex behaviors.

Plasticity in functional cortex organization

Based on early work that recognized the somatotopic organization of the cortex, it was believed that somatotopic representations were fixed by the peripheral anatomy (*53*). This was later challenged by the demonstration that peripheral nerve lesions resulted in spatial rearrangement of cortical maps – a processed termed cortical remapping (*54, 55*).

Cortical remapping has been extended to the principle that sensory deprivation results in cortical "takeover" by spared senses, and this phenomenon has been reported in experimental animals and humans with sensory deficits. Sensory-deprivation induced remapping occurs with long-term deprivation as with peripheral nerve injury, or blindness, but it can also occur with more rapid experimental deprivation via anesthetic nerve block of blindfolding (*56, 57*). In addition, there is evidence that extensive activities can expand pertinent cortical representations, as in musicians and cab drivers (*58, 59*). Taken together, this suggests that experience dependent plasticity actively modulates cortical maps throughout life.

Likewise, sensory experience and learning can modulate spontaneous ISA patterns at the systems-scale. Specifically, visual and motor learning (*34, 60*), extended Law School Admission Test (LSAT) preparation (*61*), early-age blindness (*62-65*), and peripheral nerve injury (*66-68*) have all been demonstrated to alter ISA correlation in humans.

In these examples, the functional connectivity changes occur with topographic specificity. For paradigms involving learning tasks inside the scanner, functional connectivity changes occurred between regions activated during the learning task. Further, in examples involving sensory deprivation, functional connectivity changes involved the deprived cortical regions. In addition, the magnitude of the effects induced by visual perception learning correlated with behavioral measurements of degree of perceptual learning (*60*). This suggest that functional connectivity is a critical component of systems-level brain plasticity, and specific functional connections can be selectively modified with certain maneuvers.

Understanding these systems-level changes may improve our therapeutic approach to many neurologic diseases. More specifically, neurodegeneration, psychiatric disease, developmental delay disorders, stroke, all demonstrate relationships in deficits and functional brain organization (*43-45, 69-71*). So far neuroimaging findings have largely been used as a biomarker for disease status in these conditions, but modulating cortical representations and resting-state relationships may have unrealized therapeutic potential.

The finding that sensory deprivation can alter functional representations and resting-state relationships with anatomical specificity suggests that targeted sensory deprivation may facilitate cortical plasticity and improve function. In addition, sensory deprivation is likely to trigger genetic cascades that allow cortical plasticity, and these genetic programs may be therapeutically important. Unfortunately, little is known regarding the mechanisms underlying systems-level modulation of spontaneous ISA organization.

A leading hypothesis is that experience-dependent ISA modulation reflects “brain plasticity.” It is widely believed that plasticity at the systems level may be driven by mechanisms at the molecular level, especially those involving the modulation of synaptic strengths. However, there has been to date no evidence linking synaptic plasticity mechanisms, which operate on the spatial scale of microns (*72*), with the systems-scale ISA modulations occurring on the scale of centimeters (*34, 60-63*).

Functional cortical reorganization in ischemic stroke

As mentioned above, stroke results in task evoked maps and resting-state network changes that correlate with behavioral outcomes (*69, 70, 73-75*). In the case of focal ischemia involving the cortex, there is an acute loss of behavioral capability associated with the infarcted region. Recovery occurs in parallel with the reappearance of an effective functional representation in perilesional cortex in the weeks to months following infarction (*73, 74, 76-80*). This process,

termed remapping, has been observed in both animal models and human patients recovering from focal ischemic injury (*73, 74, 81-83*).

The cellular and molecular mechanisms that drive remapping are unknown. Physiologically, remapping involves perilesional neurons shifting their receptivity from uninvolved limbs to the injured limb (*78*). Taken with the finding that injured limb activity is required for remapping to occur (*76*), this suggests remapping may involve an activity-dependent competition for cortical neuron representation. If this is the case, it suggests certain approaches that might facilitate remapping for therapeutic gain.

In addition to disrupting infarcted representations, stroke can cause remote dysfunction in distant but functionally connected regions of the brain (diaschisis). It is well known that stroke disrupts spontaneous correlation networks, and that acute disability correlates with the degree of functional connectivity decrement between specific regions (*69, 75, 84*). Behavioral deficits are especially profound when interhemispheric functional connectivity in the somatomotor network is disrupted: a finding that has been shown both in humans and rodent models (*69, 70, 75*). Furthermore, functional connectivity patterns normalize in parallel with behavioral recovery, and the extent of behavioral recovery correlates with the extent of normalization in correlation strength (*70, 75*).

Thus facilitating representation remapping and spontaneous network normalization may be critical targets for raising the recovery ceiling. Unfortunately, our current understanding is limited to the observed correlation between the alterations in functional architecture and behavior capability. Furthermore, it's not clear how the cortex can be manipulated to facilitate functional reorganization for therapeutic gain.

Understanding the molecular mechanisms involved in reorganization of functional brain arrangement may offer insight into how these plastic changes may be manipulated for therapeutic gain.

Parallels between developmental critical periods and recovery after injury

Understanding the development of functional organization in the cortex is likely to be valuable for understanding network changes after injury in adults. Neuroimaging has revealed robust functional network development at a very young age (*85-88*). It is reasonable to suspect that functional network disruption may play a role in neurologic developmental disorders, and there is evidence for this in schizophrenia, bipolar disorder, and autism (*71, 87, 89-92*).

Interestingly, much of the reported network development in humans appears to happen late *in utero* or within the first 2 years of life (*85-88*), a time that contains developmental critical periods (*93*). Developmental critical periods have been studied at length, and many molecular mechanisms involved in experience-dependent changes in visual critical periods are known.

Ocular dominance plasticity has been a particularly valuable model for understanding mechanisms of experience-dependent plasticity during critical periods. Non-human primates, cats, ferrets, and rodents have all demonstrated that monocular deprivation during the critical periods results in depression of deprived eye visual responses and potentiation of spared eye visual responses (*94*). This model has combined well with the genetic and molecular toolset available in mice to demonstrate a diverse set of mechanisms that drive ocular dominance plasticity during early development and subsequently lock these changes in place throughout adult life.

During the visual critical period, there are robust changes at both excitatory and inhibitory synapses that alter excitatory-inhibitory balance in order to allow plastic change and subsequently lock it in place (*95*). GABAergic signaling changes were one of the first recognized mechanisms of critical period. Critical period studies have demonstrated a dramatic experience-driven increase in proteins specific to inhibitory interneurons and GABAergic receptors (*95-97*). Parvalbumin, a Ca2+ binding protein thought to be critical for rapid spiking, is exclusively present in a class of inhibitory interneurons (termed fast spiking or parvalbumin inhibitory interneurons) (*98*). Increased

parvalbumin expression and GABA receptor expression correlated with increased inhibitory tone and more selective receptive fields in excitatory primary visual cortex neurons (*96*). This suggested that specificity gained during development was achieved by inhibitory influences that gate excitatory neuron responses (*95*).

GABAergic blockade, whether pharmacologic or genetic, has been shown to play an essential role in critical period ocular dominance plasticity (*95, 99-101*). However, reversible GABAergic blockade prevented critical period closure whereas GABAergic agonists cause early and shortened critical periods (*95, 99-101*). Thus, GABAergic signaling is thought to drive non-reversible changes that result in cortex maturation.

Much of this synaptic development appears to be driven by brain derived neurotrophic factor (BDNF), and it was thought that BDNF's expression during the critical period drove inhibitory synapse plasticity exclusively (*95, 102-104*). However, more recent work has demonstrated AMPA receptor plasticity within excitatory neurons plays a critical role in visual critical period ocular dominance plasticity (*105*).

This has been best demonstrated by a lack of ocular dominance plasticity in mice deficient for activity-regulated cytoskeleton-associated protein (Arc), a protein selectively expressed in glutamatergic neurons (*105, 106*). Arc plays a role in altering excitatory synapse strength via endocytosis of AMPA receptor subunits (*107*). Interestingly, actively differences within individual synapses of the same neuron enable Arc to selectively endocytose AMPA receptors at silent synapses (*108*). This mechanism may be important for experience-directed strengthening and weakening of specific connections that drive ocular dominance plasticity.

Arc activity is also driven by BDNF (*109-111*). Thus, critical period BDNF signaling likely drives changes at both excitatory and inhibitory synapses. Subtle differences in the development trajectories between excitation and inhibition allow for a short periods of high excitability that

allows plasticity to occur that is followed by durable period of increased excitation that cements these plastic changes in place (*95*).

These critical period findings have remarkable parallels to preclinical models of recovery after focal ischemic injury. Pioneering work has shown that GABAergic antagonists and AMPA receptor potentiation both improve behavioral recovery after stroke (*13, 14*). This may result from increasing the excitatory-inhibitory ratio to create an effective "critical period opening" in the post-injury environment that facilitates plasticity and improves recovery.

Thus, development and recovery after brain injury may rely on a core set of neurologic plasticity pathways. Understanding these pathways may enable therapies that allow reshaping of the cortex's functional organization in order to treat systems-level neurologic disease. While this idea may be promising, it is not entirely clear how these mechanisms tie into functional cortex plasticity. Indeed, ocular dominance plasticity involves functional representation changes within the visual system, but it is unclear how these changes interact with the cortex at large. In addition, while some cellular and genetic processes have been implicated in behavioral recovery after stroke, the role of these genes in cortical functional organization plasticity is unknown.

Summary of findings

The central hypothesis of this dissertation is that the molecular mechanisms responsible for synaptic-scale plasticity during development drive experience-dependent functional cortex plasticity during health and disease. Using functional neuroimaging in mice, I've taken advantage of the molecular tools readily available in mouse models to examine how functional map plasticity is influenced by specific genes. More specifically, I demonstrate that Arc, a gene critical for experience-dependent synaptic plasticity in excitatory neurons, plays a role in vision-dependent changes in spontaneous activity networks as well as remapping and behavioral recovery after focal ischemic injury. In addition, I show that focal sensory deprivation can lead to targeted changes in functional brain organization. Lastly, I show that inhibitory interneuron gap junctions

modulate functional specific functional networks. This work starts to establish a molecular basis for targeted functional cortical map plasticity and suggests molecular pathways and maneuvers that may be an important therapeutic target for neurological disease that involve disruption of systems organization.

References

1. E. J. Benjamin *et al.*, Heart Disease and Stroke Statistics-2017 Update: A Report From the American Heart Association. *Circulation* **135**, e146-e603 (2017).
2. P. W. Duncan, L. B. Goldstein, D. Matchar, G. W. Divine, J. Feussner, Measurement of motor recovery after stroke. Outcome assessment and sample size requirements. *Stroke* **23**, 1084-1089 (1992).
3. S. L. Wolf *et al.*, Effect of constraint-induced movement therapy on upper extremity function 3 to 9 months after stroke: the EXCITE randomized clinical trial. *JAMA* **296**, 2095-2104 (2006).
4. F. Chollet *et al.*, Pharmacological therapies in post stroke recovery: recommendations for future clinical trials. *J Neurol* **261**, 1461-1468 (2014).
5. R. M. Levy *et al.*, Epidural Electrical Stimulation for Stroke Rehabilitation: Results of the Prospective, Multicenter, Randomized, Single-Blinded Everest Trial. *Neurorehabil Neural Repair* **30**, 107-119 (2016).
6. J. Seniow *et al.*, Transcranial magnetic stimulation combined with physiotherapy in rehabilitation of poststroke hemiparesis: a randomized, double-blind, placebo-controlled study. *Neurorehabil Neural Repair* **26**, 1072-1079 (2012).
7. J. Liepert, S. Zittel, C. Weiller, Improvement of dexterity by single session low-frequency repetitive transcranial magnetic stimulation over the contralesional motor cortex in acute

stroke: a double-blind placebo-controlled crossover trial. *Restor Neurol Neurosci* **25**, 461-465 (2007).

8. E. M. Khedr, A. E. Etraby, M. Hemeda, A. M. Nasef, A. A. Razek, Long-term effect of repetitive transcranial magnetic stimulation on motor function recovery after acute ischemic stroke. *Acta Neurol Scand* **121**, 30-37 (2010).

9. E. M. Khedr, M. A. Ahmed, N. Fathy, J. C. Rothwell, Therapeutic trial of repetitive transcranial magnetic stimulation after acute ischemic stroke. *Neurology* **65**, 466-468 (2005).

10. J. B. Casals *et al.*, The use of animal models for stroke research: a review. *Comp Med* **61**, 305-313 (2011).

11. F. Fluri, M. K. Schuhmann, C. Kleinschnitz, Animal models of ischemic stroke and their application in clinical research. *Drug Des Devel Ther* **9**, 3445-3454 (2015).

12. S. T. Carmichael, Themes and strategies for studying the biology of stroke recovery in the poststroke epoch. *Stroke* **39**, 1380-1388 (2008).

13. A. N. Clarkson, B. S. Huang, S. E. Macisaac, I. Mody, S. T. Carmichael, Reducing excessive GABA-mediated tonic inhibition promotes functional recovery after stroke. *Nature* **468**, 305-309 (2010).

14. A. N. Clarkson *et al.*, AMPA receptor-induced local brain-derived neurotrophic factor signaling mediates motor recovery after stroke. *J Neurosci* **31**, 3766-3775 (2011).

15. R. J. Nudo, B. M. Wise, F. SiFuentes, G. W. Milliken, Neural substrates for the effects of rehabilitative training on motor recovery after ischemic infarct. *Science* **272**, 1791-1794 (1996).

16. J. Breasted, *The Edwin Smith surgical papyrus*. M. Friedberg, Ed., Rare Book Collection of Rush University Medical Center at the University of Chicago (University of Chicago Press, Chicago, Ill, 1930).

17. H. Damasio, T. Grabowski, R. Frank, A. M. Galaburda, A. R. Damasio, The return of Phineas Gage: clues about the brain from the skull of a famous patient. *Science* **264**, 1102-1105 (1994).

18. L. R. Squire, The legacy of patient H.M. for neuroscience. *Neuron* **61**, 6-9 (2009).

19. M. E. Raichle, A brief history of human brain mapping. *Trends Neurosci* **32**, 118-126 (2009).

20. W. Penfield, E. Boldrey, Somatic motor and sensory representation in the cerebral cortex of man as studied by electrical stimulation. *Brain* **60**, 389-443 (1937).

21. W. C. Drevets *et al.*, Blood flow changes in human somatosensory cortex during anticipated stimulation. *Nature* **373**, 249-252 (1995).

22. J. R. Simpson *et al.*, The emotional modulation of cognitive processing: an fMRI study. *J Cogn Neurosci* **12 Suppl 2**, 157-170 (2000).

23. S. E. Petersen, P. T. Fox, M. I. Posner, M. Mintun, M. E. Raichle, Positron emission tomographic studies of the cortical anatomy of single-word processing. *Nature* **331**, 585-589 (1988).

24. J. V. Pardo, P. T. Fox, M. E. Raichle, Localization of a human system for sustained attention by positron emission tomography. *Nature* **349**, 61-64 (1991).

25. M. I. Posner, S. E. Petersen, P. T. Fox, M. E. Raichle, Localization of cognitive operations in the human brain. *Science* **240**, 1627-1631 (1988).

26. J. V. Pardo, P. J. Pardo, K. W. Janer, M. E. Raichle, The anterior cingulate cortex mediates processing selection in the Stroop attentional conflict paradigm. *Proc Natl Acad Sci U S A* **87**, 256-259 (1990).

27. J. R. Simpson, Jr., A. Z. Snyder, D. A. Gusnard, M. E. Raichle, Emotion-induced changes in human medial prefrontal cortex: I. During cognitive task performance. *Proc Natl Acad Sci U S A* **98**, 683-687 (2001).

28. M. E. Raichle *et al.*, A default mode of brain function. *Proc Natl Acad Sci U S A* **98**, 676-682 (2001).

29. G. L. Shulman *et al.*, Common Blood Flow Changes across Visual Tasks: II. Decreases in Cerebral Cortex. *J Cogn Neurosci* **9**, 648-663 (1997).

30. B. Mazoyer *et al.*, Cortical networks for working memory and executive functions sustain the conscious resting state in man. *Brain Res Bull* **54**, 287-298 (2001).

31. M. E. Raichle, The restless brain: how intrinsic activity organizes brain function. *Philos Trans R Soc Lond B Biol Sci* **370**, (2015).

32. M. D. Fox *et al.*, The human brain is intrinsically organized into dynamic, anticorrelated functional networks. *Proc Natl Acad Sci U S A* **102**, 9673-9678 (2005).

33. A. Mitra, A. Z. Snyder, T. Blazey, M. E. Raichle, Lag threads organize the brain's intrinsic activity. *Proc Natl Acad Sci U S A* **112**, E2235-2244 (2015).

34. A. Mitra, A. Z. Snyder, C. D. Hacker, M. E. Raichle, Lag structure in resting-state fMRI. *J Neurophysiol* **111**, 2374-2391 (2014).

35. J. D. Power *et al.*, Functional network organization of the human brain. *Neuron* **72**, 665-678 (2011).

36. M. D. Fox, M. Corbetta, A. Z. Snyder, J. L. Vincent, M. E. Raichle, Spontaneous neuronal activity distinguishes human dorsal and ventral attention systems. *Proc Natl Acad Sci U S A* **103**, 10046-10051 (2006).

37. B. J. Shannon *et al.*, Brain aerobic glycolysis and motor adaptation learning. *Proc Natl Acad Sci U S A* **113**, E3782-3791 (2016).

38. M. D. Greicius, B. Krasnow, A. L. Reiss, V. Menon, Functional connectivity in the resting brain: a network analysis of the default mode hypothesis. *Proc Natl Acad Sci U S A* **100**, 253-258 (2003).

39. R. Cabeza, L. Nyberg, Imaging cognition II: An empirical review of 275 PET and fMRI studies. *J Cogn Neurosci* **12**, 1-47 (2000).

40. M. Corbetta, G. L. Shulman, Control of goal-directed and stimulus-driven attention in the brain. *Nat Rev Neurosci* **3**, 201-215 (2002).

41. K. A. McKiernan, J. N. Kaufman, J. Kucera-Thompson, J. R. Binder, A parametric manipulation of factors affecting task-induced deactivation in functional neuroimaging. *J Cogn Neurosci* **15**, 394-408 (2003).

42. D. A. Gusnard, M. E. Raichle, M. E. Raichle, Searching for a baseline: functional imaging and the resting human brain. *Nat Rev Neurosci* **2**, 685-694 (2001).

43. C. D. Hacker, J. S. Perlmutter, S. R. Criswell, B. M. Ances, A. Z. Snyder, Resting state functional connectivity of the striatum in Parkinson's disease. *Brain* **135**, 3699-3711 (2012).

44. G. Allen *et al.*, Reduced hippocampal functional connectivity in Alzheimer disease. *Arch Neurol* **64**, 1482-1487 (2007).

45. A. Chase, Alzheimer disease: Altered functional connectivity in preclinical dementia. *Nat Rev Neurol* **10**, 609 (2014).

46. A. Arieli, A. Sterkin, A. Grinvald, A. Aertsen, Dynamics of ongoing activity: explanation of the large variability in evoked cortical responses. *Science* **273**, 1868-1871 (1996).

47. J. Fiser, C. Chiu, M. Weliky, Small modulation of ongoing cortical dynamics by sensory input during natural vision. *Nature* **431**, 573-578 (2004).

48. R. Azouz, C. M. Gray, Cellular mechanisms contributing to response variability of cortical neurons in vivo. *J Neurosci* **19**, 2209-2223 (1999).

49. M. D. Fox, A. Z. Snyder, J. M. Zacks, M. E. Raichle, Coherent spontaneous activity accounts for trial-to-trial variability in human evoked brain responses. *Nat Neurosci* **9**, 23-25 (2006).

50. M. D. Fox, A. Z. Snyder, J. L. Vincent, M. E. Raichle, Intrinsic fluctuations within cortical systems account for intertrial variability in human behavior. *Neuron* **56**, 171-184 (2007).

51. J. L. Vincent *et al.*, Intrinsic functional architecture in the anaesthetized monkey brain. *Nature* **447**, 83-86 (2007).

52. D. Zhang *et al.*, Intrinsic functional relations between human cerebral cortex and thalamus. *J Neurophysiol* **100**, 1740-1748 (2008).

53. F. M. Woolsey, Jr., Two years of experience with two-way radio conferences for postgraduate medical education. *J Med Educ* **33**, 474-482 (1958).

54. M. M. Merzenich *et al.*, Somatosensory cortical map changes following digit amputation in adult monkeys. *J Comp Neurol* **224**, 591-605 (1984).

55. J. H. Kaas, What, if anything, is SI? Organization of first somatosensory area of cortex. *Physiol Rev* **63**, 206-231 (1983).

56. M. S. Melton *et al.*, Changes in Brain Resting-state Functional Connectivity Associated with Peripheral Nerve Block: A Pilot Study. *Anesthesiology* **125**, 368-377 (2016).

57. L. B. Merabet *et al.*, Rapid and reversible recruitment of early visual cortex for touch. *PLoS One* **3**, e3046 (2008).

58. E. A. Maguire *et al.*, Navigation-related structural change in the hippocampi of taxi drivers. *Proc Natl Acad Sci U S A* **97**, 4398-4403 (2000).

59. T. Elbert, C. Pantev, C. Wienbruch, B. Rockstroh, E. Taub, Increased cortical representation of the fingers of the left hand in string players. *Science* **270**, 305-307 (1995).

60. C. M. Lewis, A. Baldassarre, G. Committeri, G. L. Romani, M. Corbetta, Learning sculpts the spontaneous activity of the resting human brain. *Proc Natl Acad Sci U S A* **106**, 17558-17563 (2009).

61. A. P. Mackey, A. T. Miller Singley, S. A. Bunge, Intensive reasoning training alters patterns of brain connectivity at rest. *J Neurosci* **33**, 4796-4803 (2013).

62. H. Burton, A. Z. Snyder, M. E. Raichle, Resting state functional connectivity in early blind humans. *Front Syst Neurosci* **8**, 51 (2014).

63. D. Wang *et al.*, Altered resting-state network connectivity in congenital blind. *Hum Brain Mapp* **35**, 2573-2581 (2014).

64. L. Heine *et al.*, Prevalence of increases in functional connectivity in visual, somatosensory and language areas in congenital blindness. *Front Neuroanat* **9**, 86 (2015).

65. Y. Liu *et al.*, Whole brain functional connectivity in the early blind. *Brain* **130**, 2085-2096 (2007).

66. C. P. Pawela *et al.*, Interhemispheric neuroplasticity following limb deafferentation detected by resting-state functional connectivity magnetic resonance imaging (fcMRI) and functional magnetic resonance imaging (fMRI). *Neuroimage* **49**, 2467-2478 (2010).

67. B. Liu *et al.*, Changes of inter-hemispheric functional connectivity between motor cortices after brachial plexuses injury: a resting-state fMRI study. *Neuroscience* **243**, 33-39 (2013).

68. T. M. Qiu *et al.*, Sensorimotor cortical changes assessed with resting-state fMRI following total brachial plexus root avulsion. *J Neurol Neurosurg Psychiatry* **85**, 99-105 (2014).

69. A. R. Carter *et al.*, Resting interhemispheric functional magnetic resonance imaging connectivity predicts performance after stroke. *Ann Neurol* **67**, 365-375 (2010).

70. L. E. Ramsey *et al.*, Normalization of network connectivity in hemispatial neglect recovery. *Ann Neurol* **80**, 127-141 (2016).

71. N. D. Woodward, C. J. Cascio, Resting-State Functional Connectivity in Psychiatric Disorders. *JAMA Psychiatry* **72**, 743-744 (2015).

72. E. Korb, S. Finkbeiner, Arc in synaptic plasticity: from gene to behavior. *Trends Neurosci* **34**, 591-598 (2011).

73. R. M. Dijkhuizen *et al.*, Functional magnetic resonance imaging of reorganization in rat brain after stroke. *Proc Natl Acad Sci U S A* **98**, 12766-12771 (2001).

74. R. M. Dijkhuizen *et al.*, Correlation between brain reorganization, ischemic damage, and neurologic status after transient focal cerebral ischemia in rats: a functional magnetic resonance imaging study. *J Neurosci* **23**, 510-517 (2003).

75. M. P. van Meer *et al.*, Recovery of sensorimotor function after experimental stroke correlates with restoration of resting-state interhemispheric functional connectivity. *J Neurosci* **30**, 3964-3972 (2010).

76. R. J. Nudo, G. W. Milliken, W. M. Jenkins, M. M. Merzenich, Use-dependent alterations of movement representations in primary motor cortex of adult squirrel monkeys. *J Neurosci* **16**, 785-807 (1996).

77. C. Xerri, M. M. Merzenich, B. E. Peterson, W. Jenkins, Plasticity of primary somatosensory cortex paralleling sensorimotor skill recovery from stroke in adult monkeys. *J Neurophysiol* **79**, 2119-2148 (1998).

78. I. R. Winship, T. H. Murphy, In vivo calcium imaging reveals functional rewiring of single somatosensory neurons after stroke. *J Neurosci* **28**, 6592-6606 (2008).

79. C. E. Brown, K. Aminoltejari, H. Erb, I. R. Winship, T. H. Murphy, In vivo voltage-sensitive dye imaging in adult mice reveals that somatosensory maps lost to stroke are replaced over weeks by new structural and functional circuits with prolonged modes of activation within both the peri-infarct zone and distant sites. *J Neurosci* **29**, 1719-1734 (2009).

80. J. A. Jablonka, K. Burnat, O. W. Witte, M. Kossut, Remapping of the somatosensory cortex after a photothrombotic stroke: dynamics of the compensatory reorganization. *Neuroscience* **165**, 90-100 (2010).

81. C. Weiller, F. Chollet, K. J. Friston, R. J. Wise, R. S. Frackowiak, Functional reorganization of the brain in recovery from striatocapsular infarction in man. *Ann Neurol* **31**, 463-472 (1992).

82. S. C. Cramer *et al.*, A functional MRI study of subjects recovered from hemiparetic stroke. *Stroke; a journal of cerebral circulation* **28**, 2518-2527 (1997).

83. H. Reddy, N. De Stefano, M. Mortilla, A. Federico, P. M. Matthews, Functional reorganization of motor cortex increases with greater axonal injury from CADASIL. *Stroke* **33**, 502-508 (2002).

84. A. Q. Bauer *et al.*, Optical imaging of disrupted functional connectivity following ischemic stroke in mice. *Neuroimage* **99**, 388-401 (2014).

85. C. D. Smyser *et al.*, Longitudinal analysis of neural network development in preterm infants. *Cereb Cortex* **20**, 2852-2862 (2010).

86. A. T. Eggebrecht *et al.*, Joint Attention and Brain Functional Connectivity in Infants and Toddlers. *Cereb Cortex* **27**, 1709-1720 (2017).

87. J. D. Lewis *et al.*, The Emergence of Network Inefficiencies in Infants With Autism Spectrum Disorder. *Biol Psychiatry*, (2017).

88. J. R. Pruett, Jr. *et al.*, Accurate age classification of 6 and 12 month-old infants based on resting-state functional connectivity magnetic resonance imaging data. *Dev Cogn Neurosci* **12**, 123-133 (2015).

89. N. D. Woodward, H. Karbasforoushan, S. Heckers, Thalamocortical dysconnectivity in schizophrenia. *Am J Psychiatry* **169**, 1092-1099 (2012).

90. J. T. Baker *et al.*, Disruption of cortical association networks in schizophrenia and psychotic bipolar disorder. *JAMA Psychiatry* **71**, 109-118 (2014).

91. A. Hahamy, M. Behrmann, R. Malach, The idiosyncratic brain: distortion of spontaneous connectivity patterns in autism spectrum disorder. *Nat Neurosci* **18**, 302-309 (2015).

92. R. A. Muller *et al.*, Underconnected, but how? A survey of functional connectivity MRI studies in autism spectrum disorders. *Cereb Cortex* **21**, 2233-2243 (2011).

93. T. L. Lewis, D. Maurer, Multiple sensitive periods in human visual development: evidence from visually deprived children. *Dev Psychobiol* **46**, 163-183 (2005).

94. A. Ranson, F. Sengpiel, K. Fox, The role of GluA1 in ocular dominance plasticity in the mouse visual cortex. *J Neurosci* **33**, 15220-15225 (2013).

95. T. K. Hensch, Critical period plasticity in local cortical circuits. *Nat Rev Neurosci* **6**, 877-888 (2005).

96. M. A. Long, S. J. Cruikshank, M. J. Jutras, B. W. Connors, Abrupt maturation of a spike-synchronizing mechanism in neocortex. *J Neurosci* **25**, 7309-7316 (2005).

97. B. Morales, S. Y. Choi, A. Kirkwood, Dark rearing alters the development of GABAergic transmission in visual cortex. *J Neurosci* **22**, 8084-8090 (2002).

98. K. G. Baimbridge, M. R. Celio, J. H. Rogers, Calcium-binding proteins in the nervous system. *Trends Neurosci* **15**, 303-308 (1992).

99. M. Fagiolini *et al.*, Specific GABAA circuits for visual cortical plasticity. *Science* **303**, 1681-1683 (2004).

100. T. K. Hensch *et al.*, Local GABA circuit control of experience-dependent plasticity in developing visual cortex. *Science* **282**, 1504-1508 (1998).

101. Y. Iwai, M. Fagiolini, K. Obata, T. K. Hensch, Rapid critical period induction by tonic inhibition in visual cortex. *J Neurosci* **23**, 6695-6702 (2003).

102. L. Gianfranceschi *et al.*, Visual cortex is rescued from the effects of dark rearing by overexpression of BDNF. *Proc Natl Acad Sci U S A* **100**, 12486-12491 (2003).

103. J. L. Hanover, Z. J. Huang, S. Tonegawa, M. P. Stryker, Brain-derived neurotrophic factor overexpression induces precocious critical period in mouse visual cortex. *J Neurosci* **19**, RC40 (1999).

104. Z. J. Huang *et al.*, BDNF regulates the maturation of inhibition and the critical period of plasticity in mouse visual cortex. *Cell* **98**, 739-755 (1999).

105. C. L. McCurry *et al.*, Loss of Arc renders the visual cortex impervious to the effects of sensory experience or deprivation. *Nat Neurosci* **13**, 450-457 (2010).

106. K. H. Wang *et al.*, In vivo two-photon imaging reveals a role of arc in enhancing orientation specificity in visual cortex. *Cell* **126**, 389-402 (2006).

107. S. Chowdhury *et al.*, Arc/Arg3.1 interacts with the endocytic machinery to regulate AMPA receptor trafficking. *Neuron* **52**, 445-459 (2006).

108. H. Okuno *et al.*, Inverse synaptic tagging of inactive synapses via dynamic interaction of Arc/Arg3.1 with CaMKIIbeta. *Cell* **149**, 886-898 (2012).

109. Y. Yin, G. M. Edelman, P. W. Vanderklish, The brain-derived neurotrophic factor enhances synthesis of Arc in synaptoneurosomes. *Proc Natl Acad Sci U S A* **99**, 2368-2373 (2002).

110. S. W. Ying *et al.*, Brain-derived neurotrophic factor induces long-term potentiation in intact adult hippocampus: requirement for ERK activation coupled to CREB and upregulation of Arc synthesis. *J Neurosci* **22**, 1532-1540 (2002).

111. S. D. Kuipers *et al.*, BDNF-induced LTP is associated with rapid Arc/Arg3.1-dependent enhancement in adult hippocampal neurogenesis. *Sci Rep* **6**, 21222 (2016).

Chapter 2

Sensory Deprivation Following Focal Ischemia Accelerates Remapping and Improves Behavioral Recovery through Arc-Dependent Synaptic Plasticity

Preface

This chapter contains a manuscript that is under review:

Kraft A.W. et al. Sensory Deprivation Following Focal Ischemia Accelerates Remapping and Improves Behavioral Recovery through Arc-Dependent Synaptic Plasticity. Manuscript under review.

Author Contributions for the citation above:

AWK, AQB, JPC, JML designed experiments. AWK collected data. AWK, AQB processed and analyzed data. AQB provided training in imaging. AWK, JML wrote the manuscript with help from all co-authors. All authors read and approved the final manuscript. JML supervised all aspects of the project.

Abstract

Recovery after stroke, the leading cause of adult disability, is often unpredictable and incomplete. Behavioral recovery is associated with functional remapping to perilesional regions, suggesting that mechanisms underlying remapping may be important therapeutic targets to enhance recovery. However, molecular mechanisms underlying remapping are poorly understood, and it is unclear if modifying remapping alters behavioral recovery. We photothrombosed forepaw somatosensory cortex in mice, and followed remapping using Optical Intrinsic Signal imaging and behavioral recovery using the cylinder rearing test. Focal sensory deprivation targeted to the perilesional whisker barrel (via whisker trimming) accelerated forepaw sensory remapping into the whisker barrel cortex and improved the extent of sensorimotor behavioral recovery. Further, these improvements persisted even after targeted sensory deprivation was ceased. Mice deficient in Arc, a gene critical for activity-dependent synaptic plasticity, failed to remap or recover sensorimotor function. These results suggest that post-stroke remapping occurs through Arc-mediated synaptic plasticity and is required for behavioral recovery. Furthermore, recovery may be improved with maneuvers that enhance perilesional cortical plasticity.

Introduction

Ischemic stroke is the leading cause of disability throughout the world (*1*), resulting in deficits that can be profoundly debilitating (*2-4*). While some recovery may occur in the weeks to months following the initial ischemic event, this recovery is unpredictable and often incomplete (*2-4*). Thus, recovery can be expected to plateau well below baseline levels leaving patients in a state of chronic disability (*2-4*). Because limited recovery can occur, it is clear that endogenous repair mechanisms exist. Several plasticity mechanisms driving repair and recovery have been uncovered in animal models of focal brain ischemia, and enhancing these pathways can improve behavioral outcomes (*5-8*).

In the case of focal ischemia involving the cortex, there is an acute loss of function associated with the infarcted region. Functional recovery occurs in parallel with the reappearance of an effective functional representation in perilesional cortex in the weeks to months following infarction (*9-14*). This process, termed remapping, has been observed in both animal models and human patients recovering from stroke (*15-17*). Remapping has not only been demonstrated following lesions limited to sensory or motor cortex, it has also been demonstrated following infarction of subcortical structures (*18*). However, the role of remapping in recovery remains correlational; it is unclear if remapping is a necessary step for behavioral recovery. Moreover, the cellular and molecular mechanisms responsible for remapping are only beginning to be elucidated. Early studies examining recovery after motor cortex lesions in non-human primates demonstrated that activity in the affected limb was required for motor remapping to occur (*9*). Subsequent work using multiphoton imaging with cellular resolution on mice with genetic calcium reporters revealed that remapping after sensory cortex infarction involved changes in somatic sensory receptivity at the level of individual neurons (*11*). Thus, sensory remapping may involve competing somatosensory input from affected somatic regions and adjacent non-affected somatic regions (with intact sensation) that vie for receptivity of common neurons in the somatosensory cortex.

In the absence of injury, competition for cortical sensory representation can also occur in the setting of sensory deprivation—a maneuver well-known to induce cortical plasticity (*19, 20*). Amputation of limbs or digits, trimming of whiskers, and visual deprivation, each result in expanded representation of spared sensory modalities into the deprived cortical regions (*19-22*). While the effects of deprivation may be most dramatic during development, sensory deprivation also induces plasticity in the adult brain (*19, 23-26*).

These studies raise the exciting possibility that focal sensory deprivation after cortical infarction could enhance plasticity in a manner that facilitates remapping and improves behavioral recovery. Furthermore, there may be substantial overlap between the mechanisms driving plasticity induced by sensory deprivation in the uninjured brain and those involved in remapping in the injured brain. Of note is activity-regulated cytoskeleton-associated protein (Arc), which has been demonstrated to play a critical role in experience-dependent synaptic plasticity (*27*). Arc gene deletion attenuates LTD and LTP consolidation *in situ* and memory consolidation *in vivo (31)*. Furthermore, Arc is required for ocular dominance plasticity (ODP) in the visual cortex during critical period monocular deprivation (*29*). Arc mediates these effects via coordinated AMPA receptor endocytosis (*32*) and can be targeted at individual synapses. This mechanism permits the selective weakening of inactive synapses and potentiation of active synapses (*33*), making Arc-mediated synaptic plasticity a strong candidate pathway for mediating remapping and recovery after focal ischemia.

To examine this possibility, we turned to a previously established mouse model of focal cortical ischemia that is consistently followed by remapping and recovery. Primary forepaw somatosensory cortex photothrombotic infarction results in acute behavioral deficits and loss of somatosensory forepaw (S1FP) evoked responses (*11, 12*). We followed S1FP remapping and behavioral recovery in mice subjected to chronic whisker trimming, depriving sensory input to the perilesional whisker barrel cortex (S1WB). To determine if remapping and recovery was

dependent on activity-dependent synaptic plasticity, mice with genetic deletion of *Arc* (*28*) were subjected to the infarct-remapping-recovery paradigm. We have found that sensory deprivation accelerates remapping and improves behavioral recovery in wild-type mice, whereas Arc-/- mice demonstrated no remapping and persistent behavioral deficits.

Results

Mice were subjected to right S1FP photothrombosis (right forepaw somatosensory representation on left cortical hemisphere) and followed for 8 weeks after ischemia. Forepaw mapping and behavioral testing were performed prior to and at multiple timepoints following ischemia (Fig. 2.2.1). This study consisted of 4 experimental groups 1) Arc+/+ mice (WT-Control); 2) Arc+/+ mice with sensory deprivation (WT-Depriv); 3) Arc-/- mice (Arc-Control); 4) Arc-/- mice with sensory deprivation (Arc-Depriv). S1FP photothrombotic infarct volume and perilesional astrogliosis were not different between WT and Arc-/- mice (Figs. S1,S2). Throughout the study period, all mice were housed in enriched environments to expand the dynamic range for behavioral recovery.

Remapping is accelerated and redirected to the whisker barrel cortex in whisker deprived mice

To determine if post-infarct remapping can be altered by targeted perilesional sensory deprivation, we trimmed all contralesional (right) mystacial whiskers starting 48 hours after ischemia to deprive the barrel cortex adjacent to S1FP. Whiskers were kept under 1mm for the entire recovery time-course (for 8 weeks). Right forepaw stimulation resulted in consistent activation of S1FP cortex on the left hemisphere in all groups prior to photothrombosis (Figs. 2, S3, S4). Photothrombosis targeted to right S1FP (left hemisphere) resulted in loss of evoked right forepaw responses in the first week following injury in all groups (Figs. 2, S3, S4). Photothrombosis did not affect the evoked responses of the left forepaw or the right hindpaw in any of the groups (Fig. 2.2.3), and left forepaw activations were stable across imaging time points (Fig. 2.2.S5). Evoked right forepaw responses reappeared 8 weeks after infarction in WT mice, and were focused to regions anterior to the infarct (near motor cortex). In whisker-deprived mice, reappearance of S1FP maps

occurred earlier (4 week time-point), and remapping was observed in regions posterior to the infarct, within the whisker barrel cortex. At 8 weeks post-ischemia, the right forepaw evoked response was still present in the whisker cortex. Thus, focal sensory deprivation influenced both the timing and location of remapping.

While substantial evidence suggests that cortical plasticity is dependent on the dynamic changes in synaptic structure and function, it is unclear if similar mechanisms are required for remapping following cortical injury. To determine if activity-dependent synaptic plasticity was required for post-infarct remapping and recovery, we subjected Arc-/- mice to photothrombosis and followed S1FP remapping. In our experiments baseline sensory-evoked responses in Arc-/- mice were similar in location and amplitude to that in WT mice. After photothrombosis, right forepaw evoked responses did not reappear in the whisker-deprived Arc-/- mice even out to 8 weeks after ischemia; nor did remapping occur in the Arc-/- mice with intact whiskers. Collectively, these data show that Arc is required for infarct-induced cortical remapping (Figs. 2, S3, S4) and suggests that cortical remodeling following focal ischemia shares essential components with mechanisms involved in synaptic plasticity.

Whisker deprivation improves behavioral recovery following focal ischemia

To determine if whisker deprivation altered sensorimotor behavioral recovery, we used the cylinder rearing test—an observational sensorimotor test that assesses lateralized forelimb use during spontaneous exploratory behavior inside of a glass cylinder (Fig. 2.4). Healthy animals explore the walls of the cylinder while rearing using both forepaws equally. However, immediately after sensory or motor cortex photothrombosis, mice preferentially use the unaffected limb; this asymmetric forelimb use is followed by recovery of symmetry within 8 weeks after infarction (*7, 12, 34*). A major advantage of this test is that it does not involve any training—an essential requirement for the examination of Arc-/- mice, which have significant learning deficits (*31*).

At baseline, all groups demonstrated symmetrical forelimb use (Fig 3). S1FP photothrombosis resulted in use asymmetry due to relative decreases in right forelimb use that was consistent across all groups examined (Fig. 2.4). In WT-Control mice, limb use symmetry was significantly improved at WK7 compared to WK1, but the WK7 limb use was still statistically asymmetric compared to baseline (partial recovery). This time course is in agreement with previous studies utilizing small photothrombotic lesions isolated to the primary sensory cortex (*12*). In the whisker-deprived WT mice, recovery showed marked acceleration as use-symmetry returned to baseline levels by 3 weeks post-ischemia (complete recovery) which persisted to week 7. Thus, focal sensory deprivation via whisker trimming improved both the rate and extent of behavioral recovery. Arc-/- mice (both whisker-deprived and whisker-intact) showed persistent use-asymmetry throughout the 8-week timeline, indicating the absence of behavioral recovery (Fig. 2.4). Whisker deprivation alone (in the absence of cortical photothrombosis) for 3 weeks, did not result in any limb use-asymmetry (Fig. 2.S10).

Dendritic spine density is enhanced in remapped cortex

Turnover of dendritic spines is likely an important mechanism involved in brain repair after focal ischemia. Within hours of an ischemic insult, a marked decrease in perilesional dendritic spine density is observed (*35-38*). In the following weeks, spine turnover increases dramatically with spine generation outpacing spine removal. This results in spine accumulation and gradual recovery of perilesional spine density in the weeks after ischemia (*38*). This process may reflect the initial loss of structural and functional connectivity that occurs following infarction and the subsequent synaptic rearrangement in perilesional cortex that is required for remapping and recovery. Furthermore, it has been shown that recovery of spine density correlates with behavioral recovery (*39*), suggesting the synaptic changes reflected by spine density are important for recovery.

We quantified dendritic spine density 3 weeks after ischemia in layers II/III and IV at three cortical locations: 1) anterior perilesional (near motor cortex); 2) posterior perilesional (whisker barrel); and 3) distant site (1.5mm medial to the lesion; Fig. 2.5). Overall, we found decreased dendritic spine density at the perilesional locations compared to the distant site (far away from infarction)—a finding consistent with previous studies (*38*). However, in the WT mice, spine density in the anterior perilesional location (where remapping occurred) was significantly higher than all other groups. In contrast, WT mice subjected to whisker deprivation had increased spine density at the posterior perilesional location (within whisker barrel cortex) compared to all other groups. In both groups the location of increased spine density corresponded to the region of remapping. The Arc-/- mice did not show any increase in spine density at any location examined, regardless of whisker trimming status. Collectively, our data demonstrate that cortical regions of remapping demonstrate increased dendritic spine density.

Deprivation-induced remapping and behavioral improvement are stable after whisker regrowth

To determine the stability of deprivation-induced remapping and behavioral recovery, we examined remapping and behavioral performance after allowing whisker regrowth (Fig. 2.6). Using the previous recovery paradigm, we performed whisker trimming for 8 weeks and then allowed whiskers to regrow for 4 weeks (Fig. 2.6). Whiskers regrow at a rate of >1mm per day, and were fully grown after 1 week. Further, 4 weeks of whisker regrowth has been previously shown to reverse deprivation-induced cortical evoked response changes in the setting of uninjured CNS (*40*).

Using WT mice with and without sensory deprivation via whisker trimming (WT-Control and WT-Depriv), we examined right forepaw evoked responses 8 weeks after photothrombosis. At this point, whiskers were allowed to regrow in the WT-Depriv group, and forepaw maps were reexamined 4 weeks later (12 weeks post-photothrombosis, see Fig. 2.6 for timeline). At the 8 week time point, we found that right S1FP maps in WT-Control and WT-Depriv mice were in

significantly different locations (Fig. 2.7G), as seen in the previous experiment (Fig. 2.2). After 4 weeks of whisker regrowth, the right S1FP maps for each group remained in the same location (significant overlap) compared to their respective 8-week maps (Fig. 2.7K,L). These data suggest that whisker regrowth and concomitant whisker sensory input did not adversely affect the S1FP remapped area which remained stable during this period of regrowth (Fig. 2.7H).

To determine the spatial relationship between the S1FP remapped region and the whisker sensory area, we examined right whisker evoked responses 12 weeks post-photothrombosis (Fig. 2.7). Both Control and Depriv groups showed robust whisker-evoked maps; however, the Depriv maps were significantly smaller than those of the Control mice (Fig. 2.7K, Fig. 2.S9). Moreover, the smaller Depriv whisker maps were restricted to the posterior-lateral region of the WT-Control whisker maps (Fig. 2.7M). Superimposing the S1FP remapped regions onto the whisker map, revealed little overlap between these two sensory maps, and the spatial distributions of the S1FP and S1WB maps were statistically distinct (Fig. 2.7J). While the display comparisons shown in Fig. 2.7 show the 65% incidence contour, it is important to note that all statistical comparisons were made independent of any %incidence threshold (see Methods, Fig. 2.7. Fig. 2.S9). Altogether, these data suggest that whisker-deprivation enhances remapping into the whisker somatosensory cortex and that this remapping occurs at the spatial expense of the whisker map. Moreover, this remapped S1FP remains stable despite whisker regrowth.

To determine if withdrawal of whisker sensory deprivation altered forepaw use, we performed serial cylinder rearing tests during and after whisker trimming (Fig. 2.6). During the period of whisker trimming, the Depriv group showed accelerated and complete recovery by 5 weeks after photothrombosis. Even after whisker regrowth, this improved performance persisted in the Depriv group, whereas control mice demonstrated a continued behavioral deficit (Fig. 2.8). These data suggest that adjacent focal sensory deprivation accelerates and improves the extent of behavioral

recovery following ischemic injury; and that this recovery is durable despite the resumption of sensory input.

Discussion

It has long been speculated that brain plasticity with concomitant functional remapping is important for behavioral recovery after focal brain injury (*9, 10, 15, 17, 41*). In this study, we provide evidence that experimental manipulation of cortical plasticity can alter remapping and enhance behavioral recovery. We show that remapping can be directed to specific cortical regions using focal sensory deprivation targeted to perilesional regions. Focal sensory deprivation (via whisker deprivation) resulted in earlier remapping, improved behavioral recovery, and increased synaptic spine density within the remapped areas (whisker barrel cortex). This remapping and improved recovery persists even after the resumption of sensory input. Furthermore, we show that remapping and behavioral recovery require Arc, suggesting the importance of mechanisms involved in synaptic plasticity.

Our finding that sensory deprivation modifies post-ischemic remapping is consistent with the effects of sensory experience in the uninjured brain. More specifically, selective sensory deprivation in both young and mature animals leads to the contraction of deprived sensory cortical representations and concomitant expansion of neighboring, spared cortical representations (*19, 20, 22-26, 42, 43*). A well-studied example of this phenomenon is ocular dominance plasticity with monocular deprivation, where ocular dominance columns from the normal eye expand into columns representing the deprived eye (*20, 26, 42*). The same principle applies to the somatosensory system where removal of select whiskers results in expansion of neighboring spared whiskers barrel fields into the deprived barrels (*19, 23, 24, 43, 44*), and transection of the infraorbital nerve in adult rats results in expansion of the forepaw digit somatosensory representations into the barrel cortex (*22*). Our studies demonstrate that focal sensory deprivation targeted to perilesional cortex can enhance remapping, suggesting that cortical plasticity is

heightened by functional non-use of the targeted cortical region. Moreover, our data suggest that this remapping may occur at the spatial expense of the cortical region targeted for sensory deprivation.

Receptivity shifts after photothrombosis observed with OIS (e.g. remapping) have been shown to involve receptivity shifts in individual perilesional neurons (*11*). More specifically, perilesional hindlimb S1 neurons are initially unaffected by S1FP photothrombosis and respond only to himdlimb stimulation. However, weeks later, these same perilesional hindlimb S1 cortical neurons are excitable by both forelimb and hindlimb stimulation. Eventually these neurons become selectively responsive to forepaw stimulation, and this process reflects what is seen with OIS remapping studies (*11*). It is likely that the sensory input from each somatic region influences changes in cortical representation. Thus, whisker activity may compete with forepaw activity for cortical representation. By eliminating whisker activity (and thereby a competing stimulus), one might enhance receptivity of neurons in the whisker barrel to competing forepaw stimuli, thereby boosting remapping potential of the forepaw somatosensory cortex.

While we observe remapping in cortical regions, the precise cellular “reconnections” that are required for remapping and recovery of function are unclear. It is possible that surviving cortical neurons representing the affected limb form new connections to adjacent cortex, thereby creating a new representation (i.e. remapping). Alternatively, it has been suggested that pre-existing silent, or sub-threshold, thalamocortical synapses may be strengthened to allow remapping to occur (*5*). While thalamocortical plasticity has been postulated to be generally limited in mature mice (*45, 46*), it is possible that ischemic injury initiates plasticity mechanisms to allow these thalamocortical neurons to extend axons to form new synapses in adjacent surviving cortex. In addition to potentiation of pre-existing connections, formation of *de novo* connections appears to be important as well. In the weeks after cortical infarction, upregulation of various genes, including

GDF10, results in robust axonal sprouting that increases cortical connectivity and plays a role in behavioral recovery (*6, 8*).

Photothrombosis in wild-type mice without intervention resulted in remapping, suggesting injury itself may also trigger plasticity and remapping. Ischemia induces post-stroke cascades that alter gene expression (*6, 8, 47-49*), and accumulating evidence suggests that some of these pathways are critical for plasticity required for recovery. For example, ischemia results in HIF-1 induced VEGF expression that results in angiogenesis critical for neurovascular remodeling (*50*). Inflammation induced by ischemia leads to production and elaboration of matrix metalloproteases which play a critical role in neurovascular remodeling and behavioral recovery weeks after the initial injury (*51*). Furthermore, ischemia induces perilesional expression of factors that induce axonal sprouting—a critical element of behavioral recovery (*6, 8*). Indeed, there are likely many endogenous mechanisms beyond these examples involved in recovery, and our study suggests that these endogenous mechanisms can be enhanced to accelerate, and improve the extent of behavioral recovery.

The behavioral recovery advantage of focal perilesional sensory deprivation was persistent even after the reintroduction of sensory input. Four weeks after whisker regrowth, the S1FP remapped area remained stable, as did the behavioral recovery. S1FP remapping occurred within the original whisker barrel cortex, compressing the sensory map of the regrown whiskers to the posterior-lateral region of the original whisker barrel cortex. The finding that whisker-evoked responses remained robust after deprivation suggests that the whisker somatosensory system is functional. However, it is unclear if this whisker map contraction reflects compromised whisker sensory function, as this was not formally tested. It should be noted that constraint-induced movement therapy (CIMT), a standard neurorehabilitative intervention, uses a similar approach (in principle) of movement restriction of the arm contralateral to the paretic arm. There is no evidence for deficits induced by CIMT, though it has not been carefully examined (*52-54*).

While the results in the current study may be the first study to implicate Arc in post-ischemic remapping, extensive work has implicated Arc in cortical plasticity following sensory deprivation in the uninjured brain. Sensory deprivation alone results in the induction of cAMP response element-binding protein (CREB) related genes, and plays a critical role in modifying post-synaptic neurons to allow expansion of adjacent functional regions (*44*). Arc, an immediate early gene regulated by CREB, has been specifically demonstrated to be required in ocular dominance plasticity with monocular deprivation (*29*). In addition to its role in ocular dominance plasticity, Arc is also required for orientation learning in the visual cortex and long term memory consolidation seen in behavioral learning paradigms (*31*). Arc-deficient brain slices show attenuated LTP and LTD consolidation and Arc-/- mice have profound learning deficiencies, suggesting these higher-level deficits result from dysfunction of synaptic plasticity. Arc mediates synaptic change by regulating glutamate receptors in the dendritic spines of excitatory neurons (*32*). Arc can regulate synaptic strength at the level of single synapses or whole-neurons (*33, 55*). Interestingly, excitation at active synapse can induce Arc-mediated AMPAR removal and synaptic weakening at silent or inactive synapses selectively (*33*)—and this pathway may enable the activity-dependent modulation of select synapses required for receptivity field changes seen with cortical remapping.

Importantly, prior work has demonstrated that Arc-/- are remarkably normal: Compared to WT mice, Arc-/- mice have normal weigh and fertility (*28, 29*); Detailed examination of the visual system retino-thalamic neuroanatomy is normal (*29*); and functional retionotopic representations in the visual cortex are not altered in Arc-/- mice (*29*). Moreover, cortical neuron membrane excitability and sensory evoked-response potentials are virtually identical to WT neurons (*28-30*). Thus the experience-dependent plasticity attenuated in Arc-/- mice is not due to generalized neuronal dysfunction, but due to specific disruption of experience-dependent change. Our data is

consistent with this as Arc-/- mice have normal baseline somatosensory maps but lack the post-ischemic plasticity that drives remapping and behavioral recovery.

Previous examination of perilesional synapses at the level of dendritic spines reveals enhanced spine loss and spine generation. This suggests old connections are replaced with new ones, a process likely critical for receptivity switches in perilesional neurons. Here, we show that post-ischemic spine density recovers selectively in cortical regions where remapping occurs, and that Arc is required for this increase in dendritic spine density. These results are consistent with previous work from sensory deprivation paradigms (without CNS injury) where robust anatomical plasticity was associated with changes in dendritic spines in deprived cortex (*56, 57*). Similar to what is seen in perilesional cortex after ischemia, sensory deprivation results in increased spine turnover implicating similar programs for structural and functional connectivity in deprived cortex (*56*). Arc is known to regulate dendritic spine dynamics through its interaction with actin-regulating proteins in dendritic spines (*58-60*). Thus, it is not surprising that post-ischemic spine density remains low in Arc-deficient mice. However, post-ischemic dendritic spine recovery reflects the new synapses that form through Arc-mediated mechanisms.

Implications for therapy

Current rehabilitative strategies for motor recovery have focused on increasing use of disabled limbs through “forced use” or constraint-induced movement therapy (CIMT) (*52-54*). While this therapeutic strategy takes advantage of use-dependent competition for perilesional cortical representation, it neglects competition from perilesional cortex representing unaffected somatic regions. Thus, rehabilitation might be more effective when coupling forced-use with focal deprivation of motor activity represented in targeted perilesional cortex. Such an approach might involve focal sensory deprivation or motor restraint, whether through mechanical or pharmacological means. Our results suggest that this therapy may only need to be applied temporarily, which is consistent with improvements demonstrated with CIMT (*52-54*). Current

rehabilitative deprivation approaches have not demonstrated negative impact on functionality after deprivation is ceased (*52-54*), but the potential for negative consequences must be considered in clinical trials assessing this strategy.

Methods

Study Design

The aim of this study was to determine if post-stroke remapping could be manipulated (both spatially and temporally) to alter behavioral recovery; and to determine if remapping was dependent on activity-dependent synaptic plasticity. Toward this end, we performed photothrombosis targeted at the forepaw somatosensory cortex in mice. Half of the mice were randomly selected to receive focal sensory deprivation (via contralesional whisker trimming), a maneuver known to enhance cortical plasticity (*19*) in the perilesional cortex. Remapping after injury was assessed using OIS imaging (*11, 12*), and sensorimotor behavioral recovery was assessed using the cylinder rearing test (*6, 7, 12*). Sample size and specific time points were selected based on previous studies examining behavioral recovery after forepaw somatosensory cortex photothrombosis (*6, 7, 12*). To determine if activity-dependent synaptic plasticity was required for remapping and recovery, Arc+/+ and Arc-/- mice were subjected to photothrombosis and focal sensory deprivation, and assessed for remapping and behavioral recovery (as described above). In a separate cohort of mice, dendritic spines were quantified after Golgi-Cox staining, 4 weeks after photothrombosis in 3 regions of the cortex: 1) anterior to infarction, 2) posterior to infarction (in whisker barrel cortex), and distant to the infarction (ipsi-lesional). Sample size was selected based on previous studies examining dendritic spine density dynamics after photothrombosis (*36, 37*). Image processing and data analysis was performed by an examiner blinded to group and/or genotype. All experiments were performed in accordance with animal protocols approved by the Washington University Animal Studies Committee in compliance with AAALAC guidelines.

Mice

Colonies of Arc+/+ (WT) and Arc-/- mice on a pure C57Bl6/J background (RRID:IMSR_JAX:007662) (*28*) were raised in standard cages with ad libitum access to food and water in a dedicated mouse facility with a 12-12 light/dark cycle

Imaging Windows

Under isoflurane (3.0% induction, 1.5% maintenance), the scalp and periosteal membranes were reflected from the skull, and Plexiglas imaging windows were fixed to the skull with clear metabond dental cement as described previously (*61*), to provide a wide field of view of the dorsal cortex. The windows provided a stable imaging platform for serial imaging throughout the study period. Windows were examined for development of infectious abscesses, and any mice that developed window infections were immediately sacrificed in accordance with our animal protocol (WT Control n=1; WT Depriv. n=2; Arc-/- Control n=0; Arc-/- Depriv. n=1).

Whisker Trimming

Mice were lightly anesthetized with isoflurane anesthesia, and all right mystacial whiskers where cut to <1mm with surgical scissors. Mice that did not receive whisker trimming were subjected to the same anesthetic protocol.

Enriched Environments and housing

For all recovery studies, mice were housed in 24” x 17” x 8” cages (Nalgene) with the following environmental enrichment components: Mouse Arch, Mouse Huts, Mouse Igloos, Mouse Tunnels, Fast Trac (bio-serv) and Environdri crinkle paper.

Photothrombosis

Under isoflurane anesthesia (see above), mice were placed in a stereotactic frame. A 532nm green DPSS laser (Shanghai Laser & Optics Century) collimated to a 0.5mm spot was centered

on S1FP (0.5mm anterior to bregma, 2.2mm left of bregma) at low power (<0.25mW). The laser was turned off, and mice were then given 200uL Rose Bengal dissolved in saline (10g/L) via I.P. injection. After 4 minutes, the laser was powered to 23mW (centered on S1FP), and targeted to S1FP for 10 minutes. This approach lead to thrombosis of all blood vessels in the target region.

Cylinder Rearing

Cylinder rearing recording and analysis was done as previously described (*7, 12, 34*). Briefly, mice were placed in a 1000 mL glass beaker and video recorded for 5 minutes. Group identity was masked and a custom MATLAB interface was used to manually analyze videos to determine the amount of time that the 1) right paw, 2) left paw, or 3) both paws made contact with the glass walls, and the percent of total forepaw contact time was calculated for each condition. Paw-use asymmetry was calculated as (% left paw contact time – % right paw contact time). Any mice that were not spontaneously active during any of the behavioral timepoints were excluded from analysis (WT Control n=0; WT Depriv. n=5; Arc-/- Control n=1; Arc-/- Depriv. n=0).

Imaging animal prep

As reported previously (*62*), anesthesia was initiated via i.p. injection with a bolus of ketamine-xylazine (5μL per gram; drug concentration: 86.9 mg/kg ketamine, 13.4 mg/kg xylazine dissolved in saline) and animals were allowed 15 minutes for anesthetic induction. After induction, the animal was placed on a heating pad maintained at 37°C via feedback from a rectal probe (mTCII, Cell Microcontrols) and its head secured in a stereotactic frame. While under ketamine-xylazine anesthesia, forelimb and hindlimb stimulation electrodes were placed (see below); the cortex was positioned in focus of the camera, and the animals were then transitioned to isoflurane anesthesia (<0.5%) for stimulation studies.

Paw Stimulation

Transcutaneous electrical stimulation was applied to the forepaw or hindpaw by placing microvacular clips (Roboz) on either side of the wrists or ankles. Electrical stimulation was provided in a block design (AM Systems Model 2100) with the following parameters: 5 seconds rest, 1 second stimulation (0.5 mA, 5ms duration, 100Hz) 24 seconds rest as previously described in other S1FP remapping studies (*11, 12*).

Whisker Stimulation

Whiskers where stimulated via mechanically displacement by placing all mystacial whiskers through an aluminum screen attached to a piezoelectric bending actuator (Piezo Systems). A 2° anterior-direction deflection occurred for 5ms and the piezo was allowed to fall back to the neutral position. This was presented at 10Hz with the following parameters: 5 seconds rest, 1 second stimulation.

Image acquisition

Sequential illumination was provided at four wavelengths by a ring of light emitting diodes (LEDs) placed approximately 10 cm above the mouse's head. The field of view included most of the cerebral cortex (approximately $1cm^2$). Diffuse reflected light was detected by a cooled, frame-transfer EMCCD camera (iXon 897, Andor Technologies); the LED ring and the camera were time-synchronized and controlled via computer using custom-written software (MATLAB, Mathworks) at a full frame rate of 30 Hz.

Image Processing

Data from all mice were subject to an initial quality check prior to spectroscopic analysis. Data blocks in which reflected light level intensity (mean value over the brain) varied as a function of time by greater than 1% for any wavelength were excluded from further analysis. Further, data blocks that had movement contamination were excluded. For subsequent analysis, image light intensity at each wavelength was interpreted using the Modified Beer-Lambert Law, usually

expressed as: $\Phi(\mathbf{r},t) = \Phi_0 * \exp(-\Delta\mu_a(\mathbf{r},t) * L)$. Here, $\Phi(\mathbf{r},t)$ is the measured light intensity, Φ_0 is the baseline light intensity, $\Delta\mu_a(\mathbf{r}, t)$ is the change in absorption coefficient due to hemodynamic changes, and L is the optical path length factor for photons in the tissue (*63*). We normalized relative to the average light intensity at each pixel, resulting in differential measures of absorption at each wavelength at each pixel: $\Delta\mu_{a,\lambda}(\mathbf{r},t) = -\ln(\Phi_\lambda(\mathbf{r},t)/\langle \Phi_{0\lambda}(\mathbf{r},t)\rangle)/L_\lambda$. Absorption coefficient data were converted to hemoglobin (Hb) concentration changes by inverting the system of equations, $\Delta\mu_{a,\lambda}(\mathbf{r},t) = E_{\lambda,i}\, \Delta[Hb_i](\mathbf{r},t)$ (where E is the extinction coefficient matrix, and *i* runs over hemoglobin species). This inversion was performed using least-squares methods, yielding changes in oxygenated hemoglobin (HbO) at each pixel at each time point. Each pixel's time series was downsampled from 30 Hz to 1 Hz, and all further analysis was performed only on those pixels labeled as brain using a manually-constructed brain mask. The time traces of all pixels defined as brain were averaged to create a global brain signal. This global signal was regressed from every pixel's time trace to remove global sources of variance; global signal regression was applied independently on each stimulation block. Since the spectral content of the OIS signal is known to be roughly "1/f", we excluded runs in which 50% of the power of the regressed data was found above 0.04 Hz to exclude data strongly contaminated by oscillatory vascular artifact (*64*). 34% of all imaging blocks were rejected.

Creating Somatosensory Maps

Oxy-hemoglobin was used for this study because it offers the greatest contrast to noise of all of our spectral components (Fig. 2.S11). For each mouse, stimulation blocks were averaged together. From that average response, baseline images (1s prior to stimulation) were subtracted from post-stimulation images (2s after stimulation) to generate the response image. All pixels that were >%50 of the maximum amplitude were defined as activated as reported previously (*11, 12*). To create individual binary activation maps, a minimum intensity threshold of 35% of the respective baseline amplitude (averaged over all groups) was required for pixels to be included

(this was required to view percent incidence maps at the group level). Percent maps were calculated at the group level by determining the percentage of mice for which each pixel was activated. Mean intensity maps were generated by averaging the intensity maps together without applying a minimum intensity cutoff. Maps of p-values were determined via Student's t test between all baseline and activated oxy-hemoglobin images for all group members at each time point.

Image Co-registration

Image sequences of each mouse (as well as the brain mask for each mouse) were affine-transformed to a common atlas space determined by the positions of the junction between the coronal suture and sagittal suture (posterior to the olfactory bulb and cerebrum along midline) and lambda as we have done previously (*65*). Bregma was not visible in all mice, and was calculated based on the above two anatomical landmarks. The anterior-posterior stretch was set equal to the medial-lateral stretch, and all transformed images were centered at bregma. The intersection of every brain mask was calculated and made symmetric by reflection across the midline allowing all subsequent comparisons to be performed on shared brain areas across all mice.

Dendritic Spines

Brains were harvested from all groups (WT-Control, n=5; WT-Depriv., n=5; Arc-Control, n=4; Arc-Depriv., n=4) 25 days after photothrombosis. The Histo Golg-Cox OptimStain (Hitobiotech) was used to label spines per kit instructions. Brains were embedded in low melting point gelatin, coronal slices at 200 microns with a vibratome, and mounted on gelatin coated slides. Spines were examined in layers II/II and IV. Images were taken at 67X using Microbrightfield Stereology to systematically collect image stacks (25 images per site, 1 micron separation) and generate minimum intensity projections (MIPs). 3 MIPs were collected at each sampled location, resulting in an average of 570 spines being imaged per mouse at each location. All spines in the images areas were analyzed. Spine counting and dendrite length was performed on MIPs in ImageJ. For

each mouse, a spine density was calculated at each sample location. At each location, spine density was compared across groups.

Histology

7 days following S1FP infarction, mice (WT, n=4; Arc, n=4) were deeply anesthetized and transcardiac perfusion with PBS followed by 4% PFA was performed. Brains were submerged in 4% PFA for 24 hours, then kept in cryoprotectant solution for 72 hours before slicing. Brains were sliced at 50 micron thickness on a sliding microtome. To determine infarction volume, slices were stained with Cresyl Violet. Stained sections were imaged with a Nanozoomer and infarction volume was quantified in ImageJ. GFAP immunostaining was performed using anti-GFAP antibodies (Sigma) and developed using the Vector Laboratories 3,3'-diaminobenzidine ABC developing kit (Vector). Perilesional images of GFAP-labeled sections were taken with a 40X objective using Microbrightfield Stereology to systematically collect image stacks and generate minimum intensity projections (MIPs). MIPs were intensity-thesholded, and %area of GFAP immunoreactivity was calculated for each mouse.

Statistical analysis

For evoked maps, P-values were calculated for each pixel by comparing Oxy-Hb values at baseline and after stimulus using all images within each group at each time point. Clusters of 75 or more pixels with uncorrected P values $<e^{-10}$ were considered statistically significant. For cylinder rearing testing, differences between groups were analyzed using one-way ANOVA with repeated measures and Newman–Keuls' multiple pair-wise comparisons as has been done previously (*7*). The level of significance was set at $P<0.05$. For spine density analysis, differences between groups were analyzed using two-way ANOVA with Bonferroni correction for multiple comparisons with the level of significance was set at $P<0.05$. For infarction volume studies, Student's t-test was used with the level of significance was set at $P<0.05$. Statistical map comparisons (Figure 7) were performed by summing the dot products for the %incidence maps

for the two maps being compared (the sum of the element-wise produce of both %incidence maps being compared). This produced a single value, termed “overlap,” that was used as the test statistic. A “overlap” null distribution for each comparison was calculated by calculating the overlap for 10000 random groupings of the mice involved in the comparison (Fig. 2.S8). Statistical significance was set at $P<0.007$ ($P<0.05$ / 7 comparisons).

Acknowledgements

This work was supported in part by National Institutes of Health grants R01NS084028 (J.-M.L), F31NS089135 (A.W.K), R01NS078223 (J.P.C.), P01NS080675 (J.P.C.), K25NS083754 (A.Q.B) and American Heart Association grants 13POST14240023 (A.Q.B) and 14PRE18410013 (A.W.K).

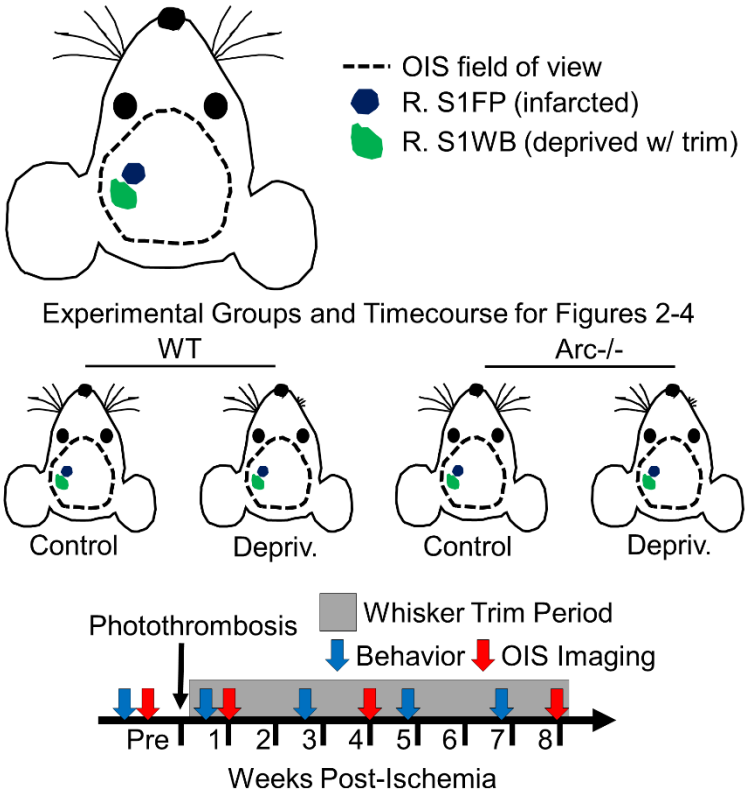

Figure 2.1. Experimental design and timecourse. Wildtype (WT) and Arc knockout (Arc -/-) mice were subjected to right forepaw somatosensory (S1FP) photothrombosis. Half of the mice in each group underwent right whisker trimming every other day for the duration of the experiment. Cranial windows were created in order to permit serial OIS imaging prior to and after photothrombosis (as indicated in timeline). Mice were also serially tested for behavioral recovery using the cylinder rearing test (as indicated in timeline).

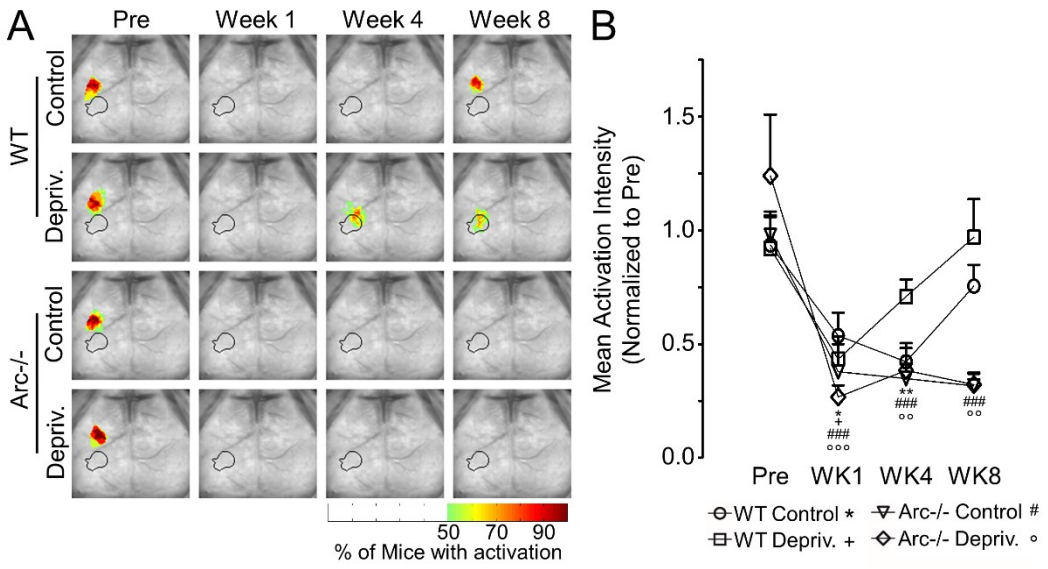

Figure 2.2. Whisker deprivation accelerates S1FP remapping after photothrombosis. **(A)** All groups showed similar evoked maps following right forepaw stimulation at baseline (Pre). Photothrombosis targeted to right S1FP (left hemisphere) resulted in acute loss of right forepaw response in all groups at week 1. 8 weeks post-photothrombosis, WT mice demonstrated remapping anterior to the infarct. Remapping in whisker-deprived mice occurred earlier (week 4), and was located within the barrel cortex (black outline, posterior to the infarct). Remapping did not occur in Arc-/- mice. Maps shown are activation density maps projected onto a white light cortical image. The whisker barrel cortex, delineated using whisker stimulation-evoked mapping with OIS imaging, is outlined in black. **(B)** Mean activation intensity after RFP stimulation for each group over the recovery time course. Intensity response is determined for each mouse prior to being group-averaged, and this reflects the remapping see in (A). * P≤0.05, ** P≤0.01, *** P≤0.001 compared to baseline time-point using ANOVA with repeated measures. WT Control, n=11; WT Depriv., n=10; Arc-/- Control, n=8; Arc-/- Depriv., n=7.

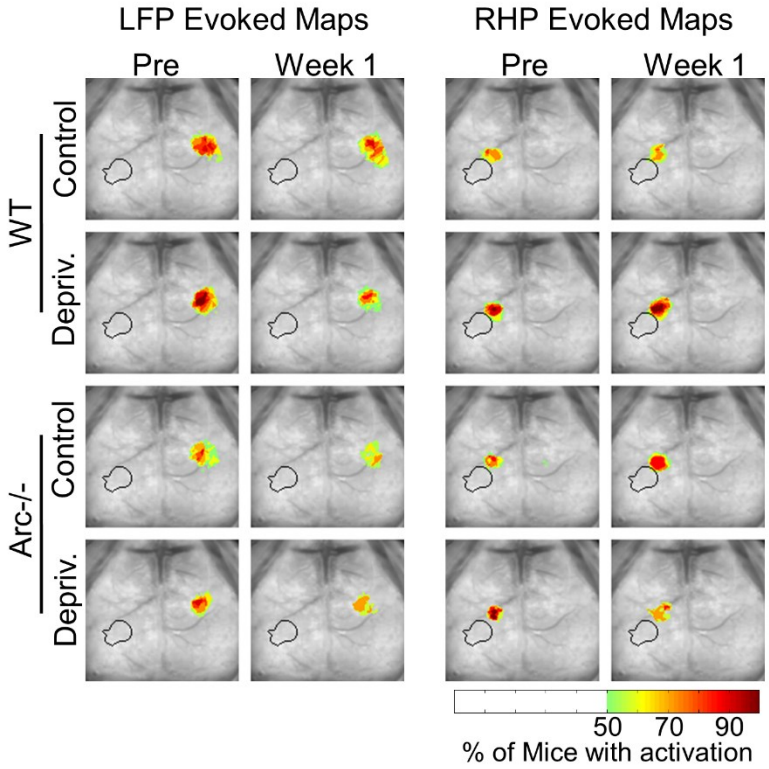

Figure 2.3. Right S1FP phothrombosis is functionally selective. Evoked maps for left forepaw (LFP) and right hindpaw (RHP) are shown prior to and 1 week after photothrombosis. In all groups, evoked maps were unaffected by right S1FP photothrombosis. WT Control, n=11; WT Depriv., n=10; Arc-/- Control, n=8; Arc-/- Depriv., n=7.

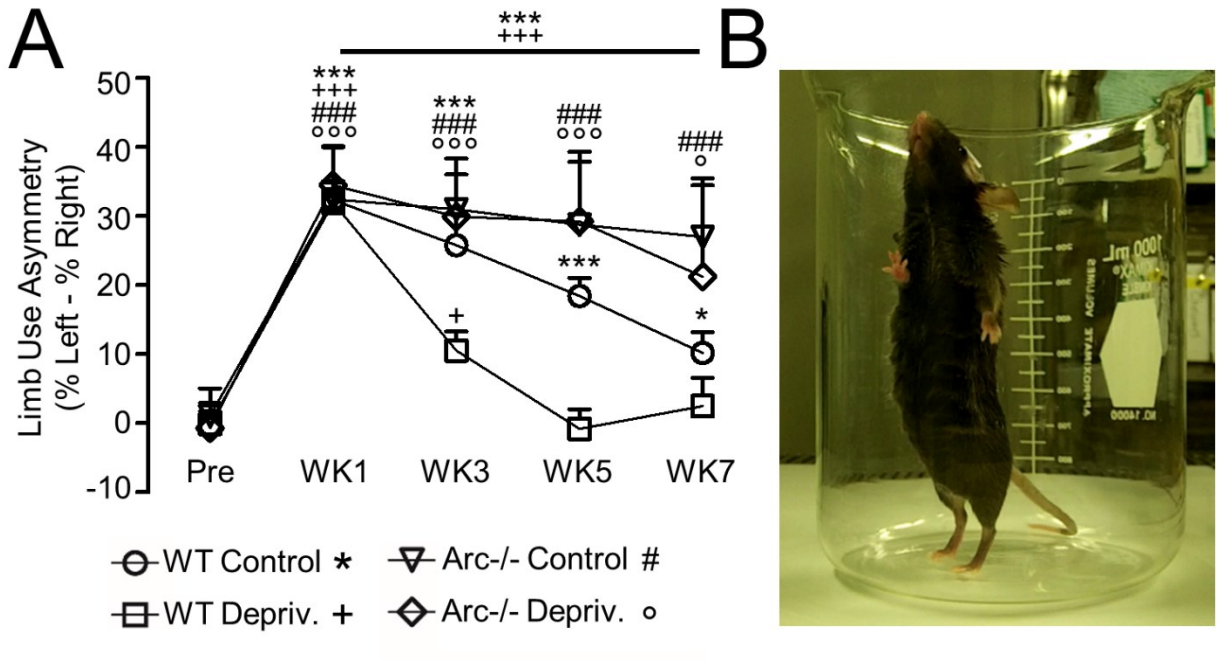

Figure 2.4. Whisker deprivation accelerates and enhances behavioral recovery after S1FP photothrombosis. **(A)** Limb use, measured with the cylinder rearing test, was completely symmetrical at baseline in all groups (Pre). Photothrombosis resulted in use asymmetry due to decreased use of the right forelimb within the first week. WT mice (WT Control) demonstrated significant improvement by week 7, but a deficit was still present compared to baseline (partial recovery). Whisker trimmed WT mice (WT Depriv.) showed more rapid return to symmetric forelimb use by 3 weeks post-photothrombosis (complete recovery) which persisted to week 7. Arc-/- mice with or without whisker deprivation had persistent use asymmetry through the entire recovery time-course (absent recovery). **(B)** Example image of rearing with right forepaw use. * P≤0.05, ** P≤0.01, *** P≤0.001 compared to baseline time-point (Pre), using ANOVA with repeated measures and Newman–Keuls' multiple pair-wise comparisons. WT Control, n=22; WT Depriv., n=16; Arc-/- Control, n=7; Arc-/- Depriv., n=7.

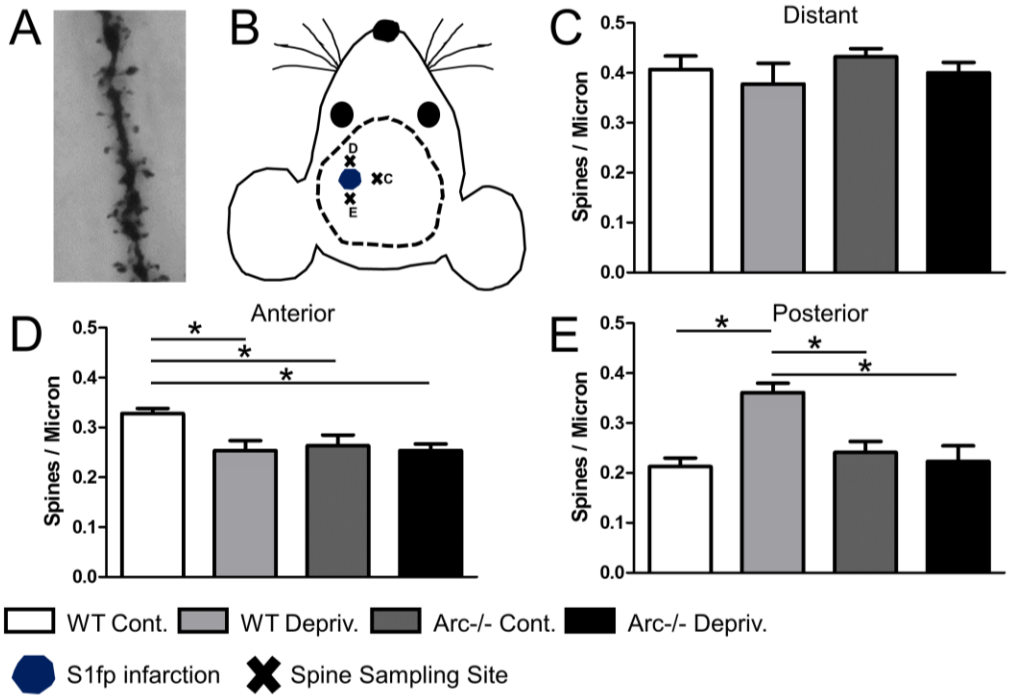

Figure 2.5. Region of remapping demonstrates increased dendritic spine density. **(A)** Example of golgi-cox stained dendritic spines. **(B)** Spines were sampled at three locations: 1) distant; 2) anterior perilesional; 3) posterior perilesional. **(C)** At the distant site, spine density was not different between the 4 groups. **(D-E)** At all perilesional locations, overall spine density was decreased compared to the distant location. **(D)** At the anterior perilesional location, spine density was significantly greater in WT mice (in region of remapping). **(E)** At the posterior perilesional location, spine density was significantly greater in the whisker-deprivation mice (in region of remapping). At each location, spine density was compared between all groups using ANOVA with Bonferroni correction for multiple comparisons. All statistically significant differences are shown (* P≤0.05). WT Control, n=5; WT Depriv., n=5; Arc-/- Control, n=4; Arc-/- Depriv., n=4.

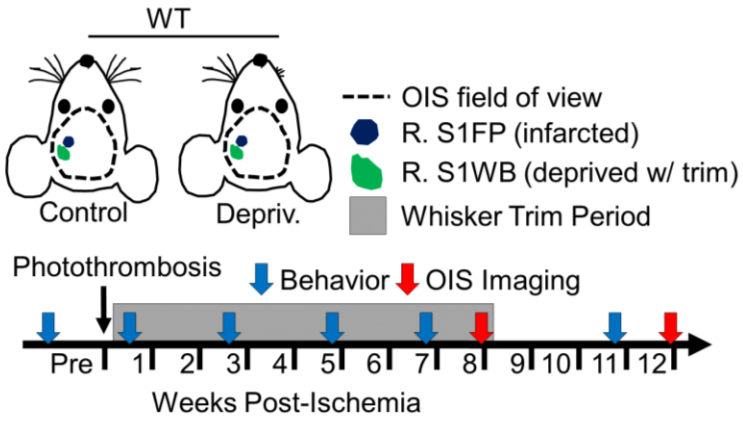

Figure 2.6. Experimental design and timecourse for whisker trimming and regrowth (Figs. 7-8). Wildtype (WT) were subjected to right forepaw somatosensory (S1FP) photothrombosis. Half of the mice underwent right whisker trimming every other day for the first 8 weeks of the experiment. After 8 weeks, trimming was halted and whisker were allowed to regrow and limb behavior and S1 maps were assessed at the times indicated.

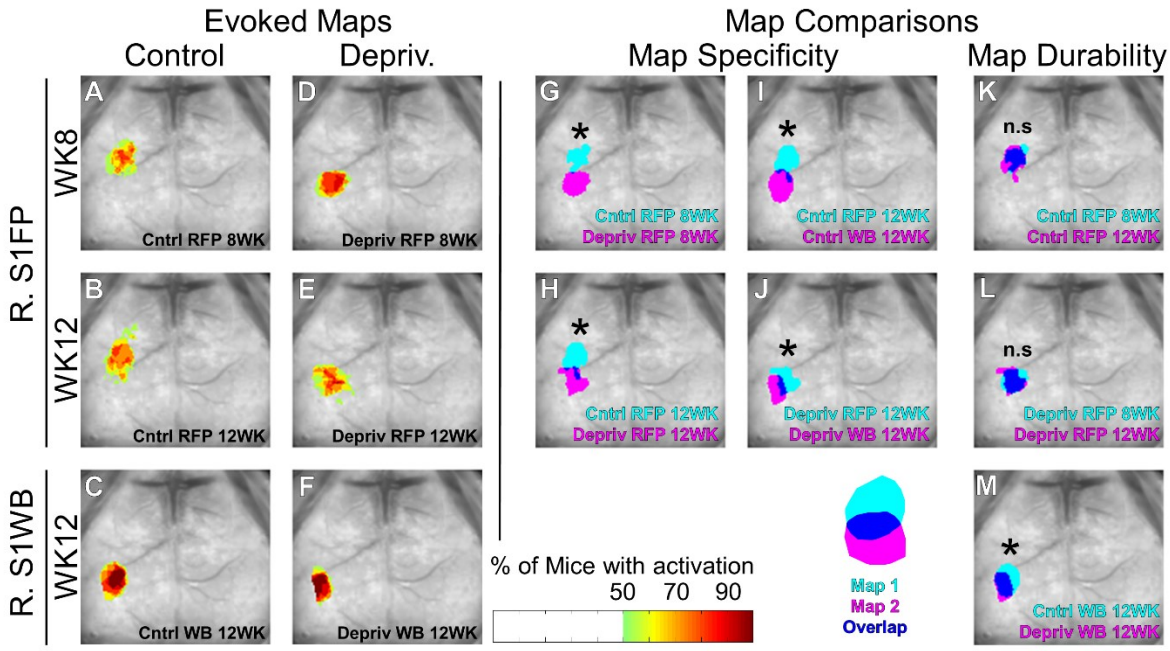

Figure 2.7. Deprivation-induced remapping is stable beyond the deprivation period. **(A-F)** Evoked response density maps showing R. S1FP maps 8 and 12 weeks after photothrombosis and R. S1WB maps 12 weeks after photothrombosis in **(A-C)** WT Control and **(D-F)** WT Depriv. Groups. Consistent with Fig. 2.2, sensory deprivation via whisker trimming altered the remapping location at WK8. **(G-M)** Map Comparisons. Displayed are maps of the >65% density response for each map. Map identity is indicated by the label in each image, and yellow represents overlap between the maps. The >65% cut off was used only for display, and statistical comparisons were independent of this cut off. * Indicates a statistically significant difference in spatial distribution between the evoked responses compared (see Fig. 2.S8 and methods for more detail). **(G,I)** Significant spatial differences between the WT Control and WT Depriv. R. S1FP maps demonstrates that remapping occurs in separate locations. **(H,J)** Significant spatial differences between the forepaw and whisker maps demonstrates specific between distinct peripheral representations. **(K,L)** For both groups group, the R. S1FP location was stable between 8 and 12 weeks, demonstrating that regrowth of whiskers did not disrupt deprivation-facilitated remapping. **(M)** WT Control and WT Depriv whisker maps were significantly altered, suggesting chronic deprivation did affect that deprived cortical representation. WT Control, n=11; WT Depriv., n=11.

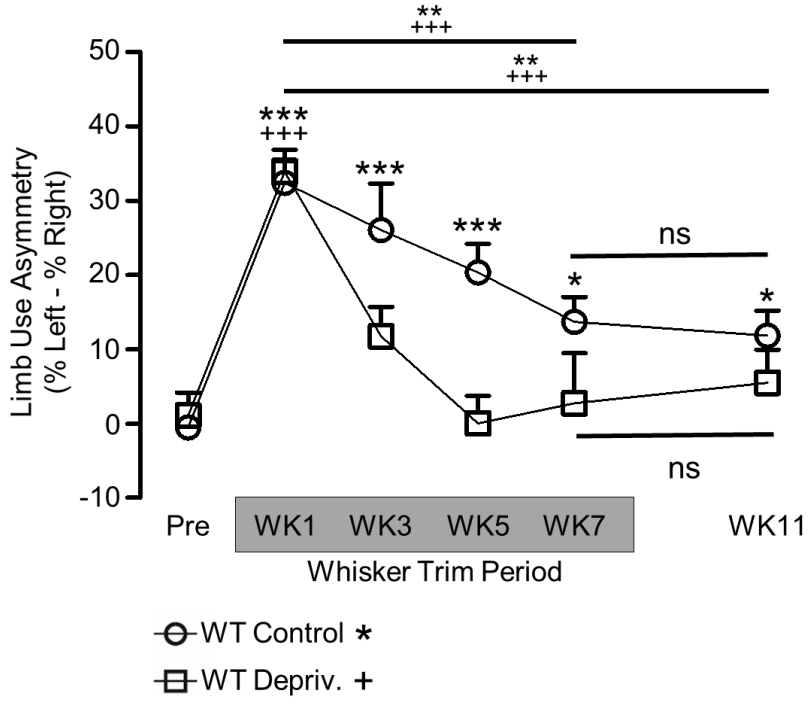

Figure 2.8. Deprivation-induced behavioral recovery persist beyond the deprivation period. R. S1FP photothrombosis resulted in acute limb use asymmetry in both WT Control and WT Depriv. groups. As in Fig. 2.4, recovery was accelerated and extent was improved by whisker trimming (WT Depriv. mice). After 8 weeks of whisker trimming, whiskers were allowed to regrow and limb use was assessed at WK11. Limb use asymmetry at WK8 and WK11 were not statistically different within each group by ANOVA and paired t-test analysis. This demonstrates that improvements to the extent of behavioral recovery from sensory deprivation were stable following deprivation withdraw. * P≤0.05, ** P≤0.01, *** P≤0.001 compared to baseline time-point (Pre), using ANOVA with repeated measures and Newman–Keuls' multiple pair-wise comparisons. WT Control, n=11; WT Depriv., n=8.

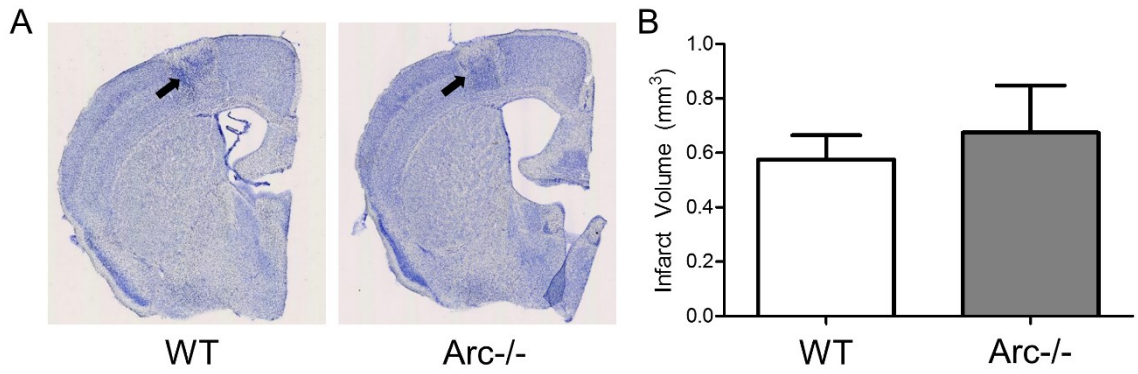

Figure 2.S1. *Arc* gene deletion does not affect infarct volume. **(A)** Representative brain slices from mice 28 days after right S1FP photothrombosis stained with cresyl violet shows equivalent infarct sizes (arrows). **(B)** Infarct volume was not different between WT and Arc-/- mice (P=0.3; n=4 per group).

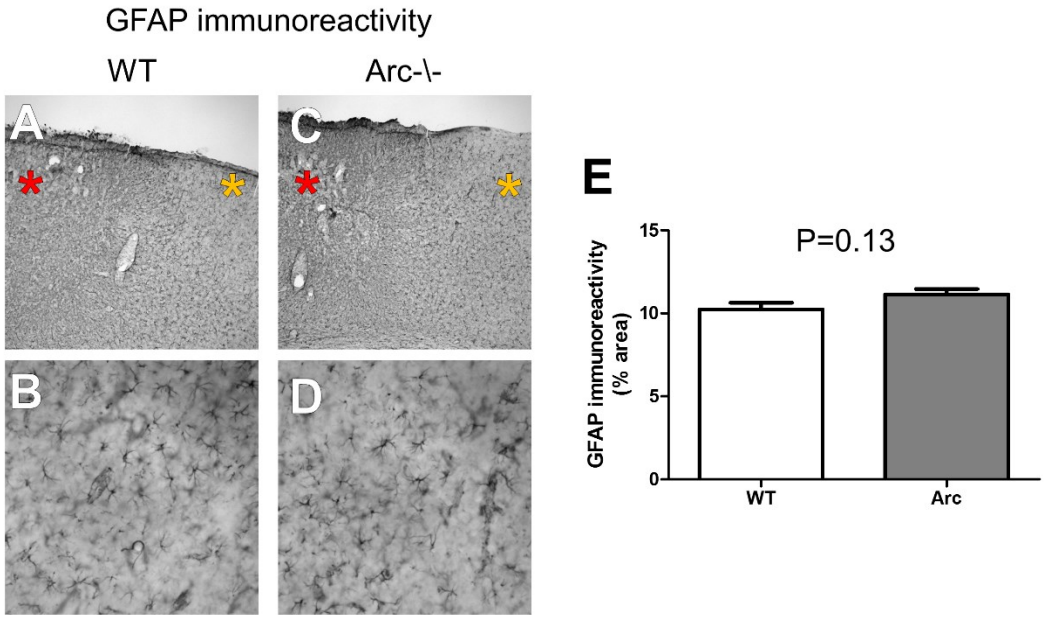

Figure 2.S2. *Arc* gene deletion does not alter perilesional reactive astrocytosis. GFAP immunoreactivity in **(A,B)** WT and **(C,D)** Arc-/- mice 7 days after photothrombosis. **(A,C)** Low magnification view of the infarction (red star) and perilesional territory (orange star). **(B,D)** High power magnification of the perilesional terrirotry. **(E)** Quantification of perilesional GFAP-immunoreactivity demonstrates no difference in astrocytosis between WT and Arc-/- mice.

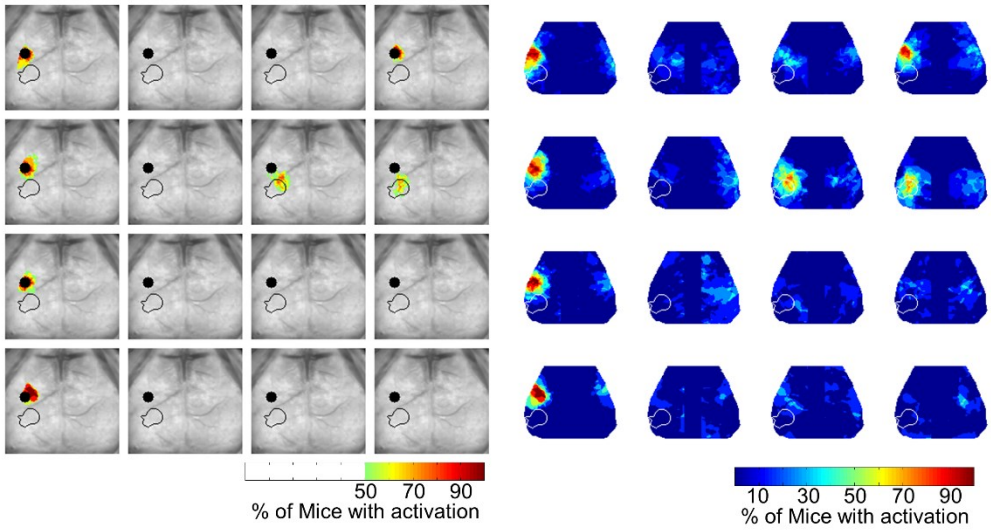

Figure 2.S3. Right S1FP remapping density maps, extended (from Fig. 2.2). **(A)** R. S1FP density maps with a black circle showing the photothrombosis target and black outline showing whisker barrel cortex. **(B)** R. S1FP density maps showing the full range of density values.

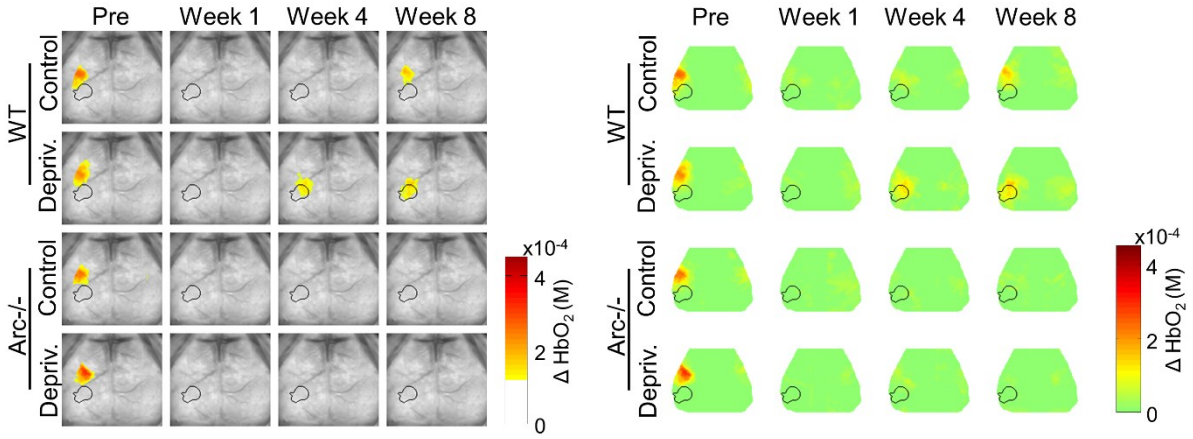

Figure 2.S4. Right S1FP remapping with mean HbO_2 intensity maps (from Fig. 2.2). For each mouse, activation intensity <50% of the maximum amplitude was set to zero. No minimum intensity was required for a response to be considered an activation. The group-averaged response intensity is shown **(A)** overlayed on the brain image with an intensity cut off, and **(B)** without any intensity cut off. Consistent with % activation maps (Figure 2), remapping is seen earlier and within the deprived S1WB in WT Deprived mice. Remapping does not occur in Arc-/- mice. Black outline indicates whisker barrel cortex.

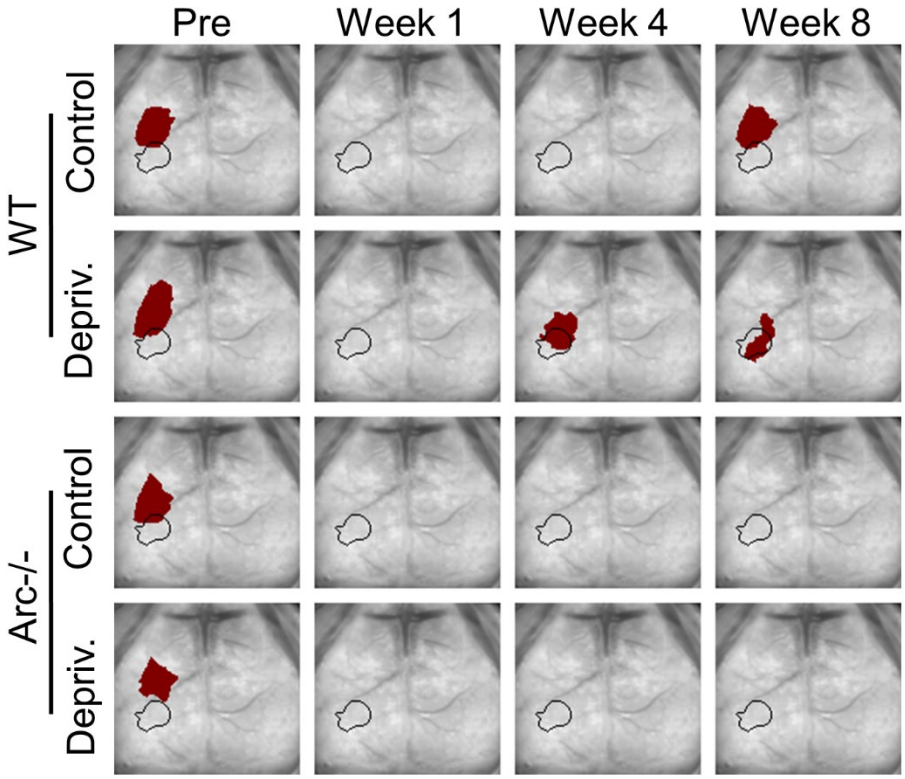

Figure 2.S5. Right S1FP remapping with statistical threshold maps (from Fig. 2.2). Statistical right S1FP evoked maps demonstrate remapping consistent with prior metrics (Figure 2, Figure S1). P values were calculated by comparing oxy-hemoglobin values at baseline and post-activation. Pixel clusters with $P < e^{-10}$ are shown in red. Right S1FP remapping is consistent in maps calculated with this method (see methods). Black outline indicates whisker barrel cortex.

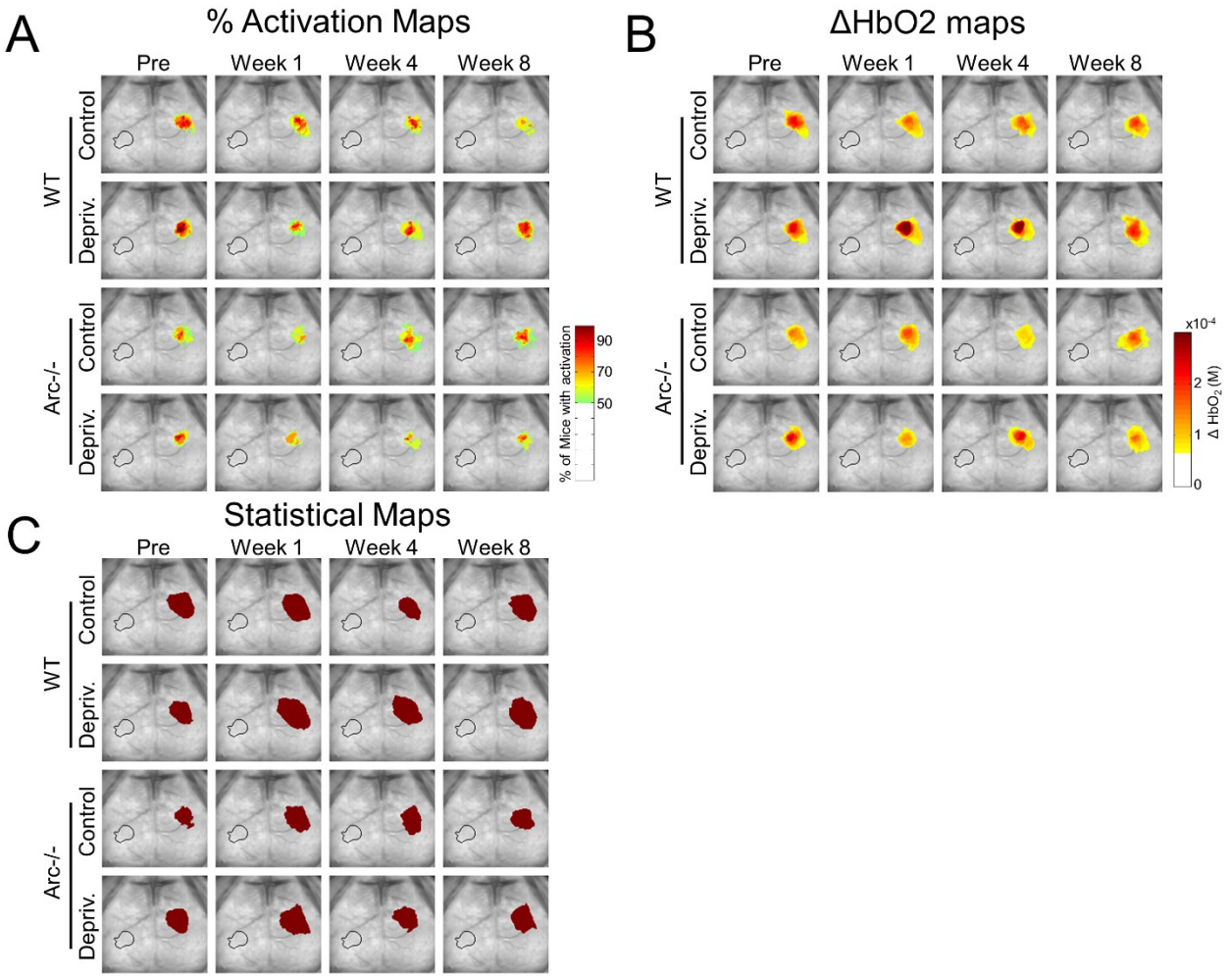

Figure 2.S6. Left S1FP activation remains intact throughout injury and recovery. Complete timecourse of left S1FP evoked maps shown with **(A)** activation density, **(B)** mean intensity **(C)**, and statistical threshold maps. All metrics show consistent Left S1FP maps throughout the recovery timecourse. Black outline indicates whisker barrel cortex.

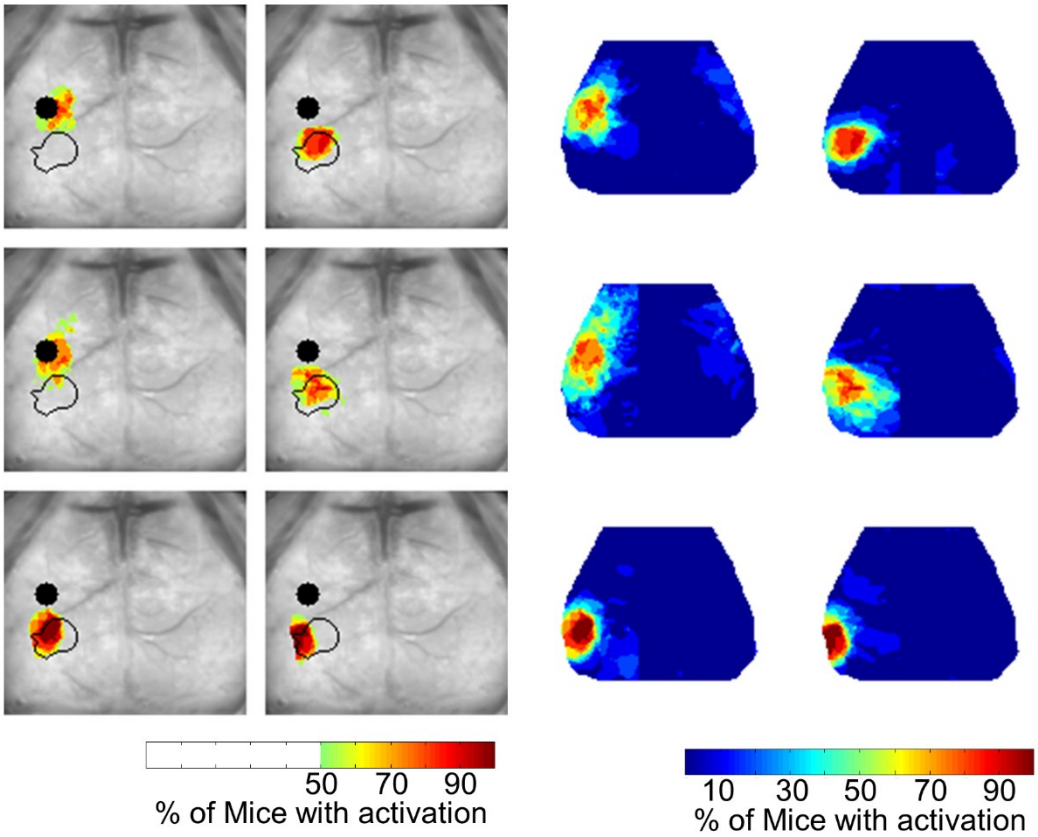

Figure 2.S7. Fig. 2.7 S1 evoked response density maps, extended. **(A)** R. S1FP density maps with a black circle showing the photothrombosis target and black outline indicates whisker barrel cortex. **(B)** R. S1FP density maps showing the full range of density values.

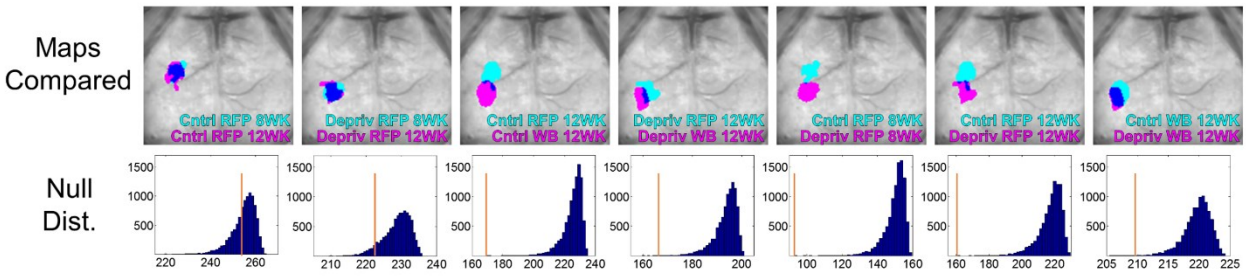

Overlap	253.5531	222.6347	169.1293	166.3151	92.9128	160.7343	209.5685
P value	0.3365	0.0825	$<10^{-4}$	$9x10^{-4}$	$<10^{-4}$	$<10^{-4}$	0.0027

Figure 2.S8. Spatial statistical analysis for Fig. 2.7. The 65% density contour is shown for the listed comparison. A spatial test statistic, termed "Overlap" was calculated from the summed dot products of the two full-range density maps (orange line in "Null Dist." histogram). The null distribution was calculated for each comparison by calculating the Overlap value for 10000 random group combinations. Statistical significance was set at P<0.007 (0.05 / number of comparisons).

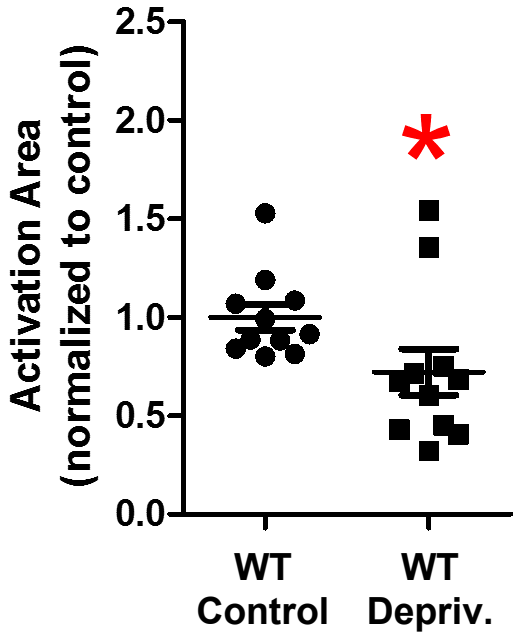

Figure 2.S9. Right S1WB representation area from WT-Control and WT-Depriv groups. Right S1WB activation area for each mouse was defined as the all pixels that were >50% of the maximum response amplitude. S1WB activation are was smaller in WT Depriv. mice compared to WT Control mice. * $P<0.05$, Student's t test.

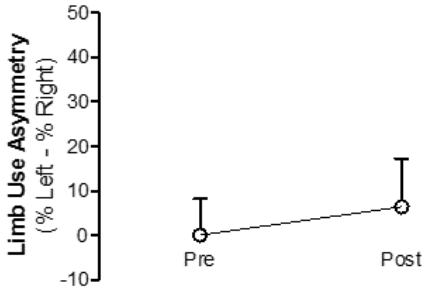

Figure 2.S10. Whisker deprivation does not affect limb use symmetry. Mice were tested with the cylinder rearing test 3 weeks after chronic right whisker trimming. Whisker trimming had no effect on limb use symmetry (P=0.7; n=5 per group).

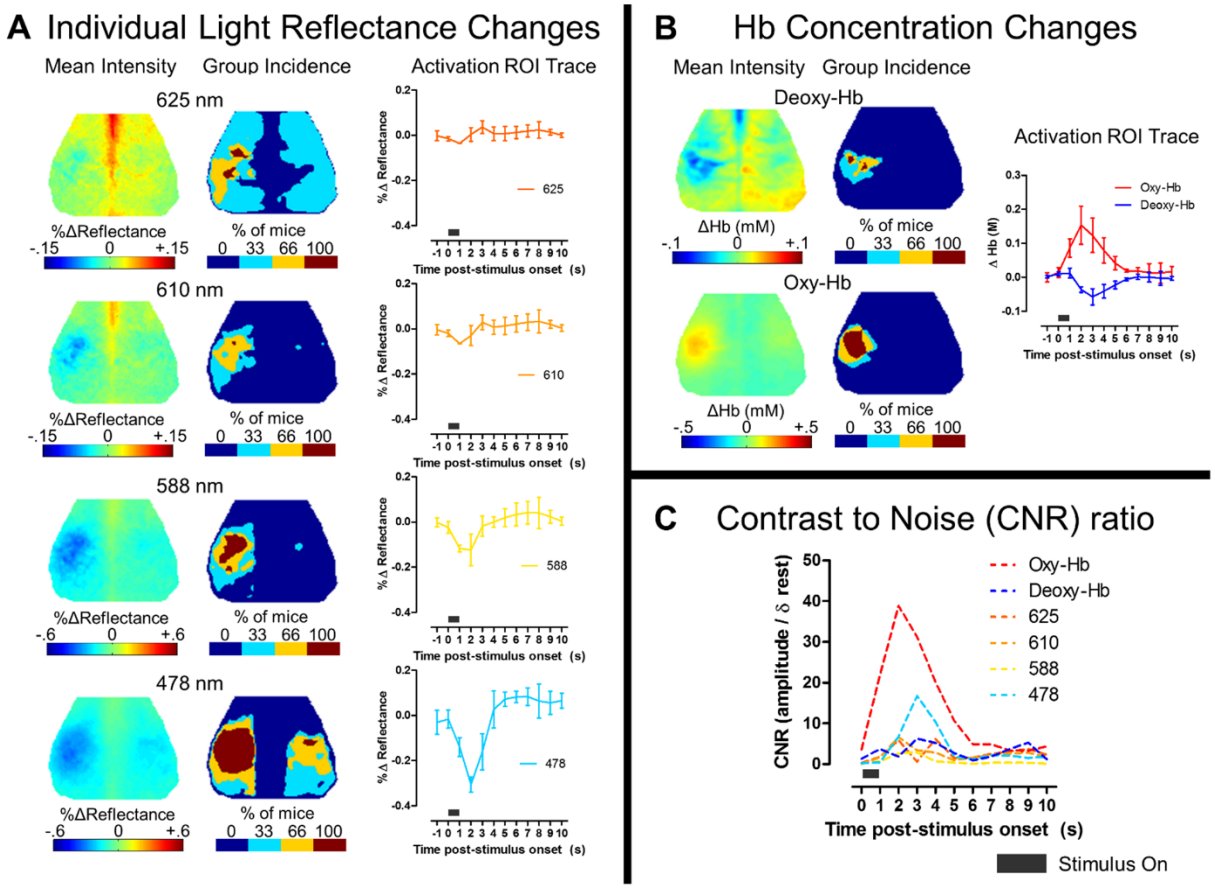

Figure 2.S11. Contrast comparisons for raw light and spectroscopy-derived Hb signals. RFP mapping was performed on 3 mice. **(A)** For each wavelength used, group averaged reflectance changes are shown next two the full-width at half max defined ROI for each mouse. The averaged reflectance time-trace over the ROI is shown. **(B)** Group averaged Hb concentration changes, full-width at half max ROIs, and response time traces are shown for oxy- and deoxy-hemoglobin. **(C)** CNR is shown for each contrast at varying times after stimulus initiation. σ_{rest} was defined from the variance of signals that occurred in the 5 seconds prior to stimulation. The peak CNR is found with oxy-Hb 2 seconds after stimulus onset. In addition, Oxy-Hb shows the most spatial consistency as demonstrated by the ROI maps.

References

1. E. J. Benjamin *et al.*, Heart Disease and Stroke Statistics-2017 Update: A Report From the American Heart Association. *Circulation* **135**, e146-e603 (2017).

2. A. Kertesz, P. McCabe, Recovery patterns and prognosis in aphasia. *Brain* **100 Pt 1**, 1-18 (1977).

3. D. B. Hier, J. Mondlock, L. R. Caplan, Recovery of behavioral abnormalities after right hemisphere stroke. *Neurology* **33**, 345-350 (1983).

4. P. W. Duncan, L. B. Goldstein, D. Matchar, G. W. Divine, J. Feussner, Measurement of motor recovery after stroke. Outcome assessment and sample size requirements. *Stroke* **23**, 1084-1089 (1992).

5. T. H. Murphy, D. Corbett, Plasticity during stroke recovery: from synapse to behaviour. *Nat Rev Neurosci* **10**, 861-872 (2009).

6. S. Li *et al.*, GDF10 is a signal for axonal sprouting and functional recovery after stroke. *Nat Neurosci* **18**, 1737-1745 (2015).

7. A. N. Clarkson, B. S. Huang, S. E. Macisaac, I. Mody, S. T. Carmichael, Reducing excessive GABA-mediated tonic inhibition promotes functional recovery after stroke. *Nature* **468**, 305-309 (2010).

8. S. Li *et al.*, An age-related sprouting transcriptome provides molecular control of axonal sprouting after stroke. *Nat Neurosci* **13**, 1496-1504 (2010).

9. R. J. Nudo, G. W. Milliken, W. M. Jenkins, M. M. Merzenich, Use-dependent alterations of movement representations in primary motor cortex of adult squirrel monkeys. *J Neurosci* **16**, 785-807 (1996).

10. C. Xerri, M. M. Merzenich, B. E. Peterson, W. Jenkins, Plasticity of primary somatosensory cortex paralleling sensorimotor skill recovery from stroke in adult monkeys. *J Neurophysiol* **79**, 2119-2148 (1998).

11. I. R. Winship, T. H. Murphy, In vivo calcium imaging reveals functional rewiring of single somatosensory neurons after stroke. *J Neurosci* **28**, 6592-6606 (2008).

12. C. E. Brown, K. Aminoltejari, H. Erb, I. R. Winship, T. H. Murphy, In vivo voltage-sensitive dye imaging in adult mice reveals that somatosensory maps lost to stroke are replaced over weeks by new structural and functional circuits with prolonged modes of activation within both the peri-infarct zone and distant sites. *J Neurosci* **29**, 1719-1734 (2009).

13. R. M. Dijkhuizen *et al.*, Functional magnetic resonance imaging of reorganization in rat brain after stroke. *Proc Natl Acad Sci U S A* **98**, 12766-12771 (2001).

14. J. A. Jablonka, K. Burnat, O. W. Witte, M. Kossut, Remapping of the somatosensory cortex after a photothrombotic stroke: dynamics of the compensatory reorganization. *Neuroscience* **165**, 90-100 (2010).

15. C. Weiller, F. Chollet, K. J. Friston, R. J. Wise, R. S. Frackowiak, Functional reorganization of the brain in recovery from striatocapsular infarction in man. *Ann Neurol* **31**, 463-472 (1992).

16. S. C. Cramer *et al.*, A functional MRI study of subjects recovered from hemiparetic stroke. *Stroke; a journal of cerebral circulation* **28**, 2518-2527 (1997).

17. H. Reddy, N. De Stefano, M. Mortilla, A. Federico, P. M. Matthews, Functional reorganization of motor cortex increases with greater axonal injury from CADASIL. *Stroke* **33**, 502-508 (2002).

18. R. M. Dijkhuizen *et al.*, Correlation between brain reorganization, ischemic damage, and neurologic status after transient focal cerebral ischemia in rats: a functional magnetic resonance imaging study. *J Neurosci* **23**, 510-517 (2003).

19. K. Fox, Anatomical pathways and molecular mechanisms for plasticity in the barrel cortex. *Neuroscience* **111**, 799-814 (2002).

20. T. K. Hensch, Critical period plasticity in local cortical circuits. *Nat Rev Neurosci* **6**, 877-888 (2005).

21. M. M. Merzenich *et al.*, Somatosensory cortical map changes following digit amputation in adult monkeys. *J Comp Neurol* **224**, 591-605 (1984).

22. K. Korodi, J. Toldi, Does the cortical representation of body parts follow both injury to the related sensory peripheral nerve and its regeneration? *Neuroreport* **9**, 771-774 (1998).

23. S. Glazewski, M. McKenna, M. Jacquin, K. Fox, Experience-dependent depression of vibrissae responses in adolescent rat barrel cortex. *Eur J Neurosci* **10**, 2107-2116 (1998).

24. S. Glazewski, C. M. Chen, A. Silva, K. Fox, Requirement for alpha-CaMKII in experience-dependent plasticity of the barrel cortex. *Science* **272**, 421-423 (1996).

25. N. B. Sawtell *et al.*, NMDA receptor-dependent ocular dominance plasticity in adult visual cortex. *Neuron* **38**, 977-985 (2003).

26. Y. Tagawa, P. O. Kanold, M. Majdan, C. J. Shatz, Multiple periods of functional ocular dominance plasticity in mouse visual cortex. *Nat Neurosci* **8**, 380-388 (2005).

27. E. Korb, S. Finkbeiner, Arc in synaptic plasticity: from gene to behavior. *Trends Neurosci* **34**, 591-598 (2011).

28. K. H. Wang *et al.*, In vivo two-photon imaging reveals a role of arc in enhancing orientation specificity in visual cortex. *Cell* **126**, 389-402 (2006).

29. C. L. McCurry *et al.*, Loss of Arc renders the visual cortex impervious to the effects of sensory experience or deprivation. *Nat Neurosci* **13**, 450-457 (2010).

30. M. Ren, V. Cao, Y. Ye, H. K. Manji, K. H. Wang, Arc regulates experience-dependent persistent firing patterns in frontal cortex. *J Neurosci* **34**, 6583-6595 (2014).

31. N. Plath *et al.*, Arc/Arg3.1 is essential for the consolidation of synaptic plasticity and memories. *Neuron* **52**, 437-444 (2006).

32. S. Chowdhury *et al.*, Arc/Arg3.1 interacts with the endocytic machinery to regulate AMPA receptor trafficking. *Neuron* **52**, 445-459 (2006).

33. H. Okuno *et al.*, Inverse synaptic tagging of inactive synapses via dynamic interaction of Arc/Arg3.1 with CaMKIIbeta. *Cell* **149**, 886-898 (2012).

34. Y. K. Baskin, W. D. Dietrich, E. J. Green, Two effective behavioral tasks for evaluating sensorimotor dysfunction following traumatic brain injury in mice. *J Neurosci Methods* **129**, 87-93 (2003).

35. B. B. Johansson, P. V. Belichenko, Neuronal plasticity and dendritic spines: effect of environmental enrichment on intact and postischemic rat brain. *J Cereb Blood Flow Metab* **22**, 89-96 (2002).

36. S. Zhang, J. Boyd, K. Delaney, T. H. Murphy, Rapid reversible changes in dendritic spine structure in vivo gated by the degree of ischemia. *J Neurosci* **25**, 5333-5338 (2005).

37. C. E. Brown, C. Wong, T. H. Murphy, Rapid morphologic plasticity of peri-infarct dendritic spines after focal ischemic stroke. *Stroke* **39**, 1286-1291 (2008).

38. C. E. Brown, P. Li, J. D. Boyd, K. R. Delaney, T. H. Murphy, Extensive turnover of dendritic spines and vascular remodeling in cortical tissues recovering from stroke. *J Neurosci* **27**, 4101-4109 (2007).

39. F. Wu *et al.*, Urokinase-type plasminogen activator promotes dendritic spine recovery and improves neurological outcome following ischemic stroke. *J Neurosci* **34**, 14219-14232 (2014).

40. D. B. Polley, C. H. Chen-Bee, R. D. Frostig, Two directions of plasticity in the sensory-deprived adult cortex. *Neuron* **24**, 623-637 (1999).

41. S. C. Cramer *et al.*, A functional MRI study of subjects recovered from hemiparetic stroke. *Stroke* **28**, 2518-2527 (1997).

42. T. N. Wiesel, D. H. Hubel, Comparison of the effects of unilateral and bilateral eye closure on cortical unit responses in kittens. *J Neurophysiol* **28**, 1029-1040 (1965).

43. A. Skibinska, S. Glazewski, K. Fox, M. Kossut, Age-dependent response of the mouse barrel cortex to sensory deprivation: a 2-deoxyglucose study. *Exp Brain Res* **132**, 134-138 (2000).

44. S. Glazewski *et al.*, Impaired experience-dependent plasticity in barrel cortex of mice lacking the alpha and delta isoforms of CREB. *Cereb Cortex* **9**, 249-256 (1999).

45. T. A. Woolsey, J. R. Wann, Areal changes in mouse cortical barrels following vibrissal damage at different postnatal ages. *J Comp Neurol* **170**, 53-66 (1976).

46. H. Van der Loos, T. A. Woolsey, Somatosensory cortex: structural alterations following early injury to sense organs. *Science* **179**, 395-398 (1973).

47. S. T. Carmichael, Cellular and molecular mechanisms of neural repair after stroke: making waves. *Ann Neurol* **59**, 735-742 (2006).

48. S. Li, S. T. Carmichael, Growth-associated gene and protein expression in the region of axonal sprouting in the aged brain after stroke. *Neurobiol Dis* **23**, 362-373 (2006).

49. S. T. Carmichael *et al.*, Growth-associated gene expression after stroke: evidence for a growth-promoting region in peri-infarct cortex. *Exp Neurol* **193**, 291-311 (2005).

50. H. J. Marti *et al.*, Hypoxia-induced vascular endothelial growth factor expression precedes neovascularization after cerebral ischemia. *Am J Pathol* **156**, 965-976 (2000).

51. B. Q. Zhao *et al.*, Role of matrix metalloproteinases in delayed cortical responses after stroke. *Nat Med* **12**, 441-445 (2006).

52. E. Taub *et al.*, An operant approach to rehabilitation medicine: overcoming learned nonuse by shaping. *J Exp Anal Behav* **61**, 281-293 (1994).

53. W. H. Miltner, H. Bauder, M. Sommer, C. Dettmers, E. Taub, Effects of constraint-induced movement therapy on patients with chronic motor deficits after stroke: a replication. *Stroke* **30**, 586-592 (1999).

54. S. L. Wolf, D. E. Lecraw, L. A. Barton, B. B. Jann, Forced use of hemiplegic upper extremities to reverse the effect of learned nonuse among chronic stroke and head-injured patients. *Exp Neurol* **104**, 125-132 (1989).

55. E. Korb, C. L. Wilkinson, R. N. Delgado, K. L. Lovero, S. Finkbeiner, Arc in the nucleus regulates PML-dependent GluA1 transcription and homeostatic plasticity. *Nat Neurosci* **16**, 874-883 (2013).

56. A. Holtmaat, L. Wilbrecht, G. W. Knott, E. Welker, K. Svoboda, Experience-dependent and cell-type-specific spine growth in the neocortex. *Nature* **441**, 979-983 (2006).

57. A. Majewska, M. Sur, Motility of dendritic spines in visual cortex in vivo: changes during the critical period and effects of visual deprivation. *Proc Natl Acad Sci U S A* **100**, 16024-16029 (2003).

58. C. L. Peebles *et al.*, Arc regulates spine morphology and maintains network stability in vivo. *Proc Natl Acad Sci U S A* **107**, 18173-18178 (2010).

59. E. Messaoudi *et al.*, Sustained Arc/Arg3.1 synthesis controls long-term potentiation consolidation through regulation of local actin polymerization in the dentate gyrus in vivo. *J Neurosci* **27**, 10445-10455 (2007).

60. T. Tsubota *et al.*, Cofilin1 controls transcolumnar plasticity in dendritic spines in adult barrel cortex. *PLoS Biol* **13**, e1002070 (2015).

61. G. Silasi, D. Xiao, M. P. Vanni, A. C. Chen, T. H. Murphy, Intact skull chronic windows for mesoscopic wide-field imaging in awake mice. *J Neurosci Methods*, (2016).

62. B. R. White *et al.*, Imaging of functional connectivity in the mouse brain. *PLoS One* **6**, e16322 (2011).

63. S. R. Arridge, M. Cope, D. T. Delpy, The theoretical basis for the determination of optical pathlengths in tissue: temporal and frequency analysis. *Phys Med Biol* **37**, 1531-1560 (1992).

64. J. R. Bumstead, A. Q. Bauer, P. W. Wright, J. P. Culver, Cerebral functional connectivity and Mayer waves in mice: Phenomena and separability. *J Cereb Blood Flow Metab* **37**, 471-484 (2017).

65. A. Q. Bauer *et al.*, Optical imaging of disrupted functional connectivity following ischemic stroke in mice. *Neuroimage* **99**, 388-401 (2014).

Chapter 3

Early visual experience modulates spatiotemporal relationships in infra-slow activity between distinct cortical regions through an Arc-dependent mechanism

Preface

This chapter contains a manuscript that is under review:

Kraft A.W. et al. Early visual experience modulates spatiotemporal relationships in infra-slow activity between distinct cortical regions through an Arc-dependent mechanism. Manuscript under review.

Author Contributions for the citation above:

AWK, AQB, JPC, JML designed experiments. AWK collected data. AM, AWK, AQB processed and analyzed data. AQB provided training in imaging. AWK, AM, AZS, JML wrote the manuscript with help from all co-authors. All authors read and approved the final manuscript. JML supervised all aspects of the project.

Abstract

Decades of work in experimental animals has established the importance of visual experience during critical periods for the development of normal sensory-evoked responses in the visual cortex. However, much less is known concerning the impact of early visual experience on the systems-level organization of spontaneous activity. Human resting-state fMRI has revealed that infra-slow fluctuations in spontaneous activity are organized into stereotyped spatiotemporal patterns across the entire brain. Furthermore, the organization of spontaneous infra-slow activity (ISA) is plastic in that it can be modulated by learning and experience, suggesting heightened sensitivity to change during critical periods. Here we used wide-field optical intrinsic signal imaging in mice to examine whole-cortex spontaneous ISA patterns. Using monocular or binocular visual deprivation, we examined the effects of critical period visual experience on the development of ISA correlation and latency patterns within and across cortical resting-state networks. Visual modification with monocular lid suturing reduced correlation between left and right cortices (homotopic correlation) within the visual network, but had little effect on inter-network correlation. In contrast, visual deprivation with binocular lid suturing resulted in increased visual homotopic correlation and increased anti-correlation between the visual network and several extra-visual networks, suggesting cross-modal plasticity. These network-level changes were markedly attenuated in mice with genetic deletion of Arc, a gene known to be critical for activity-dependent synaptic plasticity. Taken together, our results suggest that critical period visual experience induces global changes in spontaneous ISA relationships, both within the visual network and across networks, through an Arc-dependent mechanism.

Introduction

During the visual critical period, neurons within the visual cortex exhibit robust plasticity in response to visual stimuli. Binocular visual input during this period is required for the proper development of normal visual cortex function (1-5). This experience-dependent activity drives a cascade of events leading to the development of mature response properties, such as ocular dominance, orientation selectivity, spatial acuity, and others, to produce normal adult vision (1-11). As first demonstrated by Hubel and Wiesel, binocular and monocular deprivation alter the response of visual cortex neurons to visual stimuli in distinct ways: Binocular deprivation prevents maturation of normal visual responses, causing immature visual responses to be retained; while monocular deprivation induces robust ocular dominance plasticity (ODP), actively depressing deprived eye responses (1, 2, 4-7). These effects have been demonstrated at multiple spatial scales spanning single neuron electrophysiology (4, 6) to entire visual hemi-cortex responses (12-14) in several species including primates, cats, ferrets, rats, and mice (1, 4-8, 12, 13, 15). Moreover, the visual deprivation paradigm has illuminated the molecular mechanisms that drive experience-dependent visual plasticity. However, the outcome measure in almost all prior studies has been limited to visual stimulus-evoked responses within the visual cortex.

Notwithstanding the scientific gains obtained by studying sensory-evoked responses, it is increasingly recognized that spontaneous (intrinsic) neural activity represents a complementary and productive line of investigation (16-18). Spontaneous activity accounts for the majority of brain activity and is thought to play a critical role in brain function (19-21). The brain exhibits spontaneous activity at multiple temporal scales. Spontaneous infra-slow activity (ISA; 0.01-0.1 Hz), while initially regarded as “noise” (22), is now known to reflect properties of whole-brain network organization (23-28). Organized spontaneous activity has been observed using multiple imaging modalities, including resting state functional magnetic resonance imaging (RS-fMRI) and optical imaging, in multiple species, including humans, non-human primates, and rodents

(19, 20, 23, 29-31). More specifically, network organization is observed by patterns of spontaneous ISA correlation (termed functional connectivity, FC) and spontaneous ISA propagation speed between separate brain regions.

Human RS-fMRI studies have shown that the general organization of spontaneous ISA correlation and propagation is quite stable within and across individuals (26, 32). However, sensory experience and learning can modulate spontaneous ISA patterns at the systems-scale. Specifically, motor learning (25, 33), extended Law School Admission Test (LSAT) preparation (34), and early-age blindness (35-38) have all been demonstrated to alter ISA correlation in humans. Moreover, the magnitude of these effects correlated with behavioral measures (33). However, little is known regarding the mechanisms underlying systems-level modulation of spontaneous ISA organization. A leading hypothesis is that experience-dependent ISA modulation reflects “brain plasticity.” It is widely believed that plasticity at the systems level may be driven by mechanisms at the molecular level, especially those involving the modulation of synaptic strengths. However, there has been to date no evidence linking synaptic plasticity mechanisms, which operate on the spatial scale of microns (39), with the systems-scale ISA modulations occurring on the scale of centimeters (25, 33-36).

Of particular interest is that these spontaneous activity changes involve relationships between distinct functional systems, suggesting a paradigm of experience-dependent cross-modal plasticity that operates at the level of spontaneous activity. Although there already exists substantial evidence that visual loss in humans has extra-visual, or cross-modal effects on spontaneous ISA organization throughout the cerebral cortex (35, 36), the role of critical period visual input on whole-cortex spontaneous ISA spatiotemporal organization has not been examined.

In order to understand how critical period visual experience modulates whole-cortex ISA, we utilized functional optical intrinsic signal (fOIS) imaging in mice after binocular deprivation (BD) or

monocular deprivation (MD) during the visual critical period. We subsequently tested the role of synaptic plasticity in systems-level ISA reorganization by applying this paradigm to mice with genetic deletion of activity-dependent cytoskeleton-associated protein (Arc). Several studies performed on a fine-spatial scale have established that Arc is essential for experience-dependent synaptic plasticity, largely through action on glutamate receptors (40-43). However, a role for Arc in systems-level ISA plasticity has not been studied.

Results

Visual deprivation and ISA imaging paradigm

We manipulated visual experience via lid suturing in mice at the beginning of the visual critical period (immediately after weaning at P21). Littermates were subjected to either: 1) binocular lid suturing (i.e., binocular deprivation; BD), 2) monocular right lid suturing (i.e., monocular deprivation; MD), or 3) no lid suturing (Normal Vision; NV). A schematic of the experimental design is depicted in Figure 3.1. After lid suturing, mice were returned to cages with littermates. Two weeks later (P35), fOIS imaging was performed to measure ISA. All mice tolerated the suturing and imaging procedures well without mortality or morbidity.

ISA spatiotemporal organization analysis

As shown in Figure 3.2, we examined two features of the spatiotemporal organization in spontaneous ISA: zero-lag temporal correlations (functional connectivity; FC) and temporal delays (propagation latency). Zero-lag correlations spatially partition the cortex into segregated functional networks known as resting state networks (RSNs) that provide a spatial view of the system-level cortical organization (26, 44, 45). More recent work has shown that ISA also exhibits temporal relationships manifesting as reproducible propagation latency patterns, which can be computed by analyzing temporal delays (24, 25). Figure 2 illustrates how correlation and propagation latency metrics were derived from a sample 20 second epoch of spontaneous ISA

data from a single mouse (Fig. 3.2A). ISA correlation in the present report is described both in terms of left visual-seeded correlation maps (corresponding to right-eye visual manipulation; Fig. 3.2C) as well as RSN-sorted correlation matrices (Fig. 3.2D). Propagation was examined with left visual-seeded latency maps displaying the earliness or lateness of each pixel relative to the left visual area (Fig. 3.2E; described further in methods). Together, these approaches were used to quantify the effects that critical period visual experience had on the correlation and propagation latency patterns in spontaneous cortical ISA.

Visual deprivation alters ISA correlation (functional connectivity)

To determine if visual manipulation during the critical period alters ISA correlation, we examined visual-seeded correlation maps in wild type (WT) mice with normal visual experience (WT-NV), binocular deprivation (WT-BD), and monocular deprivation (WT-MD) at P35 (after 2 weeks of visual deprivation; Fig. 3.3A-C). We chose to examine correlations for each pixel relative to the average signal of all left visual RSN pixels, since MD was applied to the right eye. In all groups, left visual-seeded correlation maps demonstrated high correlation with the right visual cortex and anti-correlation to the more anterior regions, especially on the contralateral hemisphere. Statistical significance of correlation differences between groups was assessed with a spatial cluster-wise basis using threshold-extent criteria computed by extensive permutation resampling (Fig. 3.3, D,E; see Methods for further detail). Comparing WT-BD to WT-NV demonstrated that BD resulted in increased homotopic correlation within the visual RSN (increased correlation between the interhemispheric visual areas) and increased anti-correlation between the visual and anterior areas (Fig. 3.3D). More specifically, these anterior areas included the primary motor (M1) and secondary motor (M2) areas as well as the anterior edge of the cingulate/retrosplenial area (Fig. 3.3D. Many pixels with significantly altered correlation to the left visual area fell just outside of the PCA derived RSNs; according to Paxinos atlas coordinates, the area of increased anti-correlation (blue) was in anterior cingulate cortex (Fig. 3.S1A). MD, on the other hand, resulted in

dramatically decreased homotopic visual correlation (within the visual network), but very little change in extra-visual network correlation (Fig. 3.3E, Fig. 3.S1B), effects in stark contrast to those found with BD.

Interestingly, with both BD and MD there were no changes in correlation between the visual cortices and adjacent brain regions: correlation changes were restricted to longer distance connections. Histograms of visual homotopic correlation values demonstrate that BD and MD were shifted in opposite directions relative to NV: BD enhanced cross-hemispheric visual correlation while MD disrupted it (Fig. 3.3F). Comparing BD to NV using anti-correlation histograms between visual and non-visual pixels showed a dramatic increase in anti-correlation between visual and extra-visual areas (Fig. 3.3G). MD, on the other hand, induced only a small effect on anti-correlation between visual and extra-visual areas (Fig. 3.3G).

To examine ISA correlation changes related to visual manipulation at a more global level, we next created RSN-sorted correlation matrices, similar to that shown in Fig. 3.2D (but using the entire group-averaged data set rather than a sample 20-second epoch). These matrices demonstrated correlation and anti-correlation between networks in all three WT groups (Fig. 3.4A-C). By definition, intra-network correlation (diagonal blocks) was high, with prominent homotopic correlation in most RSNs, as has been shown previously in multiple mammalian species using optical and magnetic resonance imaging modalities (23, 29, 46, 47). Anti-correlation was apparent along the anterior-posterior axis both within and across hemispheres. The overall qualitative topography of correlation patterns was preserved between groups, but there were clear differences in correlation values.

To examine differences quantitatively at the whole-cortex level, we examined the correlation difference (Δcorrelation) matrices calculated by subtracting the WT-BD or WT-MD correlation matrices from the WT-NV correlation matrix (Fig. 3.4D,G). These Δcorrelation matrices highlight the contrasting effects induced by BD and MD. The black outlines in Figure 3.4D and 3.4G, which

highlight the visual RSN, demonstrate the increased visual intra-network homotopic correlation seen in WT-BD vs. WT-NV (red off-diagonal blocks) and the decreased visual intra-network homotopic correlation in WT-MD vs. WT-NT (blue off-diagonal blocks). Outside of the visual RSN, the anterior-posterior inter-network correlation differences had higher magnitude and opposite direction in the WT-BD minus WT-NV Δcorrelation matrix compared to the WT-MD minus WT-NV Δcorrelation matrix. Thus, in alignment with our visual-seeded analysis, the effects of visual deprivation were most pronounced in connections involving the visual areas, with the sign of change for each connection largely opposite in the BD vs. MD groups.

To determine statistical significance of whole-cortex correlation changes in WT with NV, BD, or MD, we computed the Δcorrelation matrix (WT-BD minus WT-NV and WT-MD minus WT-NV) over all pixels in the mouse cortex (instead of the subset of pixels included in the parcellation), and subjected this whole-cortex Δcorrelation matrix to principal component analysis (PCA). True differences in ISA correlation relationships that exist between groups manifest as eigenvectors accounting for variance greater than that expected by chance, as assessed through permutation re-sampling (see Methods for further details). The topography of any statistically significant PC provides a spatial summary of correlation changes between groups (this strategy for assessing correlation differences has been previously applied in (24); see Methods for further details). This approach to statistical significance does not depend on the choice of RSNs as every pixel is included in this PCA approach. Using this method, we found one statistically significant PC (termed a Δcorrelation PC) for the correlation differences between WT-NV vs. WT-BD (Fig. 3.4E). A map of this Δcorrelation PC1 demonstrates a pronounced increase in the posterior cross-hemispheric correlation in addition to anterior-posterior anti-correlation (Fig. 3.4F). This result is consistent with the findings from the visual-seeded correlation analysis (Fig. 3.3D) and the qualitative assessment of the RSN-sorted Δcorrelation matrices (Fig. 3.4 D), which showed increased visual homotopic correlation and increased visual-anterior area anti-correlation. One

statistically significant PC was also found in the WT-NV vs. WT-MD correlation difference (Fig. 3.4H). The corresponding WT-MD vs. WT-NV Δcorrelation PC1 map showed decreases in posterior correlation values and increases in anterior correlation values (Fig. 3.4I). Compared to the WT-BD vs. WT-NV Δcorrelation PC1 (Fig. 3.4F), the WT-MD vs. WT-NV Δcorrelation PC1 showed changes of opposite direction, albeit with much lower magnitude.

Visual deprivation does not alter ISA correlation in Arc-/- mice

The previous experiments established an experimental model for experience-dependent ISA correlation plasticity in mice. To examine the role of synaptic plasticity in vision-mediated ISA changes, we used the same visual deprivation paradigm in Arc-/- mice. It is important to note that Arc-/- mice are viable, fertile, and have normal anatomy and growth curves. Furthermore, Arc-/- mice have normal LGN anatomy and visual cortex retinotopy (48), and cortical neuron membrane excitability is not altered (49). Additionally, Arc-/- mice have pre-critical period visual evoked potentials that are identical to those found in WT (48). While the visual system in pre-critical period Arc-/- mice appears normal, profound experience-dependent changes that occur during or after the critical period are absent or attenuated: In Arc-/- mice ODP plasticity was absent after monocular deprivation (48), selective responses potentiation did not occur with repeated visual presentation (48), and visual orientation learning was attenuated in adult Arc-/- mice (50). Taken together, these results suggest that experience-dependent processes that are attenuated in Arc-/- mice are not attributable to developmental aberrations that disrupt basic visual functionality, but the specific action of Arc on experience-driven synaptic change.

Prior to any correlation analysis, we examined ISA spectral content in Arc-/- groups. We found that ISA power was equivalent between all WT and Arc-/- groups, demonstrating equal amounts of spontaneous ISA was present in all groups (Fig. 3.S2). Left visual-seeded correlation maps in all Arc-/- groups exhibit the same features as those seen in WT mice: homotopic visual

correlations and posterior-anterior anti-correlation (Fig. 3.5A-C). However, in stark contrast to the WT mice, the correlation maps appeared nearly identical across Arc-NV, Arc-BD, and Arc-MD mice. Cluster-analysis revealed no statistically significant differences in left-visual seeded correlation maps between Arc-BD and Arc-NV (Fig. 3.5D) or Arc-MD and Arc-NV (Fig. 3.5E). Furthermore, the correlation histograms for both visual-visual and visual-non-visual connection showed no statistically significant group differences (Fig. 3.5F,G).

At the whole-cortex level, RSN-sorted correlation matrices were very similar between all 3 Arc-/- groups (Fig. 3.6A-C). Examination of the Δcorrelation matrices from Arc-BD minus Arc-NV and Arc-MD minus Arc-NV comparisons demonstrated markedly attenuated ISA correlation differences compared to those seen in WT mice (Fig. 3.6D,F). Furthermore, PCA revealed no statistically significant Δcorrelation PCs for Arc-BD minus Arc-NV or Arc-MD minus Arc-NV (Fig. 3.6E,G). Taken together these results establish the role of Arc mediated synaptic plasticity in experience-dependent ISA correlation plasticity. Moreover, these Arc-mediated changes in ISA correlation were not confined to the visual network, but manifested between distant networks as seen with BD manipulation.

Visual deprivation alters ISA propagation latency

Recent work in humans has demonstrated reproducible patterns of ISA propagation latency within and between brain regions (24, 25). Propagation latency can be quantified by calculating temporal delays between spontaneous activity measured at pixel pairs. Like ISA correlation, ISA propagation latency patterns can be modified by experience (25). To determine how early visual experience influences propagation latency patterns, we examined ISA propagation latency over the whole-cortex relative to visual activity in our WT and Arc-/- mice (Fig. 3.7). The methodology for computing these propagation latency maps has been previously described ((24, 25); see Methods). In brief, we compute the activity correlation curve between every pair of pixels in mouse cortex. The time corresponding to the peak of the latency correlation curve is the propagation

delay (or latency) between the pair of signals. We can thereby calculate a latency value for every pair of pixels in the mouse cortex. As with our correlation analysis, we chose to examine latencies for each pixel relative to the average signal of all left visual RSN pixels, and used this analysis to produce a left visual-seeded latency map for each experimental group (Fig. 3.7A-F).

Examination of the visual-seeded latency maps revealed common features between all WT and Arc-/- groups. Latency maps in both genotypes and all visual deprivation conditions were roughly symmetrical and showed common early (blue) and late (red) areas. In all groups, visual area activity was early relative to motor area activity, consistent with fMRI data from sleeping humans (24). However, quantitative group differences were apparent. To determine which changes after visual deprivation (BD and MD) were statistically significant, we applied spatial cluster-wise threshold-extent criteria to the relevant within-genotype Δlatency maps (Fig. 3.7G-J).

Compared to WT-NV, both WT-BD and WT-MD showed widespread changes in propagation latency. More specifically, BD resulted in elongated propagation time from motor to visual areas and visual to cingulate/retrosplenial areas; motor area activity occurred earlier (blue) and cingulate/retrosplenial area activity occurred later in WT-BD mice compared to WT-NV mice. Latency change occurred at the anterior edge of cingulate/retrosplenial RSN, in a region we identify as centered in the cingulate, using the same logic as in Figure 3.3 (see also Fig. 3.S1C,D). Propagation latency was altered in distinct locations within the visual area (Fig. 3.7G). Similarly, MD in WT mice resulted in slowing of motor-visual-cingulate signal propagation. However, changes within the visual area resulting from MD were exclusive to the left hemisphere (contralateral to the deprived eye) and included slowed propagation to the adjacent sensory area and lateral extra visual area (Fig. 3.7H). In sum, BD and MD resulted in cross-modal ISA propagation latency changes between visual and extra-visual areas separated by both short and long cortical distances.

In the Arc-/- groups, Δlatency maps thresholded for statistical significance revealed markedly attenuated changes attributable to visual deprivation (Fig. 3.7I,J). Nonetheless, a subset of the latency changes that occurred in WT mice were also found in the absence of Arc, but Δlatency magnitude within these clusters was attenuated in the Arc-/- groups. Compared to Arc-NV mice, Arc-BD demonstrated propagation slowing within the visual RNS bilaterally but lacked the motor and cingulate latency increases seen in WT mice (Fig. 3.7I). Furthermore, Arc-MD mice showed the same unilateral latency changes near the visual area seen in WT-MD, but the motor and cingulate area latency changes were absent (Fig. 3.7J). Thus, experience-dependent ISA propagation plasticity was attenuated but not completely absent in Arc-/- mice. The cross-modal latency changes that occurred adjacent to the left visual RSN in WT mice were present in the Arc-/- mice, but more distant latency effects of visual deprivation were not observed.

Discussion

The effects of critical period visual experience on sensory-evoked neuronal and microcircuit responses in the visual cortex have been well-characterized; however, its impact on whole-cortex spontaneous ISA correlation and propagation patterns has not been examined. In this study, we utilized wide-field optical imaging in mice, experimentally manipulating visual experience during the critical period, to examine effects on network-scale ISA plasticity. We found that BD and MD induced distinct effects on intra- and inter-network spontaneous ISA correlation and propagation. Moreover, we found that these effects were attenuated in Arc-/- mice.

Binocular visual deprivation alters intra- and inter-network relationships in spontaneous ISA correlation

In WT mice, BD enhanced spontaneous ISA correlation across hemispheres within the visual RSNs. Work in experimental animals has shown that complete visual deprivation stalls the critical period, preventing the development of mature response features (1, 2, 4, 6-8, 11, 15). We were surprised to find that BD increased homotopic visual functional connectivity, given that decreased

ISA correlation generally is a reliable biomarker of CNS disease (51-53). Rather, these findings suggest that normal visual development results in “functional pruning” that tunes correlation in spontaneous activity between homotopic visual hemi-cortices to a specific range.

At the level of individual neurons, BD is known to impair the maturation of feature detection (4, 5, 7, 8). During normal development, visual cortex neurons become more selective, for both receptive fields and specific features, the differences encoded in individual visual cortex neurons may become increasingly divergent. With each visual hemi-cortex being largely monocular in mice, normal visual disparity between separate visual fields may result in decreased visual homotopic correlation.

In addition to altering visual intra-network correlation, we found that BD altered inter-network correlation between visual and extra-visual networks. We observed enhanced anti-correlation between visual areas and cingulate/retrosplenial as well as contralateral motor cortex. Thus, we infer that visual experience influences cross-modal connectivity between visual and extra-visual regions.

The concept of cross-modal plasticity was initially suggested by the observation that blind or deaf individuals have heightened auditory or visual perception, respectively (54-56). Although these findings are currently debated, it is clear that loss a single sensory modality alters anatomical and functional relationships between distinct brain systems (35, 36, 54-58). Cross-modal plasticity has been demonstrated by physiologic and molecular assays in humans (35, 36), cats (59), rodents (57), and even *C. Elegans* (60), which suggests it is a generalizable property of the nervous system. We suggest that enhanced inter-network correlation of ISA observed after BD (between visual, cingulate, and motor networks) may be a signature of cross-modal plasticity.

In experimental animals, visual deprivation results in enhanced axonal sprouting between the deprived visual area and surrounding auditory and somatosensory areas (59, 61-63). In addition to anatomic change, cross-modal plasticity also involves homeostatic plasticity mechanisms that

drive alterations in synaptic strength. Enhanced evoked responses to auditory and tactile stimuli have been reported in mice within days of deprivation (57, 64). Congenitally blind humans exhibit widespread changes in ISA correlation in multiple networks (35, 36), suggesting that cross-modal plasticity involves altered spontaneous activity relationships over long distances. Caution may be appropriate in the interpretation of these human studies as they may be confounded by heterogeneous pathologic etiologies (35, 36). Moreover, Braille experience is common in blind individuals (35), and it has been argued that decades of Braille use may drive these changes (37, 38). Our results suggest that these cross-network changes in ISA correlation can occur rapidly during the critical period (over 2 weeks in this study), and do not require lifetime use of an adaptive behavior. In this regard, it may be noted that enhanced cross-modal somatosensory performance has been reported in sighted humans following only 5 days of blindfolding (65). It is interesting to speculate that these rapid changes may precede and even facilitate the development of adaptive behaviors. Future studies will be required to understand the consequences of these internetwork changes.

Monocular visual deprivation induces intra-network change in spontaneous ISA correlation opposite to those seen with binocular deprivation

MD induces ocular dominance plasticity, which depresses the deprived eye responses and strengthens the spared eye responses (4, 6, 15, 66, 67). While the binocular zone is limited in mice, the deprived monocular zone undergoes visual response depression (67). This process manifests physiologically as changes in the visual response amplitude ratio between the spared and deprived eye (1, 2, 4-7, 15, 66, 67). In this study, we find that MD induces diminished homotopic visual correlation.

The opposed effects of BD vs. MD (compared to normal vision) suggest that the correlation of spontaneous ISA between visual hemi-cortices matches sensory input. Indeed, MD causes more sensory discordance between each hemisphere than either BD or NV. Moreover, previous work

using MD has shown that interhemispheric inhibition through callosal inputs weakens deprived eye evoked responses (68). Hypothetically, the interhemispheric inhibition provided by transcallosal connections may also contribute to the “functional pruning” that tunes ISA correlation between the visual hemi-cortices.

Modest correlation changes between visual and extra-visual areas were observed after MD. However, these changes were spatially limited and of lesser magnitude to those seen after BD. Thus, the MD-induced changes appear to be much more concentrated within the visual system. Since MD alters visual experience while BD “eliminates” visual experience, it is not surprising that extra-visual changes in ISA are less affected than in BD. However, it remains unclear why the extra-visual changes that do occur in MD mice tend towards the direction opposite to those in BD. These differences are likely to stem from the distinction between a brain that is rewiring visual-motor circuits to adapt to altered vision (MD), as opposed to the adaptations necessary to achieve motor coordination in the absence of vision (BD).

ISA propagation latency plasticity is distinct but overlaps with ISA correlation plasticity

In addition to spatial correlation relationships, experience has been shown to alter propagation latency patterns in ISA (25). Indeed, our data demonstrate that visual experience influences ISA propagation latencies in many of the same regions showing altered correlation. In mice with NV, our visual-referenced latency maps demonstrate early visual activity and late motor activity (Fig. 3.7A), a hallmark of human activity propagation during sleep (24). Following either BD or MD, motor activity was early-shifted while cingulate area activity was delayed (Fig. 3.7A-C,D,H). These effects may reflect disruption of the visual-cingulate-motor circuit following visual deprivation.

The most prominent disparity in propagation latency plasticity induced by BD vs. MD was observed near the visual RSN: in MD, these changes occurred only in the deprived hemisphere, while, in BD, these changes occurred in both hemispheres (both of which were deprived). The contrasting differences seen in correlation versus propagation change demonstrate the distinct

nature of these ISA features. Propagation latency changes induced by BD vs. MD were quite similar in areas distant from the visual cortex. In contrast, the correlation changes induced by BD vs. MD were distinct, suggesting that propagation latency and correlation patterns reflect different aspects of cross-modal communication between functional systems.

These results suggest that visual area relationships with both motor and cingulate/retrosplenial regions appear especially sensitive to visual deprivation; similar findings have been observed in early blind humans (35). Previous work has demonstrated that rodent cingulate cortex has reciprocal connections with the visual area and projects to motor areas (69, 70). In addition, visual stimulation can elicit evoked responses in the cingulate cortex (71), and direct electrical stimulation of cingulate cortex can elicit movement (72-74). Thus, converging evidence suggests that the cingulate cortex plays a role in integrating sensory information to generate behavioral outputs. Accordingly, we speculate that altered ISA relationships between visual and cingulate/retrosplenial cortex in BD mice reflects reorganization of the brain in the absence of visual input.

More broadly, our findings extend the principle, previously articulated in human studies, that the organization of spontaneous ISA is subject to experience-dependent plasticity. Several examples of this phenomenon have been described in humans: the correlation and propagation structures of the BOLD signal are known to be altered after motor learning (25, 28, 75, 76). Correlation changes have been reported in the context of exam preparation (34) as well as lifelong absence of vision (35, 36). The present results, obtained on the basis of fOIS imaging of mouse cortex, demonstrate that visual experience during the mouse critical period also induces marked changes in the correlation and propagation structure of spontaneous ISA. Therefore, although the molecular basis of experience-dependent plasticity in the organization of spontaneous ISA remains unexplored in humans, the present paradigm offers an opportunity to probe the molecular bases of this re-organization in the mouse.

Arc-dependence of spontaneous ISA plasticity

All of the changes in correlation induced by visual manipulation (intra-network changes in MD, and inter-network changes in BD) were absent in Arc-/- mice. Similarly, changes in propagation latency were largely attenuated in Arc-/- mice. These results suggest that Arc expression is required for experience-dependent changes in spontaneous activity correlation and propagation patterns that occur during the visual critical period.

Previous work has shown that visually-evoked responses in Arc-/- mice are identical to WT mice prior to the critical period, but Arc-/- failed to undergo experience-dependent changes elicited by visual experience. More specifically, Arc-/- mice did not exhibit ocular dominance plasticity with visual deprivation or stimulus-selective response potentiation after repeated visual presentations (48). A role for Arc in experience-dependent plasticity has been demonstrated more broadly in additional settings: adult Arc-/- mice have attenuated visual orientation learning with repeated orientation presentation (50); Arc-/- mice have profound deficits in memory consolidation, and brain slices from Arc-/- mice show attenuated LTP and LTD (77).

Several studies have implicated Arc as a key regulator of structural, Hebbian, and homeostatic synaptic plasticity (39). More specifically, Arc has been shown to influence dendritic spine dynamics, LTP and LTD durability, as well as whole-neuron synaptic scaling. The best understood mechanism by which Arc influences plasticity concerns its regulation of synaptic strength via control of glutamate receptors. Arc regulates glutamate receptor levels at multiple scales, from individual synapses to the entire neuron (40-43). At the individual synapse level, Arc has been shown to target silent dendrites during activation of adjacent dendrites in the same neuron (42). Through this mechanism, Arc facilitates the selective removal of silent synapses. In addition, Arc has been shown to translocate to the nucleus and initiate whole-neuron decreases in glutamate receptor production, enabling scaling of synaptic strength throughout the entire neuron (41, 43).

Given the profound control that Arc exerts on synaptic strength, it is reasonable to hypothesize that Arc has a role in maintaining systems-level organization of the brain by modulating synaptic strength between distinct brain systems. In accordance with this view, our experiments demonstrate that Arc-/- mice fail to exhibit the changes in the systems-level organization of spontaneous ISA that normally occur during the visual critical period. We were surprised that visual deprivation in Arc-/- mice modulated the short-distance temporal ISA patterns, but not the longer-distance correlation or temporal relationships that occurred in WT mice. Thus, Arc, which is capable of selective synapses removal on the basis of activity, may be especially important in regulating both the inter-hemispheric connections within the visual network and the long-distance, cross-modal connections between visual and extra-visual modalities. Indeed, it is well known that Arc acts locally within the visual system for vision-induced plasticity (48, 50). However, there must exists additional mechanisms that drive deprivation-induced ISA latency change within and near the visual system.

Importantly, prior studies have shown that Arc gene deletion does not alter growth curves, visual system anatomy, visual cortex retinotopic maps, visual evoked potentials, or cortical neuron membrane excitability (48-50). Thus, the experience-dependent processes that were attenuated in Arc-/- mice are not attributable to disrupted basic visual functionality, but to specific action of Arc on experience-driven synaptic change. Similarly, we show here that WT and Arc-/- mice exhibit equivalent ISA spectral content, demonstrating that spontaneous brain activity was equally abundant in both WT and Arc-/- mice (Fig. 3.S2), but the reorganization of ISA spatiotemporal organization was attenuated in the absence of Arc.

To conclude, our results demonstrate that critical period visual experience dramatically alters correlation and propagation latency patterns in spontaneous neural activity, both within and outside the visual cortex. Widespread alterations in neural activity after such a dramatic intervention are not surprising: a mouse with intact vision must interact with its environment very

differently compared to a mouse without any vision (BD), or a mouse with limited vision (MD). Different experience-dependent activity patterns (normal vision vs. BD vs. MD) induce the brain to converge on distinct systems-wide patterns of neural communication, as reflected by the organization of spontaneous ISA. The process of transducing experience-dependent activity patterns into altered functional organization undoubtedly requires synaptic plasticity, and our results imply that Arc-dependent mechanisms play a role in this process. It is plausible that the local activities of Arc at the single synapse and whole-neuron level are sufficient to coordinate systems-wide re-organization on the basis of coordinated experience-dependent activity. Future studies are required to investigate these possibilities. Nonetheless, despite these mechanistic uncertainties, our results clearly establish that Arc-mediated molecular plasticity mechanisms, previously studied at a fine spatial scale, are also relevant for understanding the re-organization of neural activity at a systems-level.

Limitations

All imaging performed in this study was done under ketamine/xylazine anesthesia. While anesthesia alters spontaneous neural activity, recent work in mice has shown that cortical correlations in slow activity are quite stable across wake and ketamine/xylazine anesthesia states (78). This is in agreement with data showing stability of low frequency correlation across states of consciousness in humans (79). Moreover, although the slow wave phenomenon was first reported in the context of anesthesia and slow wave sleep (80, 81), recent work has also shown that slow wave propagation is also present in awake rodents (82). Thus, in light of the work showing stability in low frequency correlations and propagation across states, it is very likely that the main findings of the paper are not driven by state effects.

Methods

Mice

All procedures described below were approved by the Washington University Animal Studies Committee in compliance with AAALAC guidelines. Male and female Arc+/+ and Arc-/- mice (RRID:IMSR_JAX:007662) on a pure C57Bl6/J background were raised in standard cages in a dedicated mouse facility with a 12-12 light/dark cycle. Pups were weaned at P21 and immediately subjected to suturing.

Lid Suture

Mice from the same litter were randomly assigned to right monocular lid suture, binocular lid suture, or no suturing (normal vision) P21 mice were anesthetized using isofluorane until unresponsive to toe pinch. Lid margins were trimmed using fine surgical scissors and sutured shut. Normal vision mice were subjected to equal lengths of anesthesia. After suturing, mice were kept in standard cages with 4-5 mice total in a semi-clean facility with a 12 - 12 light/dark cycle until P35.

Imaging animal prep

In accord with our previously published animal preparation protocol for fcOIS imaging (29), anesthesia was initiated via i.p. injection with a bolus of ketamine-xylazine (1x dose: 86.9 mg/kg ketamine, 13.4 mg/kg xylazine) and animals were allowed 15 minutes for anesthetic transition. After induction, the animal was placed on a heating pad maintained at 37°C via feedback from a rectal probe (mTCII, Cell Microcontrols) and its head secured in a stereotactic frame. The head

was shaved and cleaned, a midline incision was made along the top of the head to reflect the scalp and the skull was kept intact.

Image acquisition

Sequential illumination was provided at four wavelengths by a ring of light emitting diodes (LEDs) placed approximately 10 cm above the mouse's head. The field of view included most of the cerebral cortex (approximately $1cm^2$). Diffuse reflected light was detected by a cooled, frame-transfer EMCCD camera (iXon 897, Andor Technologies); the LED ring and the camera were time-synchronized and controlled via computer using custom-written software (MATLAB, Mathworks) at a full frame rate of 30 Hz.

Image Processing

Data from all mice were subjected to an initial quality check prior to spectroscopic analysis. Data runs (5 minutes) in which reflected light level intensity (mean value over the brain) varied as a function of time by greater than 1% for any wavelength were excluded from further analysis. This preliminary quality control yielded 10–30 minutes of data per mouse. For subsequent analysis, image light intensity at each wavelength was interpreted using the Modified Beer-Lambert Law, usually expressed as: $\Phi(\mathbf{r},t) = \Phi_0 * \exp(-\Delta\mu_a(\mathbf{r},t) * L)$. Here, $\Phi(\mathbf{r},t)$ is the measured light intensity, Φ_0 is the baseline light intensity, $\Delta\mu_a(\mathbf{r}, t)$ is the change in absorption coefficient due to hemodynamic changes, and L is the optical path length factor for photons in the tissue (83). As there is no pre-stimulus baseline in resting-state experimentation, we normalized relative to the average light intensity at each pixel, resulting in differential measures of absorption at each

wavelength at each pixel: $\Delta\mu_{a,\lambda}(\mathbf{r},t) = -\ln(\Phi_\lambda(\mathbf{r},t)/< \Phi_{0\lambda}(\mathbf{r},t)>)/L_\lambda$. Absorption coefficient data were converted to hemoglobin (Hb) concentration changes by inverting the system of equations, $\Delta\mu_{a,\lambda}(\mathbf{r},t) = E_{\lambda,i}\,\Delta[Hb_i](\mathbf{r},t)$ (where E is the extinction coefficient matrix, and *i* runs over hemoglobin species). This inversion was performed using least-squares methods, yielding changes in oxygenated hemoglobin (HbO) and deoxygenated hemoglobin (HbR) at each pixel at each time point. Differential changes in hemoglobin concentration were filtered to retain the infra-slow activity/functional connectivity band (0.009–0.08 Hz) following previous human functional connectivity algorithms (23). After filtering, each pixel's time series was downsampled from 30 Hz to 1 Hz, and all further analysis was performed only on those pixels labeled as brain using a manually-constructed brain mask. The time traces of all pixels defined as brain were averaged to create a global brain signal. This global signal was regressed from every pixel's time trace to remove global sources of variance; global signal regression was applied independently on each contiguous imaging session. Finally, data from some imaging sessions exhibited strongly oscillatory activity in the 0.04-0.08 Hz range, which that likely reflects vascular (not neural) physiology (84). Since the spectral content of the BOLD signal is known to be roughly "1/f" (85), we excluded runs in which 50% of the power of the filtered, regressed data was found above 0.04 Hz. This quality control step excludes data strongly contaminated by oscillatory vascular artifact.

Image Co-registration

Image sequences of each mouse (as well as the brain mask for each mouse) were affine-transformed to a common atlas space determined by the positions of the junction between the coronal suture and sagittal suture (posterior to the olfactory bulb and cerebrum along midline) and lambda, as previously reported (86). Bregma was not visible in all mice, and was calculated based on the above two anatomical landmarks. The anterior-posterior stretch was set equal to the

medial-lateral stretch, and all transformed images were centered at bregma. The intersection of every brain mask was calculated and made symmetric by reflection across the midline allowing all subsequent comparisons to be performed on shared brain areas across all mice.

ISA correlation (functional connectivity) analysis

Conventional (zero-lag) functional connectivity was computed using Pearson correlation on pairs of pixel time series. In figures depicting correlation matrices, for ease of display, we show only pixels corresponding to six RSNs inferred through principal components analysis (PCA) parcellation method of the fOIS neuroimaging data from this study (Fig. 3.2B) that has been used to define RSNs previously (87). Network names were assigned to PCA topographies on the basis of colocalization with Paxinos coordinates (29, 88). Note that network sorting of pixels is applied for visualization only. All analyses of the full correlation matrix were computed over all pixels in the brain.

ISA propagation latency analysis

Our method for computing propagation latency between time series has been previously published (24, 25). In brief, we determine temporal propagation latency by computing lagged cross-covariance functions:

$$C_{x_1x_2}(\tau) = \frac{1}{T}\int x_1(t+\tau)\cdot x_2(t)dt, \qquad \text{[E1]}$$

where τ is the latency (in units of time). The value of τ at which $C_{x_1x_2}(\tau)$ exhibits an extremum defines the temporal latency (equivalently, delay) between signals x_1 and x_2 (89). Although cross-

covariance functions can exhibit multiple extrema in the analysis of periodic signals, BOLD time series are aperiodic (85, 90), and almost always give rise to lagged cross-covariance functions with a single, well defined extremum, typically in the range ± 1 sec (24). We determine the extremum abscissa and ordinate using parabolic interpolation (25).

Here, we compute delays between the time-series and each pixel and the mean time-series extracted from a left visual cortex area of interest. This set of temporal delays defines a left-visual seeded propagation latency map.

Statistics

To assess the topography of pair-wise correlation changes across conditions, we computed the difference correlation matrices, and applied spatial principal components analysis to the difference matrix. Permutation re-sampling between groups was used to determine the amount of variance expected in the first eigenvalue of the PCA decomposition in the null case. Eigenvalues in the true eigenspectrum exceeding the null expectation by 2.5 standard deviations ($p < 0.05$; red line Figs. 3, 5, 6) are counted as statistically significant. Statistical significance of propagation sequence differences in spatial maps (Figs. 4-6) was assessed on a cluster-wise basis using threshold-extent criteria computed by extensive permutation resampling (91, 92).

Data and Code Availability

All presented data and analysis algorithms are available upon request.

Acknowledgements

This work was supported in part by National Institutes of Health grants R01NS084028 (J.-M.L), F31NS089135 (A.W.K), R01NS078223 (J.P.C.), P01NS080675 (J.P.C.), P30NS048056 (A.Z.S.),

NS080675 (M.E.R. and A.Z.S.), K25NS083754 (A.Q.B), F30MH106253 (A.M.) and American Heart Association grants 13POST14240023 (A.Q.B) and 14PRE18410013 (A.W.K).

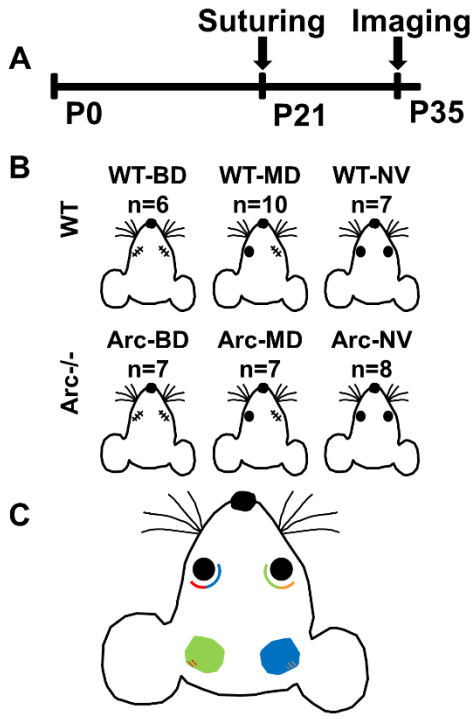

Figure 3.1: Visual deprivation paradigm. **(A)** Experimental timeline for eyelid suturing and imaging. **(B)** Genotypes and deprivation groups used in this study: wildtype (WT), Arc gene deletion (Arc-/-), binocular visual deprivation (BD), monocular visual deprivation (MD). **(C)** Cartoon of mouse visual anatomy highlighting monocular (solid) and binocular areas (striped).

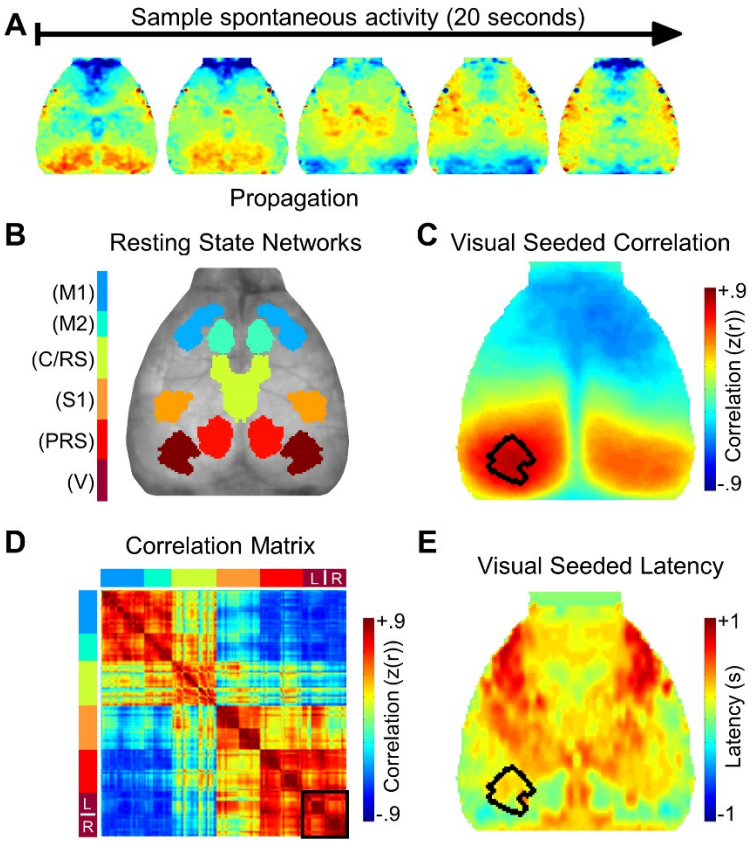

Figure 3.2: Analysis of ISA correlation and propagation patterns for 20 seconds of data from a single mouse. **(A)** Frames from a sample movie showing 20 seconds of spontaneous ISA from a single mouse. In this example, activity propagates from the posterior to anterior regions. Note that although ISA fluctuates over 10-100's of seconds, propagation occurs more quickly (~2 seconds in this example). Correlation between separate regions over the entire 20 seconds is present and especially apparent between homotopic interhemispheric regions throughout the cortex **(B)** Resting state network (RSN) parcellation of mouse cortex on the basis of principal components analysis of group-level correlation structure (see Methods). **(C)** Left visual-seeded correlation map from the sample data shows high correlation between left and right visual areas along with anti-correlation between the left visual and anterior regions. **(D)** Correlation matrix showing the correlation value for every pixel-pair in the cortex from the sample ISA in A, organized by RSNs produced from (B, color-coded on right). Within each RSN, left hemisphere pixels are sorted above right hemisphere pixels. This sorting offers a more detailed picture of correlation topography than what is viewable with a single correlation map. The visual RSN is outlined in the black box (D). The off diagonals (the top right or bottom left corner of the matrix), showed very high correlation between the left and right visual areas, in accordance with what is seen in the ISA sample in panel A and visual-seeded map in C. **(E)** Left visual-seeded activity propagation latency map of sample ISA in A shows early activity in the posterior region and later activity in the more anterior regions, consistent with what is seen in the sample ISA. M1: primary motor; M2: secondary motor; C/RS: Cingulate/Retrosplenial; S1: primary sensory; PRS: posterior retrosplenial; V: visual.

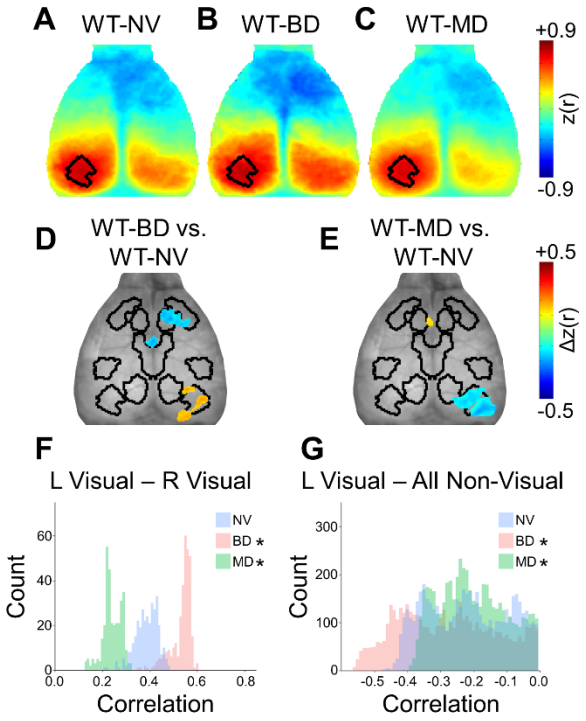

Figure 3.3: Critical period visual deprivation alters visual-seeded ISA correlation patterns. **(A-C)** Group-level correlation maps seeded in the left visual RSN in **(A)** WT-NV, (B) WT-BD, and **(C)** WT-MD mice. **(D)** Statistically significant correlation differences between WT-NV and WT-BD mice based on spatial cluster-wise threshold-extent criteria (see methods). Cool-colored pixels show decreased correlation in WT-BD compared to WT-NV, and warm-colored pixels show increased correlation in WT-BD compared to WT-NV mice. **(E)** Statistically significant correlation differences between WT-NV and WT-MD mice. **(F)** Correlation histograms between all right visual RSN pixels and the left visual RSN. **(G)** Correlation histograms between all non-visual pixels (both within and outside of RSNs in 2B) and the left visual RSN. BD enhances interhemispheric intra-network correlation and increases inter-network anti-correlation, while MD reduces intra-network correlation with little effect on inter-network correlation.

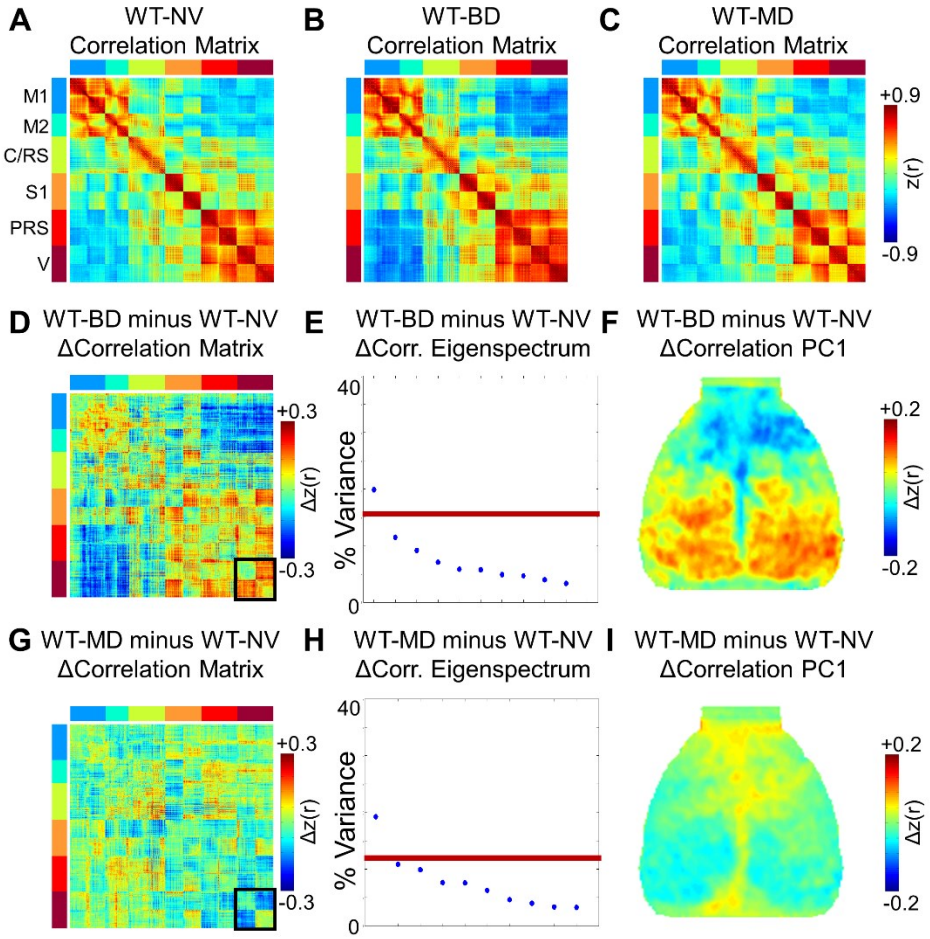

Figure 3.4: Unbiased correlation analysis over the entire cortex reveals differential influence of BD and MD on intra- and inter-network correlation. **(A-C)** Group level correlation matrices showing correlation between every pixel pair for pixels located within RSNs for **(A)** WT-NV, **(B)** WT-BD, and **(C)** WT-MD mice. The RSN pixels have been sorted as in Fig. 3.2B and D. **(D)** Correlation difference matrix calculated from WT-BD minus WT-NV demonstrates how correlation for each pixel pair differs between these two groups. The visual network is highlighted in black in panels B-D. Thus, the black outline in panel D demonstrates increase in correlation, in WT-BD vs. WT-NV, within the visual system. **(E)** To assess the full topography of pair-wise correlation changes, we applied spatial principal components analysis (PCA) to the full, unmasked correlation difference matrix. The resulting eigenspectrum (panel D) shows that there is 1 statistically significant PC (red line corresponds to $p < 0.05$, corrected; threshold computed by permutation re-sampling). **(F)** Topography of the significant PC, from which we term Δcorrelation PC1, indicates increased correlation between homotopic visual areas, and decreased correlation in the somatomotor system and cingulate areas, in accordance with the primary features of the difference correlation matrix (panel C). **(G)** Correlation difference matrix calculated as WT-MD minus WT-NV. **(H)** The eigenspectrum resulting from spatial principal components analysis (PCA) applied to the full, unmasked correlation difference matrix shows that there is 1 statistically significant PC. **(I)** Topography of the Δcorrelation PC1 indicates decreased correlation in the visual system, and increased correlation in the somatomotor system and cingulate areas.

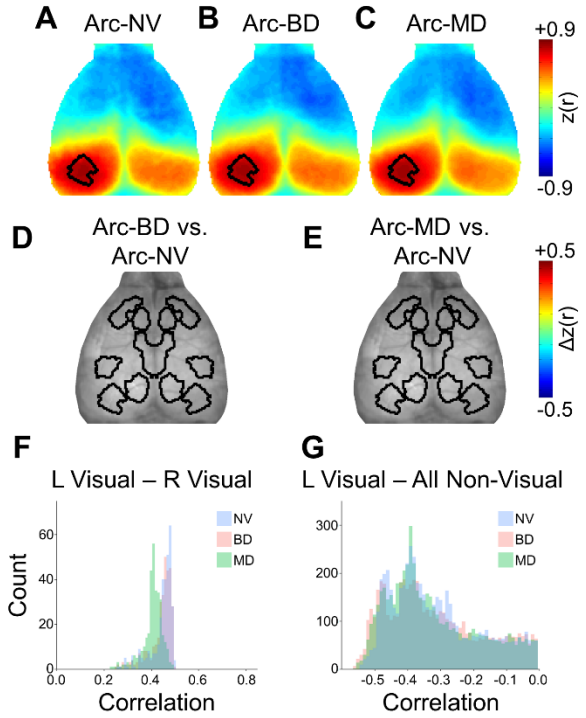

Figure 3.5: Visual deprivation does not induce visual-seeded ISA correlation change in Arc-/- mice. **(A-C)** Group-level correlation maps seeded in the left visual RSN in **(A)** Arc-NV, **(B)** Arc -BD, and **(C)** Arc -MD mice. **(D,E)** Neither BD nor MD resulted in statistically significant correlation differences compared to NV in Arc-/- mice based on spatial cluster-wise threshold-extent criteria. **(F)** Correlation histograms between all right visual RSN pixels and the left visual RSN. **(G)** Correlation histograms between all non-visual pixels (both within and outside of RSNs in 2B) and the left visual RSN.

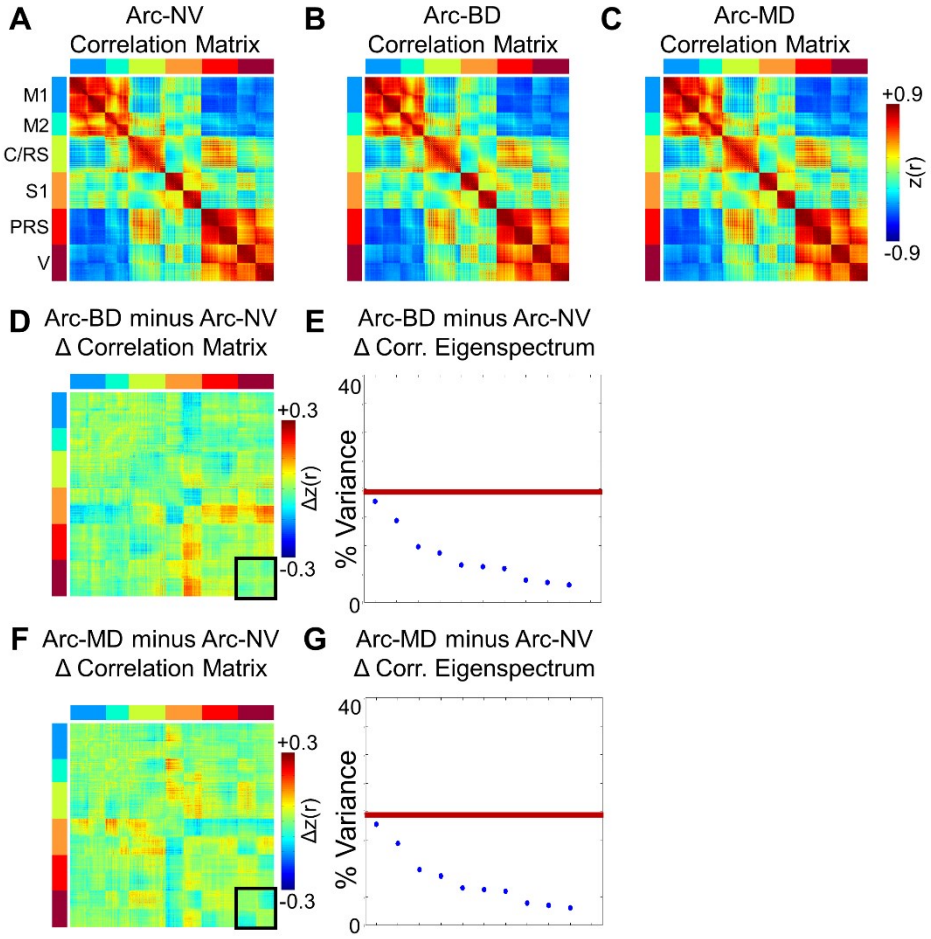

Figure 3.6: Whole-cortex correlation ISA is not altered by visual deprivation in Arc-/- mice. **(A-C)** Group level correlation matrices showing correlation between every pixel pair for pixels located within RSNs for **(A)** Arc-NV, **(B)** Arc-BD, and **(C)** Arc-MD mice. The pixels have been ordered as in Fig. 3.2B and D. **(D)** Correlation difference matrix calculated from Arc-BD minus Arc-NV, demonstrates how correlation for each pixel pair differs between these two groups. The visual network is highlighted in black in panels B-D. Thus, the black outline in panel D demonstrates increased correlation, in Arc-BD vs. Arc-NV, within the visual system. **(E)** The eigenspectrum resulting from spatial principal components analysis (PCA) to the full, unmasked correlation difference matrix shows no statistically significant PCs (red line corresponds to $p < 0.05$, corrected; threshold computed by permutation re-sampling). **(F)** Correlation difference matrix calculated from Arc-BD minus Arc-NV demonstrated how correlation for each pixel pair differs between these two groups. The visual network is highlighted in black in panels B-D. Thus, the black outline in panel D demonstrates increased correlation, in Arc-BD vs. Arc-NV, within the visual system. **(G)** The eigenspectrum resulting from spatial principal components analysis (PCA) to the full, unmasked correlation difference matrix shows no statistically significant PCs.

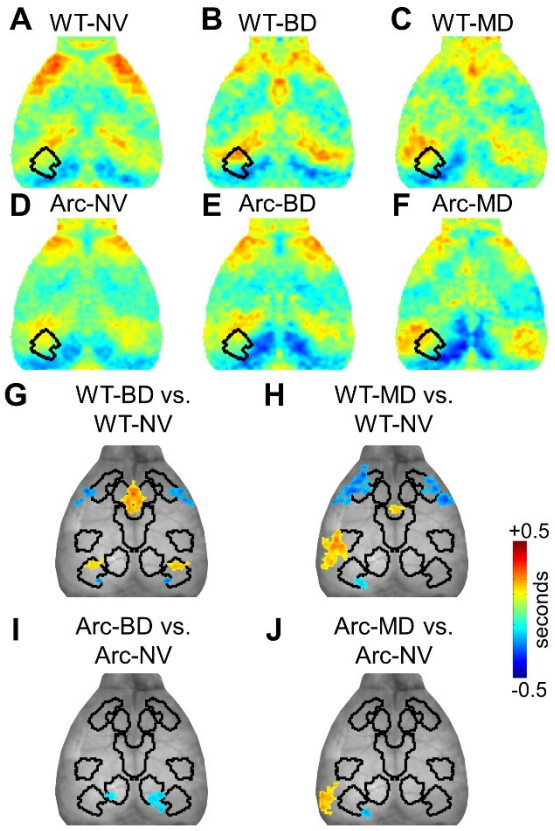

Figure 3.7: BD and MD result in selective short- and long-distance propagation latency changes involving visual, motor and cingulate/retrosplenial areas; long-distance latency changes appear to be Arc-dependent. **(A-C)** Propagation latency relative to the left visual RSN in WT groups: **(A)** WT-NV, **(B)** WT-BD, and **(C)** WT-MD groups. **(D-F)** Propagation latency relative to the left visual RSN in Arc-/- groups: **(D)** WT-NV, **(E)** WT-BD, and **(F)** WT-MD groups. **(G)** Statistically significant differences in propagation latency between WT-BD and WT-NV mice based on spatial cluster-wise threshold-extent criteria. **(H)** Statistically significant differences in propagation latency between WT-BD and WT-NV mice. **(I)** Statistically significant differences in propagation latency between Arc-BD and Arc-NV mice. **(J)** Statistically significant differences in propagation latency between Arc-BD and Arc-NV mice.

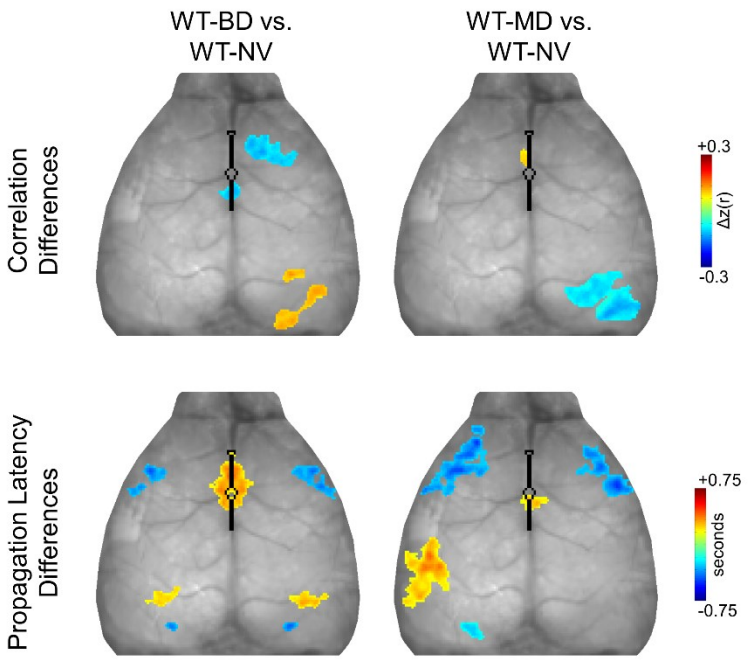

Figure 3.S1: Correlation and propagation latency difference maps shown with the cingulate cortex delineated. The cingulate perimeter is marked on the brain map in black.

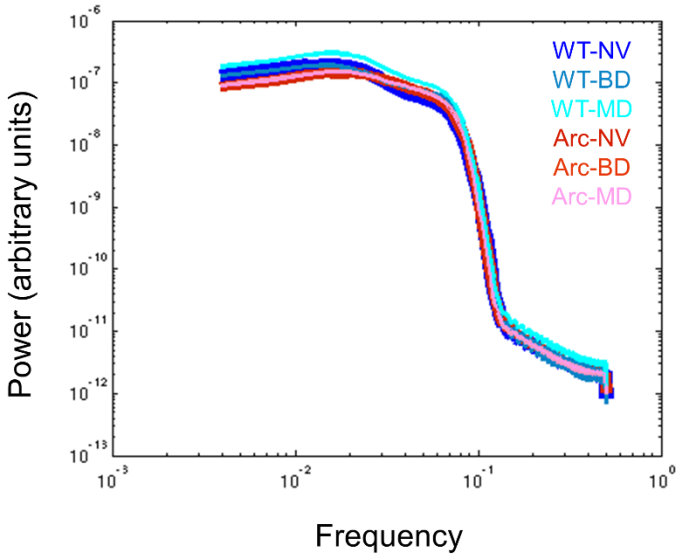

Figure 3.S2: Spontaneous infra-slow spectral content is equivalent in all WT and Arc experimental groups. The group-averaged spectral content over the infra-slow frequency band, calculated after filtering and global signal regression, is plotted for each group. This demonstrates that correlation and propagation differences in ISA patterns are not driven by differences in the amount of activity.

References

1. Crair MC, Gillespie DC, & Stryker MP (1998) The role of visual experience in the development of columns in cat visual cortex. *Science* 279(5350):566-570.

2. Fagiolini M, Pizzorusso T, Berardi N, Domenici L, & Maffei L (1994) Functional postnatal development of the rat primary visual cortex and the role of visual experience: dark rearing and monocular deprivation. *Vision Res* 34(6):709-720.

3. Wang BS, Sarnaik R, & Cang J (2010) Critical period plasticity matches binocular orientation preference in the visual cortex. *Neuron* 65(2):246-256.

4. Wiesel TN & Hubel DH (1965) Comparison of the effects of unilateral and bilateral eye closure on cortical unit responses in kittens. *J Neurophysiol* 28(6):1029-1040.

5. Chapman B & Stryker MP (1993) Development of orientation selectivity in ferret visual cortex and effects of deprivation. *J Neurosci* 13(12):5251-5262.

6. Wiesel TN & Hubel DH (1963) Single-Cell Responses in Striate Cortex of Kittens Deprived of Vision in One Eye. *J Neurophysiol* 26:1003-1017.

7. Gordon JA & Stryker MP (1996) Experience-dependent plasticity of binocular responses in the primary visual cortex of the mouse. *J Neurosci* 16(10):3274-3286.

8. Stryker MP & Harris WA (1986) Binocular impulse blockade prevents the formation of ocular dominance columns in cat visual cortex. *J Neurosci* 6(8):2117-2133.

9. Prusky GT & Douglas RM (2003) Developmental plasticity of mouse visual acuity. *Eur J Neurosci* 17(1):167-173.

10. Prusky GT, West PW, & Douglas RM (2000) Experience-dependent plasticity of visual acuity in rats. *Eur J Neurosci* 12(10):3781-3786.

11. McMullen CA, Andrade FH, & Stahl JS (2004) Functional and genomic changes in the mouse ocular motor system in response to light deprivation from birth. *J Neurosci* 24(1):161-169.

12. Kalatsky VA & Stryker MP (2003) New paradigm for optical imaging: temporally encoded maps of intrinsic signal. *Neuron* 38(4):529-545.

13. Grinvald A, Lieke E, Frostig RD, Gilbert CD, & Wiesel TN (1986) Functional architecture of cortex revealed by optical imaging of intrinsic signals. *Nature* 324(6095):361-364.

14. Blasdel GG & Salama G (1986) Voltage-sensitive dyes reveal a modular organization in monkey striate cortex. *Nature* 321(6070):579-585.

15. Espinosa JS & Stryker MP (2012) Development and plasticity of the primary visual cortex. *Neuron* 75(2):230-249.

16. Mitra A & Raichle ME (2016) How networks communicate: propagation patterns in spontaneous brain activity. *Philosophical transactions of the Royal Society of London. Series B, Biological sciences* 371(1705).

17. Raichle ME (2010) Two views of brain function. *Trends in cognitive sciences* 14(4):180-190.

18. Raichle ME (2015) The restless brain: how intrinsic activity organizes brain function. *Philosophical transactions of the Royal Society of London. Series B, Biological sciences* 370(1668).

19. Arieli A, Shoham D, Hildesheim R, & Grinvald A (1995) Coherent spatiotemporal patterns of ongoing activity revealed by real-time optical imaging coupled with single-unit recording in the cat visual cortex. *J Neurophysiol* 73(5):2072-2093.

20. Tsodyks M, Kenet T, Grinvald A, & Arieli A (1999) Linking spontaneous activity of single cortical neurons and the underlying functional architecture. *Science* 286(5446):1943-1946.

21. Kenet T, Bibitchkov D, Tsodyks M, Grinvald A, & Arieli A (2003) Spontaneously emerging cortical representations of visual attributes. *Nature* 425(6961):954-956.

22. Purdon PL & Weisskoff RM (1998) Effect of temporal autocorrelation due to physiological noise and stimulus paradigm on voxel-level false-positive rates in fMRI. *Hum Brain Mapp* 6(4):239-249.

23. Fox MD*, et al.* (2005) The human brain is intrinsically organized into dynamic, anticorrelated functional networks. *Proc Natl Acad Sci U S A* 102(27):9673-9678.

24. Mitra A, Snyder AZ, Blazey T, & Raichle ME (2015) Lag threads organize the brain's intrinsic activity. *Proc Natl Acad Sci U S A* 112(17):E2235-2244.

25. Mitra A, Snyder AZ, Hacker CD, & Raichle ME (2014) Lag structure in resting-state fMRI. *J Neurophysiol* 111(11):2374-2391.

26. Power JD*, et al.* (2011) Functional network organization of the human brain. *Neuron* 72(4):665-678.

27. Fox MD, Corbetta M, Snyder AZ, Vincent JL, & Raichle ME (2006) Spontaneous neuronal activity distinguishes human dorsal and ventral attention systems. *Proc Natl Acad Sci U S A* 103(26):10046-10051.

28. Shannon BJ*, et al.* (2016) Brain aerobic glycolysis and motor adaptation learning. *Proc Natl Acad Sci U S A* 113(26):E3782-3791.

29. White BR*, et al.* (2011) Imaging of functional connectivity in the mouse brain. *PLoS One* 6(1):e16322.

30. Grayson DS*, et al.* (2016) The Rhesus Monkey Connectome Predicts Disrupted Functional Networks Resulting from Pharmacogenetic Inactivation of the Amygdala. *Neuron* 91(2):453-466.

31. Stafford JM*, et al.* (2014) Large-scale topology and the default mode network in the mouse connectome. *Proc Natl Acad Sci U S A* 111(52):18745-18750.

32. Laumann TO*, et al.* (2015) Functional System and Areal Organization of a Highly Sampled Individual Human Brain. *Neuron* 87(3):657-670.

33. Lewis CM, Baldassarre A, Committeri G, Romani GL, & Corbetta M (2009) Learning sculpts the spontaneous activity of the resting human brain. *Proc Natl Acad Sci U S A* 106(41):17558-17563.

34. Mackey AP, Miller Singley AT, & Bunge SA (2013) Intensive reasoning training alters patterns of brain connectivity at rest. *J Neurosci* 33(11):4796-4803.

35. Burton H, Snyder AZ, & Raichle ME (2014) Resting state functional connectivity in early blind humans. *Front Syst Neurosci* 8:51.

36. Wang D*, et al.* (2014) Altered resting-state network connectivity in congenital blind. *Hum Brain Mapp* 35(6):2573-2581.

37. Heine L*, et al.* (2015) Prevalence of increases in functional connectivity in visual, somatosensory and language areas in congenital blindness. *Front Neuroanat* 9:86.

38. Liu Y*, et al.* (2007) Whole brain functional connectivity in the early blind. *Brain* 130(Pt 8):2085-2096.

39. Korb E & Finkbeiner S (2011) Arc in synaptic plasticity: from gene to behavior. *Trends Neurosci* 34(11):591-598.

40. Chowdhury S*, et al.* (2006) Arc/Arg3.1 interacts with the endocytic machinery to regulate AMPA receptor trafficking. *Neuron* 52(3):445-459.

41. Shepherd JD*, et al.* (2006) Arc/Arg3.1 mediates homeostatic synaptic scaling of AMPA receptors. *Neuron* 52(3):475-484.

42. Okuno H*, et al.* (2012) Inverse synaptic tagging of inactive synapses via dynamic interaction of Arc/Arg3.1 with CaMKIIbeta. *Cell* 149(4):886-898.

43. Korb E, Wilkinson CL, Delgado RN, Lovero KL, & Finkbeiner S (2013) Arc in the nucleus regulates PML-dependent GluA1 transcription and homeostatic plasticity. *Nat Neurosci* 16(7):874-883.

44. Smith SM*, et al.* (2009) Correspondence of the brain's functional architecture during activation and rest. *Proc Natl Acad Sci U S A* 106(31):13040-13045.

45. Yeo BT*, et al.* (2015) Functional Specialization and Flexibility in Human Association Cortex. *Cereb Cortex* 25(10):3654-3672.

46. Biswal B, Yetkin FZ, Haughton VM, & Hyde JS (1995) Functional connectivity in the motor cortex of resting human brain using echo-planar MRI. *Magn Reson Med* 34(4):537-541.

47. Nir Y*, et al.* (2008) Interhemispheric correlations of slow spontaneous neuronal fluctuations revealed in human sensory cortex. *Nat Neurosci* 11(9):1100-1108.

48. McCurry CL*, et al.* (2010) Loss of Arc renders the visual cortex impervious to the effects of sensory experience or deprivation. *Nat Neurosci* 13(4):450-457.

49. Ren M, Cao V, Ye Y, Manji HK, & Wang KH (2014) Arc regulates experience-dependent persistent firing patterns in frontal cortex. *J Neurosci* 34(19):6583-6595.

50. Wang KH*, et al.* (2006) In vivo two-photon imaging reveals a role of arc in enhancing orientation specificity in visual cortex. *Cell* 126(2):389-402.

51. Carter AR*, et al.* (2010) Resting interhemispheric functional magnetic resonance imaging connectivity predicts performance after stroke. *Ann Neurol* 67(3):365-375.

52. Allen G*, et al.* (2007) Reduced hippocampal functional connectivity in Alzheimer disease. *Arch Neurol* 64(10):1482-1487.

53. Chase A (2014) Alzheimer disease: Altered functional connectivity in preclinical dementia. *Nat Rev Neurol* 10(11):609.

54. Bavelier D & Neville HJ (2002) Cross-modal plasticity: where and how? *Nat Rev Neurosci* 3(6):443-452.

55. Kupers R*, et al.* (2011) Neural correlates of olfactory processing in congenital blindness. *Neuropsychologia* 49(7):2037-2044.

56. Pascual-Leone A & Hamilton R (2001) The metamodal organization of the brain. *Prog Brain Res* 134:427-445.

57. Lee HK & Whitt JL (2015) Cross-modal synaptic plasticity in adult primary sensory cortices. *Curr Opin Neurobiol* 35:119-126.

58. Burton H*, et al.* (2002) Adaptive changes in early and late blind: a fMRI study of Braille reading. *J Neurophysiol* 87(1):589-607.

59. Rauschecker JP, Tian B, Korte M, & Egert U (1992) Crossmodal changes in the somatosensory vibrissa/barrel system of visually deprived animals. *Proc Natl Acad Sci U S A* 89(11):5063-5067.

60. Rabinowitch I & Bai J (2016) The foundations of cross-modal plasticity. *Commun Integr Biol* 9(2):e1158378.

61. Negyessy L, Gal V, Farkas T, & Toldi J (2000) Cross-modal plasticity of the corticothalamic circuits in rats enucleated on the first postnatal day. *Eur J Neurosci* 12(5):1654-1668.

62. Toldi J, Farkas T, & Volgyi B (1994) Neonatal enucleation induces cross-modal changes in the barrel cortex of rat. A behavioural and electrophysiological study. *Neurosci Lett* 167(1-2):1-4.

63. Toldi J, Rojik I, & Feher O (1994) Neonatal monocular enucleation-induced cross-modal effects observed in the cortex of adult rat. *Neuroscience* 62(1):105-114.

64. Petrus E*, et al.* (2015) Vision loss shifts the balance of feedforward and intracortical circuits in opposite directions in mouse primary auditory and visual cortices. *J Neurosci* 35(23):8790-8801.

65. Merabet LB*, et al.* (2008) Rapid and reversible recruitment of early visual cortex for touch. *PLoS One* 3(8):e3046.

66. Hensch TK (2005) Critical period plasticity in local cortical circuits. *Nat Rev Neurosci* 6(11):877-888.

67. Ranson A, Sengpiel F, & Fox K (2013) The role of GluA1 in ocular dominance plasticity in the mouse visual cortex. *J Neurosci* 33(38):15220-15225.

68. Restani L*, et al.* (2009) Functional masking of deprived eye responses by callosal input during ocular dominance plasticity. *Neuron* 64(5):707-718.

69. Vogt BA & Miller MW (1983) Cortical connections between rat cingulate cortex and visual, motor, and postsubicular cortices. *J Comp Neurol* 216(2):192-210.

70. Zhang S*, et al.* (2016) Organization of long-range inputs and outputs of frontal cortex for top-down control. *Nat Neurosci* 19(12):1733-1742.

71. Cuenod M, Casey KL, & MacLean PD (1965) Unit analysis of visual input to posterior limbic cortex. I. Photic stimulation. *J Neurophysiol* 28(6):1101-1107.

72. Woolsey CN, Erickson TC, & Gilson WE (1979) Localization in somatic sensory and motor areas of human cerebral cortex as determined by direct recording of evoked potentials and electrical stimulation. *J Neurosurg* 51(4):476-506.

73. Lende RA & Woolsey CN (1956) Sensory and motor localization in cerebral cortex of porcupine (Erethizon dorsatum). *J Neurophysiol* 19(6):544-563.

74. Kaada BR (1951) Somato-motor, autonomic and electrocorticographic responses to electrical stimulation of rhinencephalic and other structures in primates, cat, and dog; a study of responses from the limbic, subcallosal, orbito-insular, piriform and temporal cortex, hippocampus-fornix and amygdala. *Acta Physiol Scand Suppl* 24(83):1-262.

75. Albert NB, Robertson EM, & Miall RC (2009) The resting human brain and motor learning. *Curr Biol* 19(12):1023-1027.

76. Hardwick RM, Rottschy C, Miall RC, & Eickhoff SB (2013) A quantitative meta-analysis and review of motor learning in the human brain. *Neuroimage* 67:283-297.

77. Plath N*, et al.* (2006) Arc/Arg3.1 is essential for the consolidation of synaptic plasticity and memories. *Neuron* 52(3):437-444.

78. Silasi G, Xiao D, Vanni MP, Chen AC, & Murphy TH (2016) Intact skull chronic windows for mesoscopic wide-field imaging in awake mice. *J Neurosci Methods* 267:141-149.

79. Picchioni D, Duyn JH, & Horovitz SG (2013) Sleep and the functional connectome. *Neuroimage* 80:387-396.

80. Amzica F & Steriade M (1995) Short- and long-range neuronal synchronization of the slow (< 1 Hz) cortical oscillation. *J Neurophysiol* 73(1):20-38.

81. Steriade M, Nunez A, & Amzica F (1993) A novel slow (< 1 Hz) oscillation of neocortical neurons in vivo: depolarizing and hyperpolarizing components. *J Neurosci* 13(8):3252-3265.

82. Petersen CC, Hahn TT, Mehta M, Grinvald A, & Sakmann B (2003) Interaction of sensory responses with spontaneous depolarization in layer 2/3 barrel cortex. *Proc Natl Acad Sci U S A* 100(23):13638-13643.

83. Arridge SR, Cope M, & Delpy DT (1992) The theoretical basis for the determination of optical pathlengths in tissue: temporal and frequency analysis. *Phys Med Biol* 37(7):1531-1560.

84. Bumstead JR, Bauer AQ, Wright PW, & Culver JP (2017) Cerebral functional connectivity and Mayer waves in mice: Phenomena and separability. *J Cereb Blood Flow Metab* 37(2):471-484.

85. He BJ, Zempel JM, Snyder AZ, & Raichle ME (2010) The temporal structures and functional significance of scale-free brain activity. *Neuron* 66(3):353-369.

86. Bauer AQ*, et al.* (2014) Optical imaging of disrupted functional connectivity following ischemic stroke in mice. *Neuroimage* 99:388-401.

87. Carbonell F, Bellec P, & Shmuel A (2011) Global and system-specific resting-state fMRI fluctuations are uncorrelated: principal component analysis reveals anti-correlated networks. *Brain Connect* 1(6):496-510.

88. Franklin K & Paxinos G (2008) *The Mouse Brain in Stereotactic Coordinates* (Academic Press, New York).

89. Konig P (1994) A method for the quantification of synchrony and oscillatory properties of neuronal activity. *J Neurosci Methods* 54(1):31-37.

90. Maxim V*, et al.* (2005) Fractional Gaussian noise, functional MRI and Alzheimer's disease. *Neuroimage* 25(1):141-158.

91. Hayasaka S & Nichols TE (2003) Validating cluster size inference: random field and permutation methods. *Neuroimage* 20(4):2343-2356.

92. Hacker CD, Perlmutter JS, Criswell SR, Ances BM, & Snyder AZ (2012) Resting state functional connectivity of the striatum in Parkinson's disease. *Brain* 135(Pt 12):3699-3711.

Chapter 4

Electrically coupled inhibitory interneuron networks limit spontaneous activity coupling between distant cortical regions

Preface

This chapter contains a manuscript in preparation:

Kraft A.W. et al. Electrically coupled inhibitory interneuron networks limit spontaneous activity coupling between distant cortical regions. Manuscript in preparation.

Author Contributions for the citation above:

AWK and JML designed experiments. AWK and ZR collected data. AM and AWK processed and analyzed data. AWK and AM wrote the manuscript with help from all co-authors. All authors read and approved the final manuscript. JML supervised all aspects of the project.

Abstract

Spontaneous infra-slow brain activity (ISA) exhibits a high degree of temporal synchrony, or correlation, between distant brain regions. Spatial organization of ISA coordination is not explained by anatomy alone, suggesting active processes modulate spontaneous activity. Inhibitory interneurons (IIN) form electrically coupled networks with the gap junction protein connexin 36 (Cx36), and these IIN networks may be one biological mechanism that influences functional organization of neural activity. Deleting Cx36 disrupts electrical coupling in IIN networks and attenuates theta and gamma local field potential oscillations, but the role of electrically coupled IIN networks in regulating ISA organization over the entire brain is unknown. In this study, we performed OIS imaging on Cx36-/- mice to examine the role of this gap junction in ISA coordination across the entire cortex. We show that Cx36 deletion increased long-distance intra-hemispheric anti-correlations and inter-hemispheric correlation in spontaneous ISA. In addition, local correlation was unaltered, or in certain locations increased, in Cx36-/- mice. This suggests that electrically coupled IIN networks are involved in decoupling infra-slow spontaneous activity between distant brain regions.

Introduction

At rest, the brain is continuously oscillating over a wide frequency range (<0.01Hz – 600Hz) (*1*). Infra-slow activity (ISA), activity between 0.1 and 0.01 Hz, dominates the power spectrum of spontaneous brain activity and occurs with precise spatiotemporal organization. More specifically, spontaneous ISA across distinct brain regions is temporally synchronous, and these patterns of correlated activity between regions define functionally connected networks (*2-4*). Spontaneous activity correlation patterns (often termed functional connectivity) are remarkably stable within and between individuals (*4, 5*). Moreover, these patterns are present with remarkable homology in non-human primates and rodents (*6-9*). This suggest that these resting state correlation patterns may be fundamental to neurological function. Consistent with this, decreased network correlation is a common feature of neurological disease (*10-12*).

While there is some overlap between neuroanatomy and spontaneous ISA correlation, the bulk of functionally connected systems do not have a clear anatomical connection (*3, 4, 6, 13, 14*). Furthermore, correlation strength varies widely between functional networks for unknown reasons. Thus, correlation is not merely a readout of anatomical connectivity, and other biological mechanisms must be modulating brain activity to shape synchrony in spontaneous activity.

Inhibitory interneuron (IIN) networks may be one system that modulates temporally synchronous networks. IINs form robust interconnections amongst each other using both chemical and electrical synapses (*15-17*). The electrical synapses are formed by Connexin 36 (Cx36), a gap junction protein found throughout the brain and in the cortex it is exclusively in inhibitory interneurons (*15, 16*). Deletion of Cx36 does not result in obvious deficits: Cx36-/- mice have normal anatomy, growth, fertility, and no obvious behavior deficits (*15, 16*). However, closer examinations have revealed that Cx36 deletion impairs higher-level cognitive processes including ocular dominance plasticity, LTP, and context-dependent fear learning (*18-21*).

Cx36's role in neuroplasticity is not completely clear. However, there are several demonstrations that disrupting Cx36 attenuates certain aspects of neural coordination. Cx36 enables coordinated inhibition across separate cells at distances up to 400 microns (*16*). This appears to be important for local field potential oscillations as *in vitro* and *in vivo* recordings demonstrated diminished gamma frequency (30-80Hz) power in Cx36-/- mice.

In addition, IIN modulation of these oscillations appears to be state dependent. Ocular dominance plasticity and fear learning paradigms resulted in increased hippocampal theta activity (3-12Hz) that was absent with Cx36 gene deletion or pharmacologic blockade (*19, 21*). Furthermore, motor activity results in large gamma power differences between Cx36+/+ and Cx36-/- mice that dissipate during sleep (*22*). Thus, Cx36 has a well-defined role in coordinating certain low-frequency (theta and gamma, 3Hz - 80Hz) neural oscillations within small brain volumes, and this may be important for complex behaviors and plasticity.

Given this, it is reasonable to suspect electrically coupled IIN networks play a role in coordinating ISA activity between regions separated by large distances to generate whole-brain spontaneous correlation patterns. However, the role of Cx36 in coordinating brain activity in the ISA range has not been examined. To address this, we performed wide-field optical intrinsic signal (OIS) imaging in Cx36+/+ and Cx36-/- mice to examine whole-cortex spontaneous ISA correlation organization. We found that Cx36 gene deletion resulted in enhanced inter-hemispheric ISA correlation and intra-hemispheric ISA anti-correlation between specific cortical regions. This suggests that electrically coupled inhibitory neuron networks play a role in decoupling ISA between distant cortical regions.

Results

Cx36 gene deletion influences spatial ISA correlation in specific cortical regions without altering ISA power

Given previous findings that show Cx36 gene deletion results in decreased gamma and theta LFP oscillation power (*15, 19, 21, 22*), we first examined ISA (0.1Hz – 0.01Hz) spectral power in the OIS data from Cx36+/+ and Cx36-/- mice. We found that Cx36 gene deletion had no significant effect on ISA power over the cortex as measured with OIS (Fig. 4.4.1).

To examine if electrically coupled IIN networks influence the spatial correlation observed in ISA across the brain, we looked at the relationship between intra-hemispheric distance and correlation. First we examined this relationship for every pixel: each intra-hemspheric pixel-pixel pair's correlation value and separation distance was calculated, and the average correlation vs. distance curve was generated (Fig. 4.2A). In Cx36+/+ mice this relationship shows high positive correlation values at short distances, decreasing correlation with distance, and anti-correlation occurs at longer distances. Cx36 gene deletion did not alter this relationship (Fig. 4.2A).

Given that Cx36 has a non-uniform distribution throughout the cortex (*16*), we wondered if Cx36 may have a spatially specific influence on correlation relationships. We separated our mice into two separate analysis sets. To determine pertinent ROIs, we selected 3 Cx36+/+ and 3 Cx36-/- mice at random and performed component analysis on the whole-cortex Δcorrelation matrix. The first principal component (PC) explained 28% of the variance (Fig. 4.S1) and projection of the Δcorrelation matrix on the corresponding eigenvector generated a Δcorrelation PC map (Fig. 4.2B). The Δcorrelation PC map demonstrated focal territories of correlation increases and decreases, and these areas were used to define ROIs for subsequent analysis (Fig. 4.2C).

Importantly, these ROIs were used on the separate set of mice from those used to select the ROIs (Cx36+/+ n=16, Cx36-/- n=10). We examined the intra-hemispheric spatial correlation relationship for pixels within the determined ROIs and found that for both the anterior and posterior ROIs, Cx36 deletion enhanced anti-correlation at longer distances (Fig. 4.2D,E). In addition, for pixels in the anterior ROI, Cx36 deletion increased correlation between pixels separate by very short distances (Fig. 4.2,D). For pixels outside of these ROIs, there was no difference in the spatial

correlation relationship (Fig. 4.2F). Thus, Cx36 deletion enhanced correlation and anti-correlation for selective cortical regions.

We also looked at ISA spectral power within these ROIs and found no significant differences between Cx36+/+ and Cx36-/- mice (Fig. 4.S2).

Cx36 gene deletion decreases inter-hemispheric correlation and intra-hemispheric anti-correlation in select cortical regions

We next examined the correlation between these ROIs, taking inter-hemispheric relationships into account (Fig. 4.3). First we used ROI-sorted matrices that examined the mean correlation value for every set of ROI pairs (Fig. 4.3B). Qualitative inspection of these activity correlation matrices shows a clear influence of Cx36 on the intra- and inter-hemispheric correlation relationships. Subtracting these two matrices to generate the Δcorrelation matrix for these ROIs shows that, indeed, Cx36-/- mice have increased inter-hemispheric correlation and increased intra-hemispheric anti-correlation (Fig. 4.3C). Consistent with Fig. 4.2, the intra-hemispheric Ant. ROI and Post. ROIs have increased anti-correlation in the Cx36-/- mice, and the Ant. ROIs have increased auto-correlation. In addition, this analysis shows that Cx36 deletion increases homotopic correlation between the Ant. ROIs. Homotopic correlation between the Post. ROIs was increased, but the difference did not reach statistical significance (Fig. 4.3C).

Next we calculated whole-cortex correlation maps seeded by our ROIs (Fig. 4.4). Obvious differences were present between Cx36+/+ and Cx36-/- correlation maps (Fig. 4.4A-H). Consistent with previous analyses, Cx36+/+ maps had largely attenuated inter-hemispheric correlation and intra-hemispheric anti-correlation for the ROIs examined. Statistical significance of correlation differences between groups was assessed with a spatial cluster-wise basis using threshold-extent criteria computed by extensive permutation resampling (see Methods for further detail).

An additional key finding in the statistically masked difference maps are that both the left and right Post. ROIs showed contralateral clusters of increased correlation that were centered just outside of the homotopic ROI (Fig. 4.4K,L). This suggests that for the Post. ROIs, Cx36 limits the positive correlation beyond the homotopic region. Further, the Ant. ROI in Cx36-/- mice demonstrated increased anti-correlation with the contralateral Post. ROI. Although these differences were only statistically significant for the right Ant. seeded region, they suggest Cx36 also limits off-homotopic anti-correlation.

Altogether, this analysis is consistent with what is shown be the previous metrics: Cx36 limits ISA correlation magnitude for cortical ROIs separated by long distances within and across hemispheres.

Cx36 gene deletion enhances the anterior-posterior correlation gradient boundary

The cortex can be partitioned into functional regions based on abrupt transitions in resting state correlation patterns that occur across functionally distinct ROIs. Based on this functional boundaries can be assigned to the brain (*23*). This metric reveals zones of high ISA correlation pattern similarity that are separated by narrow edges of transition (*23*).

We wondered how electrically coupled IN networks might influence functional transitions between regions. Using all imaged Cx36+/+ and Cx36-/- mice (Cx36+/+ n=19, Cx36-/- n=13), we generated correlation edge gradient maps (Fig. 4.5A,B). In Cx36+/+ mice, an anterior-posterior gradient border zone was apparent, suggesting abrupt correlation changes occur over the anterior-posterior correlation transition (Fig. 4.5A). Cx36-/- gradient maps were generally the same except that the anterior-posterior gradient was much wider and of larger magnitude (Fig. 4.5B). Subtracting the two, it is clear that Cx36+/+ mice have a much narrower correlation transition gradient along the A-P axis (Fig. 4.5C).

Using the entire set of mice, we performed PCA on the Δcorrelation matrix to generate the Δcorrelation PC map (Fig. 4.5F). This Δcorrelation PC explained 39% of the variance (Fig. 4.S3) and was consistent with the Δcorrelation PC map generated from the subset of mice in Fig. 4.2B. Overlaying the gradient changes on the Δcorrelation PC map demonstrates that Cx36 deletion resulted in a widened transition zones between the anterior and posterior regions (Fig. 4.5G). In comparing this gradient change to the Paxinos mouse brain atlas (Fig. 4.5H), it is clear that this border exists along the interface of many anatomically defined territories. Thus in addition to altering spontaneous activity correlation, Cx36 deletion causes the anterior-posterior functional border to occur over a longer distance. This suggests that electrically coupled IIN networks play a role in generating sharp transitions between functionally defined regions.

Discussion

In this study we used wide-field OIS imaging in mice deficient for Cx36, the gap junction protein that forms gap junctions between IINs, to examine the role of electrically coupled IIN networks in shaping spontaneous activity correlation patterns over the cerebral cortex. We found that disrupting electrically coupling in IIN networks resulted in increased ISA correlation magnitude between distant cortical regions both within and across hemispheres.

Cx36 influence on intra-hemispheric correlation organization

Anti-correlations in spontaneous brain activity led to some of the earliest descriptions of spontaneous activity network organization (*3, 24*). Anti-correlations are especially interesting because they separate areas that have respective increases and decreases in activity during focused tasks (*3, 24-29*). The best demonstration of this is seen in the dorsal attention networks and default mode networks in humans (*3*). Activity in the default mode decreases during attention demanding tasks, and this is thought to be driven by the brain pivoting from self-referential activity to task-directed activity requiring focused attention (*3, 30, 31*).

Our results demonstrate that electrically coupled IIN networks decrease anti-correlations in spontaneous activity. Thus some set of processes enable anti-correlations that are actively opposed by IIN networks. Spontaneous anti-correlations are thought to be important in segregating distinct processing streams, but these findings suggests electrically coupled IIN networks may play a role in limiting anti-correlation to optimally balance integration and segregation across separate systems.

Moreover, the correlation transition gradients in Cx36+/+ mice were much more narrow those in Cx36-/- mice. In human fMRI imaging, this approach allows a non-invasive method of delineating architectonic areas (*23*). We show that Cx36 deletion results in a widening of the anterior-posterior gradient intensity. This suggests that electrically coupled IIN networks play a role in generating sharp functional transitions between separate functional regions in the cortex.

Cx36 influence on inter-hemispheric correlation organization

In addition to anti-correlation enhancement in Cx36-/- mice, we also found increased correlation for certain relationships. This included increased local correlation for the Ant. ROIs and increased inter-hemispheric correlation between the Ant. and Post. ROI pairs (for the homotopic relationships, roughly speaking). Homotopic correlations are especially robust in humans and present in all species that have been examined (*2-4, 6, 8, 9, 32, 33*). Indeed, this phenomenon extends to the mouse and has been observed using fMRI, fOIS, genetically encoded calcium imaging, genetically encoded glutamate imaging, and voltage sensitive dyes (*8, 9, 32, 34-36*).

Our results suggest that electrically coupled IIN networks play a role in limiting spontaneous synchrony between homotopic cortical regions. This is especially interesting given that homotopic correlation decrement is a powerful biomarker of neurologic disease (*10, 12*). Cx36 deletion, on the other hand, enhances certain homotopic correlations but causes deficits in complex motor learning and experience-dependent plasticity (*18-21, 37*).

By partially limiting inter-hemispheric correlation, each cortical hemisphere may be able to act with more independence. This may also be the purpose for intra-hemispheric anti-correlation limits imposed by electrically coupled IINs. Ideal brain function must involve a balance between system independence and integration. Over-synchronization across all systems may limit the ability of each brain system to handle specific tasks independently. One the other hand, complete dyssynchrony may prevent the cross-system communication required for high order integration. Thus through the observed effect on ISA decoupling, electrical coupled IIN networks may enable better parallel processing for handling complex scenarios.

Anatomy of electrically coupled IIN networks and spontaneous ISA correlation organization

The spatial reach of electrically coupled IIN networks is not entirely clear. Work from brain slices showed that IPSPs correlation is present in cortical cells separated by up to 400 microns, and this correlation is dramatically reduced in Cx36-/- slices (*16*). Given this limit, it is unclear how disrupting electrically coupled IIN networks influences spontaneous ISA correlation relationships between cortical regions separated by several millimeters.

Cx36 gap junctions are present between dendrites and the extensive dendritic trees found on IIN could expand network distance. Furthermore, IIN networks involve many neurons, which could help extend the network reach. That said, electrical coupling is spatially limited as amplitude decrements with distance (*38*).

Thus, electrically coupled IIN networks may be coordinated by longer-distance axonal inputs. In the case of homotopic cortical partners, it has been suggested that transcallosal projections have both excitatory and inhibitory interhemispheric influences (*39*). Transcallosal projections may synapse on IINs (directly or indirectly) and exert coordinated interhemispheric inhibition that is carefully balanced with excitatory signaling to generate a precise excitatory/inhibitory balance. Electrical coupling amongst these IINs may be crucial for proper inhibition across hemispheres.

Likewise, long-distance intra-hemispheric connections may be important for limiting out of phase synchrony that produces anti-correlated activity.

State-dependency (Limitations – not sure about having this section)

All fOIS experiments performed in this study were done under ketamine/xylazine anesthesia. Recent work in mice has shown that cortical correlations in slow activity are quite stable across wake and ketamine/xylazine anesthesia states (*40*). This is in agreement with data showing stability of low frequency correlation across states of consciousness in humans (*41*).

Previous work using Cx36-/- brain slices *in vitro* and awake Cx36-/- mice *in vivo* have both showed decreased gamma power with Cx36 deletion. However, *in vivo* work has revealed that some differences in Cx36-/- mice are accentuated under specific conditions. More specifically gamma power differences between Cx36+/+ and Cx36-/- mice were larger during wheel running that during sleep (*22*), and theta power increases following plasticity paradigms were absent in Cx36-/- mice (*19, 21*). Thus, the resting state differences we see may not be capturing more robust network-level effects that occur during complex tasks or after learning. Future work will be required to examine this.

Methods

Mice

All procedures described below were approved by the Washington University Animal Studies Committee in compliance with AAALAC guidelines. Littermate (male and female) Cx36+/+ and Cx36-/- mice (RRID:MGI:3810169)(*15*) on a pure C57Bl6/J background were raised in standard cages in a dedicated mouse facility with a 12-12 light/dark cycle. All imaging was performed on P90 mice.

Imaging animal prep

In accord with our previously published animal preparation protocol for fOIS imaging (*9*), anesthesia was initiated via i.p. injection with a bolus of ketamine-xylazine (1x dose: 86.9 mg/kg ketamine, 13.4 mg/kg xylazine) and animals were allowed 15 minutes for anesthetic transition. After induction, the animal was placed on a heating pad maintained at 37°C via feedback from a rectal probe (mTCII, Cell Microcontrols) and its head secured in a stereotactic frame. The head was shaved and cleaned, a midline incision was made along the top of the head to reflect the scalp and the skull was kept intact.

Image acquisition

Sequential illumination was provided at four wavelengths by a ring of light emitting diodes (LEDs) placed approximately 10 cm above the mouse's head. The field of view included most of the cerebral cortex (approximately 1cm^2). Diffuse reflected light was detected by a cooled, frame-transfer EMCCD camera (iXon 897, Andor Technologies); the LED ring and the camera were time-synchronized and controlled via computer using custom-written software (MATLAB, Mathworks) at a full frame rate of 30 Hz.

Image Processing

Data from all mice were subjected to an initial quality check prior to spectroscopic analysis. Data runs (5 minutes) in which reflected light level intensity (mean value over the brain) varied as a function of time by greater than 1% for any wavelength were excluded from further analysis. This preliminary quality control yielded 10–30 minutes of data per mouse. For subsequent analysis, image light intensity at each wavelength was interpreted using the Modified Beer-Lambert Law, usually expressed as: $\Phi(\mathbf{r},t) = \Phi_0 * \exp(-\Delta\mu_a(\mathbf{r},t) * L)$. Here, $\Phi(\mathbf{r},t)$ is the measured light intensity, Φ_0 is the baseline light intensity, $\Delta\mu_a(\mathbf{r}, t)$ is the change in absorption coefficient due to hemodynamic changes, and L is the optical path length factor for photons in the tissue (*42*). As there is no pre-stimulus baseline in resting-state experimentation, we normalized relative to the average light intensity at each pixel, resulting in differential measures of absorption at each

wavelength at each pixel: $\Delta\mu_{a,\lambda}(\mathbf{r},t) = -\ln(\Phi_\lambda(\mathbf{r},t)/< \Phi_{0\lambda}(\mathbf{r},t)>)/L_\lambda$. Absorption coefficient data were converted to hemoglobin (Hb) concentration changes by inverting the system of equations, $\Delta\mu_{a,\lambda}(\mathbf{r},t) = E_{\lambda,i}\,\Delta[Hb_i](\mathbf{r},t)$ (where E is the extinction coefficient matrix, and *i* runs over hemoglobin species). This inversion was performed using least-squares methods, yielding changes in oxygenated hemoglobin (HbO) and deoxygenated hemoglobin (HbR) at each pixel at each time point. Differential changes in hemoglobin concentration were filtered to retain the infra-slow activity/functional connectivity band (0.009–0.08 Hz) following previous human functional connectivity algorithms (*3*). After filtering, each pixel's time series was downsampled from 30 Hz to 1 Hz, and all further analysis was performed only on those pixels labeled as brain using a manually-constructed brain mask. The time traces of all pixels defined as brain were averaged to create a global brain signal. This global signal was regressed from every pixel's time trace to remove global sources of variance; global signal regression was applied independently on each contiguous imaging session.

Image Co-registration

Image sequences of each mouse (as well as the brain mask for each mouse) were affine-transformed to a common atlas space determined by the positions of the junction between the coronal suture and sagittal suture (posterior to the olfactory bulb and cerebrum along midline) and lambda, as previously reported (*43*). Bregma was not visible in all mice, and was calculated based on the above two anatomical landmarks. The anterior-posterior stretch was set equal to the medial-lateral stretch, and all transformed images were centered at bregma. The intersection of every brain mask was calculated and made symmetric by reflection across the midline allowing all subsequent comparisons to be performed on shared brain areas across all mice.

ISA correlation (functional connectivity) analysis

Functional connectivity was computed using Fisher's Z transformed correlation on pairs of pixel time series. Correlation difference PCA segmentation (Figs. 2B, 5F) was performed by applying

spatial principal components analysis to the whole-cortex correlation difference matrix calculated from the difference in average correlation at each pixel between the two groups.

Statistics

All single-dimension statistical comparisons were assessed with Student's t test. The statistical threshold was set at 0.05 divided by the number of comparisons performed. Statistical significance of correlation differences in spatial maps (Fig. 4.4I-L) was assessed on a cluster-wise basis using threshold-extent criteria computed by extensive permutation resampling (*44, 45*).

Acknowledgements

This work was supported in part by National Institutes of Health grants R01NS084028 (J.-M.L), F31NS089135 (A.W.K), R01NS078223 (J.P.C.), P01NS080675 (J.P.C.), P30NS048056 (A.Z.S.), NS080675 (M.E.R. and A.Z.S.), K25NS083754 (A.Q.B), F30MH106253 (A.M.) and American Heart Association grants 13POST14240023 (A.Q.B) and 14PRE18410013 (A.W.K).

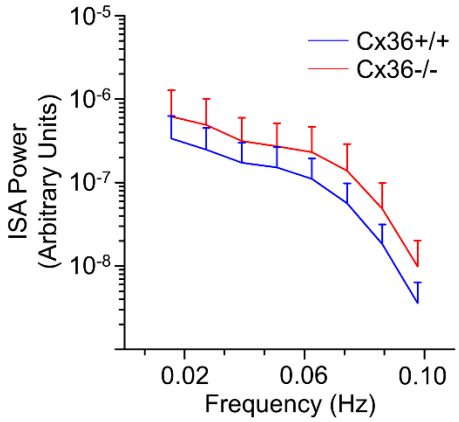

Figure 4.1. Cx36 gene deletion does not change ISA spectral power. The group-averaged spectral content over the infra-slow frequency band, calculated after filtering and global signal regression, and bin-averaging is plotted for Cx36+/+ and Cx36-/- mice. Error bars are standard deviation. For each ISA bin, differences between groups were not statistically significant. This demonstrates that the amount of ISA is not altered by Cx36 gene deletion. Error bars are standard deviation. Statistical significance was set at $P<0.0063$ (0.05/number of frequency bins; determined using Student's t test with Bonferonni correction). Cx36+/+ n=19, Cx36-/- n=13.

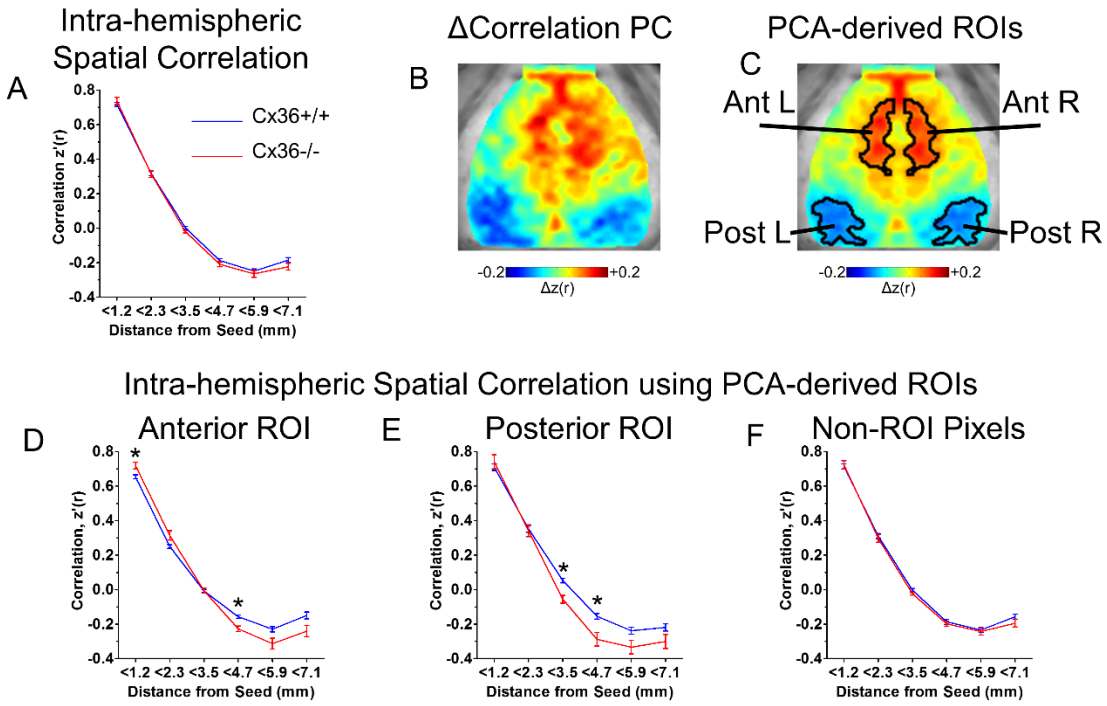

Figure 4.2. Cx36 deletion alters spatial ISA correlation relationships in specific cortical regions. **(A)** Group averaged correlation values vs. distance for every intra-hemispheric pixel. For each mouse, the correlation vs. distance curve from the left and right hemisphere were averaged before group averaging was performed. Using a subset of mice (Cx36+/+ n=3, Cx36-/- n=3), PCA was performed on the correlation differences between groups in order to find ROIs that may be selectively influenced by Cx36. **(B)** The first principal component derived from ΔCorrelation PCA reveals distinct anterior and posterior ROIs with ISA correlation patterns that differ between Cx36+/+ and Cx36-/- groups. **(C)** Anterior and Posterior ROIs defined after smoothing and bilateral averaging of the ΔCorrelation PC in (B). These ROIs were used for analysis on an independent set of mice (Cx36+/+ n=16, Cx36-/- n=10). **(D-E)** Spatial correlation values for pixels within the ROIs from (C). **(D)** Within the anterior ROI, Cx36 deletion caused increased correlation for nearby pixel pairs (<1.2mm), and increased anti-correlation for more distant pixel pairs (3.5mm-4.7mm). **(E)** Within the posterior ROI, Cx36 deletion resulted in increased anti-correlation at further distances (3.5mm-4.7mm). The correlation vs. distance curve was calculated between all pixels within the ROIs and every other pixel in the same hemisphere. **(F)** Correlation vs. distance relationship for pixels outside of the ROIs from (C). No differences were found for pixels in this area. *P<0.0083 (0.05/number of distance bins; determined using Student's t test with Bonferonni correction).

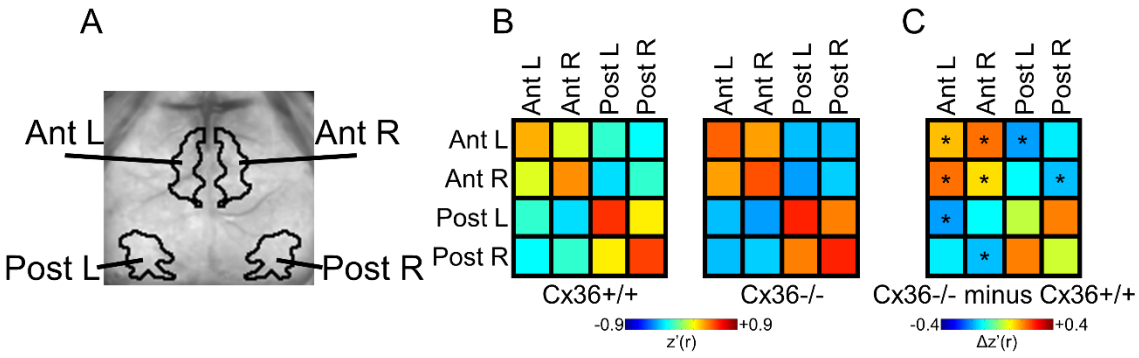

Figure 4.3. Cx36 deletion increases inter-hemispheric correlation and intra-hemispheric anti-correlation between specific ROIs. **(A)** ROIs used for analysis. **(B)** Average correlation values for all pixels within and between all ROIs in (A) in Cx36+/+ and Cx36-/- mice. **(C)** Cx36-/- minus Cx36+/+ ΔCorrelation matrix with statistically significant correlations marked. In the Ant. ROIs, within ROI correlation and homoptopic correlation was increased in Cx36-/- mice. In addition, the intra-hemispheric Ant.-Post. anti-correlation was increased in Cx36-/- mice. Post. ROI homotopic correlation was increased in Cx36-/- mice, but not statistically significant. *P<0.005 (0.05/number of correlations examined; determined using Student's t test with Bonferonni correction). Cx36+/+ n=16, Cx36-/- n=10.

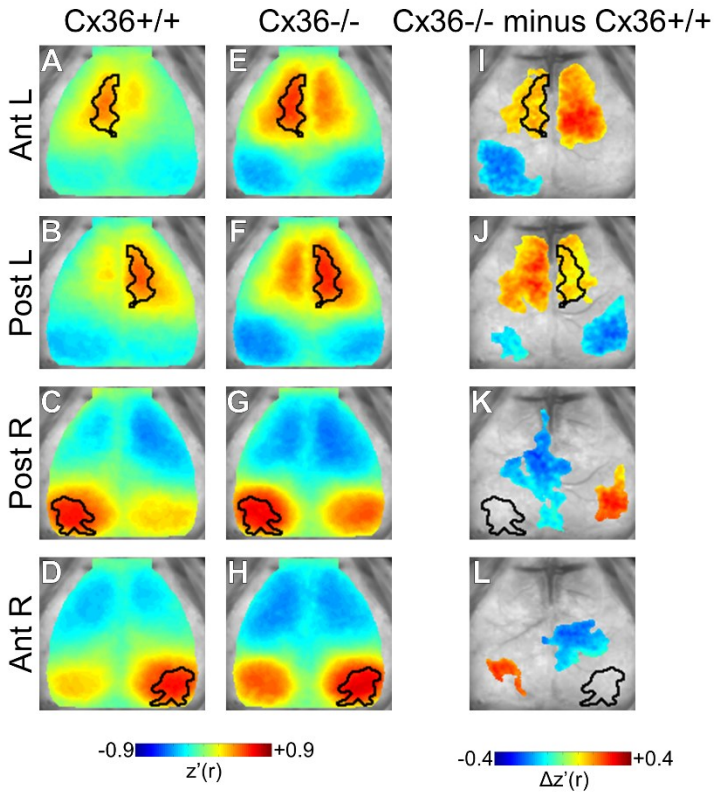

Figure 4.4. Spatial distribution of correlation changes with Cx36 deletion. Seeded correlation maps for **(A-D)** Cx36+/+ and **(E-H)** Cx36-/- mice. Seeded regions are outline in black. Enhanced homotopic correlation and intra-hemispheric anti-correlation are qualitatively apparent in Cx36-/- mice. **(I-L)** Statistically masked correlation difference maps (Cx36-/- minus Cx36+/+) for each ROI. Significance was determined using spatial cluster-wise threshold-extent criteria (see methods). **(I,J)** For Ant. ROIs, Cx36-/- mice demonstrated increased within ROI correlation, homotopic correlation was increased, and increased Ant.-Post. ROI anti-correlation for each hemisphere. **(K,L)** Post. ROIs showed regionally selective increases in intra-hemispheric anti-correlation and increased inter-hemispheric correlation. The inter-hemispheric correlation increases were centered outside of the homotopic Post. ROI. Cx36+/+ n=16, Cx36-/- n=10.

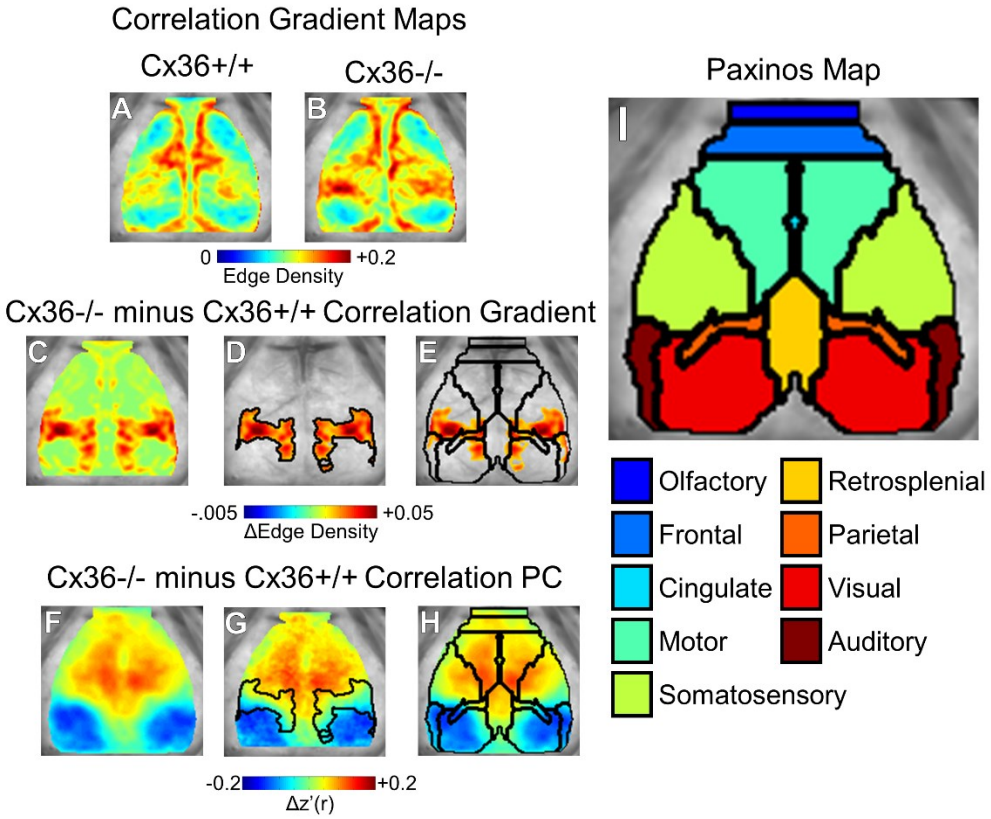

Figure 4.5. Cx36 deletion causes a more abrupt anterior-posterior correlation transition gradient. **(A-B)** Correlation gradient maps for **(A)** Cx36+/+ mice and **(B)** Cx36-/- mice. **(C)** Cx36-/- minus Cx36+/+ gradient difference map reveals a focally increased correlation transition gradient on the anterior-posterior axis. **(D)** Gradient differences threshold-masked and outlined. **(E)** Thresholded gradient differences shown with overlaid Paxinos anatomy shows that these gradient differences occur at the border of several anatomical regions separated on the anterior-posterior axis. **(F)** The Δcorrelation PC1 determined from PCA on correlation differences between all mice analyzed. This Δcorrelation PC1 is similar to the Δcorrelation PC1 found in a subset of mice in Fig. 4.2B. ΔCorrelation PC1 with overlaid **(G)** correlation gradient differences and **(H)** Paxinos anatomical boundaries. Panel G demonstrates that the correlation transition gradient was more abrupt in Cx36-/- mice. **(I)** Paxinos atlas for reference. Cx36+/+ n=19, Cx36-/- n=13.

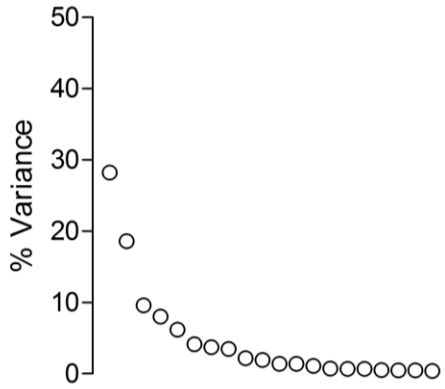

Figure 4.S1. Eigenspectrum for Δcorrelation PCA performed in Fig. 4.2B. Cx36+/+ n=3, Cx36-/- n=3. PC1 explains 28% of the variance and was used to determine ROIs for in subsequent analyses.

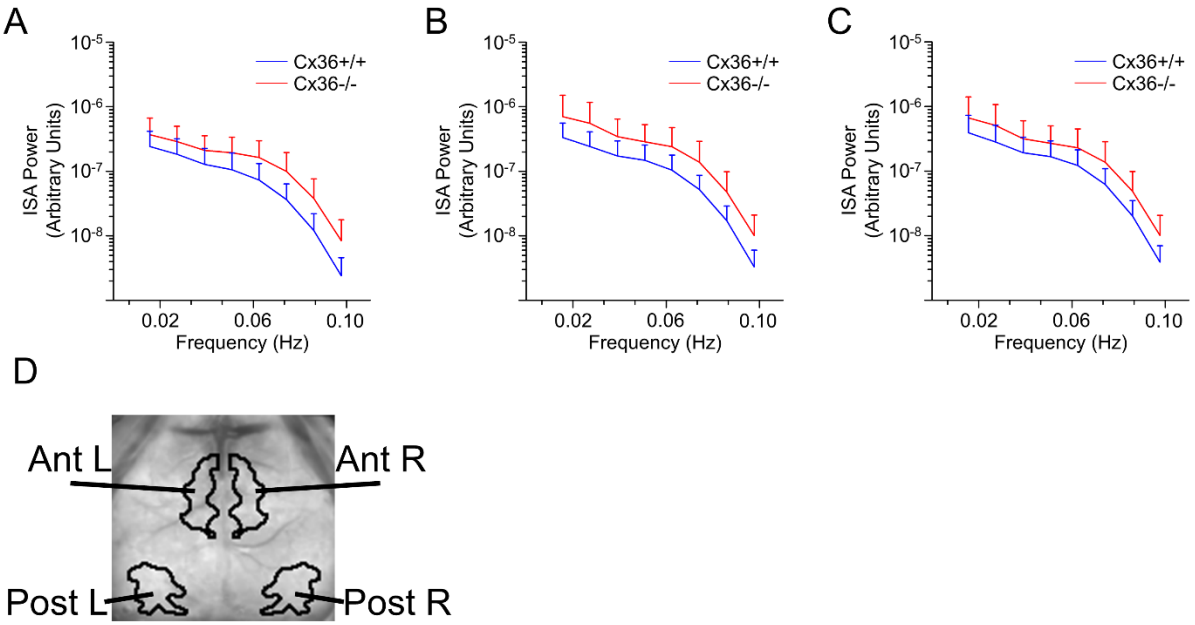

Figure 4.S2. Cx36 gene deletion does not alter ISA spectral power in Δcorrelation-derived ROIs. Correlation vs. distance for pixels in the **(A)** anterior ROIs, **(B)** posterior ROIs, and **(C)** not in any ROI. **(D)** ROI map for reference. These calculations were performed on the set of mice independent from those used to determine ROIs. Error bars are standard deviation. Statistical significance was determined using Student's t test with Bonferonni correction. Cx36+/+ n=16, Cx36-/- n=10

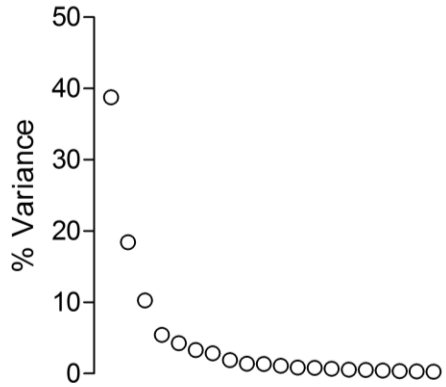

Figure 4.S3. Eigenspectrum for Δcorrelation PCA performed in Fig. 4.5F. Cx36+/+ n=19, Cx36-/- n=13. PC1 explains 39% of the variance.

References

1. B. J. He, J. M. Zempel, A. Z. Snyder, M. E. Raichle, The temporal structures and functional significance of scale-free brain activity. *Neuron* **66**, 353-369 (2010).

2. B. Biswal, F. Z. Yetkin, V. M. Haughton, J. S. Hyde, Functional connectivity in the motor cortex of resting human brain using echo-planar MRI. *Magn Reson Med* **34**, 537-541 (1995).

3. M. D. Fox *et al.*, The human brain is intrinsically organized into dynamic, anticorrelated functional networks. *Proc Natl Acad Sci U S A* **102**, 9673-9678 (2005).

4. J. D. Power *et al.*, Functional network organization of the human brain. *Neuron* **72**, 665-678 (2011).

5. T. O. Laumann *et al.*, Functional System and Areal Organization of a Highly Sampled Individual Human Brain. *Neuron* **87**, 657-670 (2015).

6. J. L. Vincent *et al.*, Intrinsic functional architecture in the anaesthetized monkey brain. *Nature* **447**, 83-86 (2007).

7. D. S. Grayson *et al.*, The Rhesus Monkey Connectome Predicts Disrupted Functional Networks Resulting from Pharmacogenetic Inactivation of the Amygdala. *Neuron* **91**, 453-466 (2016).

8. J. M. Stafford *et al.*, Large-scale topology and the default mode network in the mouse connectome. *Proc Natl Acad Sci U S A* **111**, 18745-18750 (2014).

9. B. R. White *et al.*, Imaging of functional connectivity in the mouse brain. *PLoS One* **6**, e16322 (2011).

10. A. R. Carter *et al.*, Resting interhemispheric functional magnetic resonance imaging connectivity predicts performance after stroke. *Ann Neurol* **67**, 365-375 (2010).

11. G. Allen *et al.*, Reduced hippocampal functional connectivity in Alzheimer disease. *Arch Neurol* **64**, 1482-1487 (2007).

12. A. Chase, Alzheimer disease: Altered functional connectivity in preclinical dementia. *Nat Rev Neurol* **10**, 609 (2014).

13. C. J. Honey *et al.*, Predicting human resting-state functional connectivity from structural connectivity. *Proc Natl Acad Sci U S A* **106**, 2035-2040 (2009).

14. D. Zhang *et al.*, Intrinsic functional relations between human cerebral cortex and thalamus. *J Neurophysiol* **100**, 1740-1748 (2008).

15. S. G. Hormuzdi *et al.*, Impaired electrical signaling disrupts gamma frequency oscillations in connexin 36-deficient mice. *Neuron* **31**, 487-495 (2001).

16. M. R. Deans, J. R. Gibson, C. Sellitto, B. W. Connors, D. L. Paul, Synchronous activity of inhibitory networks in neocortex requires electrical synapses containing connexin36. *Neuron* **31**, 477-485 (2001).

17. M. Galarreta, S. Hestrin, Electrical and chemical synapses among parvalbumin fast-spiking GABAergic interneurons in adult mouse neocortex. *Proc Natl Acad Sci U S A* **99**, 12438-12443 (2002).

18. Y. Wang, A. B. Belousov, Deletion of neuronal gap junction protein connexin 36 impairs hippocampal LTP. *Neurosci Lett* **502**, 30-32 (2011).

19. F. Postma *et al.*, Electrical synapses formed by connexin36 regulate inhibition- and experience-dependent plasticity. *Proc Natl Acad Sci U S A* **108**, 13770-13775 (2011).

20. C. Frisch *et al.*, Stimulus complexity dependent memory impairment and changes in motor performance after deletion of the neuronal gap junction protein connexin36 in mice. *Behav Brain Res* **157**, 177-185 (2005).

21. S. Bissiere *et al.*, Electrical synapses control hippocampal contributions to fear learning and memory. *Science* **331**, 87-91 (2011).

22. D. L. Buhl, K. D. Harris, S. G. Hormuzdi, H. Monyer, G. Buzsaki, Selective impairment of hippocampal gamma oscillations in connexin-36 knock-out mouse in vivo. *J Neurosci* **23**, 1013-1018 (2003).

23. E. M. Gordon *et al.*, Generation and Evaluation of a Cortical Area Parcellation from Resting-State Correlations. *Cereb Cortex* **26**, 288-303 (2016).

24. M. D. Greicius, B. Krasnow, A. L. Reiss, V. Menon, Functional connectivity in the resting brain: a network analysis of the default mode hypothesis. *Proc Natl Acad Sci U S A* **100**, 253-258 (2003).

25. R. Cabeza, L. Nyberg, Imaging cognition II: An empirical review of 275 PET and fMRI studies. *J Cogn Neurosci* **12**, 1-47 (2000).

26. M. Corbetta, G. L. Shulman, Control of goal-directed and stimulus-driven attention in the brain. *Nat Rev Neurosci* **3**, 201-215 (2002).

27. J. R. Simpson *et al.*, The emotional modulation of cognitive processing: an fMRI study. *J Cogn Neurosci* **12 Suppl 2**, 157-170 (2000).

28. J. R. Simpson, Jr., A. Z. Snyder, D. A. Gusnard, M. E. Raichle, Emotion-induced changes in human medial prefrontal cortex: I. During cognitive task performance. *Proc Natl Acad Sci U S A* **98**, 683-687 (2001).

29. K. A. McKiernan, J. N. Kaufman, J. Kucera-Thompson, J. R. Binder, A parametric manipulation of factors affecting task-induced deactivation in functional neuroimaging. *J Cogn Neurosci* **15**, 394-408 (2003).

30. D. A. Gusnard, M. E. Raichle, M. E. Raichle, Searching for a baseline: functional imaging and the resting human brain. *Nat Rev Neurosci* **2**, 685-694 (2001).

31. M. E. Raichle *et al.*, A default mode of brain function. *Proc Natl Acad Sci U S A* **98**, 676-682 (2001).

32. A. W. Chan, M. H. Mohajerani, J. M. LeDue, Y. T. Wang, T. H. Murphy, Mesoscale infraslow spontaneous membrane potential fluctuations recapitulate high-frequency activity cortical motifs. *Nat Commun* **6**, 7738 (2015).

33. C. P. Pawela *et al.*, Resting-state functional connectivity of the rat brain. *Magn Reson Med* **59**, 1021-1029 (2008).

34. Y. Ma *et al.*, Resting-state hemodynamics are spatiotemporally coupled to synchronized and symmetric neural activity in excitatory neurons. *Proc Natl Acad Sci U S A* **113**, E8463-E8471 (2016).

35. T. Matsui, T. Murakami, K. Ohki, Transient neuronal coactivations embedded in globally propagating waves underlie resting-state functional connectivity. *Proc Natl Acad Sci U S A* **113**, 6556-6561 (2016).

36. Y. Xie *et al.*, Resolution of High-Frequency Mesoscale Intracortical Maps Using the Genetically Encoded Glutamate Sensor iGluSnFR. *J Neurosci* **36**, 1261-1272 (2016).

37. A. Zlomuzica *et al.*, Behavioral alterations and changes in Ca/calmodulin kinase II levels in the striatum of connexin36 deficient mice. *Behav Brain Res* **226**, 293-300 (2012).

38. A. L. Hodgkin, W. A. Rushton, The electrical constants of a crustacean nerve fibre. *Proc R Soc Med* **134**, 444-479 (1946).

39. J. S. Bloom, G. W. Hynd, The role of the corpus callosum in interhemispheric transfer of information: excitation or inhibition? *Neuropsychol Rev* **15**, 59-71 (2005).

40. G. Silasi, D. Xiao, M. P. Vanni, A. C. Chen, T. H. Murphy, Intact skull chronic windows for mesoscopic wide-field imaging in awake mice. *J Neurosci Methods* **267**, 141-149 (2016).

41. D. Picchioni, J. H. Duyn, S. G. Horovitz, Sleep and the functional connectome. *Neuroimage* **80**, 387-396 (2013).

42. S. R. Arridge, M. Cope, D. T. Delpy, The theoretical basis for the determination of optical pathlengths in tissue: temporal and frequency analysis. *Phys Med Biol* **37**, 1531-1560 (1992).

43. A. Q. Bauer *et al.*, Optical imaging of disrupted functional connectivity following ischemic stroke in mice. *Neuroimage* **99**, 388-401 (2014).

44. S. Hayasaka, T. E. Nichols, Validating cluster size inference: random field and permutation methods. *Neuroimage* **20**, 2343-2356 (2003).

45. C. D. Hacker, J. S. Perlmutter, S. R. Criswell, B. M. Ances, A. Z. Snyder, Resting state functional connectivity of the striatum in Parkinson's disease. *Brain* **135**, 3699-3711 (2012).

Chapter 5

Conclusion

Summary of findings

The collection of work contained in this dissertation has demonstrated components of excitatory and inhibitory synaptic plasticity that modulate functional organization in the cortex. The specific conclusions are:

1. Focal sensory deprivation can modulate task-evoked and resting-state functional cortex organization through an Arc-dependent mechanism.
2. Focal somatosensory deprivation can accelerate and reposition functional representation remapping after somatosensory cortex infarction. This also results in improved behavioral recovery, and these changes persist after sensory deprivation is withdrawn.
3. Focal visual deprivation modifies spontaneous activity relationships involving the visual system. Partial (monocular) and complete (binocular) deprivation have differential effects, with partial deprivation resulting in intra-network correlation changes (within visual system) and complete deprivation resulting in inter-network correlation changes.
4. Arc is required for post-infarction remapping and behavioral recovery.
5. Arc is required for intra- and inter-network spontaneous activity organization plasticity.
6. Electrically coupled inhibitory interneuron (IIN) networks limit spontaneous coupling between distant cortical regions.

As predicted from the critical period literature, synaptic mechanisms within both excitatory and inhibitory neurons drive functional cortex organization plasticity. This suggests that the critical period model of excitatory-inhibitory balance controlling plasticity may also apply to functional cortex organization changes during development and in recovery following neurologic injury.

Cortical remapping as a modifiable therapeutic target

Cortical remapping after focal injury was first reported over 20 years ago (*1*). Since then, the same phenomenon has been observed in rodent models and human patients (*2*-*9*). Moreover, it was

repeatedly seen that remapping occurred in conjunction with behavioral recovery, arguing for the importance of this process in reversing disability (*2, 3, 5*). However, there was no evidence that modifying remapping influenced behavioral recovery.

Chapter 2 of this dissertation demonstrates that 1) disrupting remapping (via Arc gene deletion) prevents behavioral recovery and that 2) accelerating remapping (via whisker trimming) improves behavioral recovery. These findings establish that manipulating functional cortex organization after focal ischemic injury can influence behavioral recovery. Further, it suggests rehabilitative maneuvers, such as targeted sensory deprivation, may be an effective approach for promoting remapping in stroke patients.

Relationship between task-evoked remapping and spontaneous activity

Like task-evoked cortical remapping, spontaneous activity relationships, or functional connectivity, changes after focal ischemia are known to correlate with behavioral recovery (*10-12*). However, this relationship remains correlational and it is unclear how important functional connectivity plasticity is for recovery. Furthermore, the relationship between post-ischemic task-evoked remapping and resting-state functional connectivity plasticity remains unclear. Separate studies have shown that these two phenomena both correlate with behavioral recovery (*1-3, 10-12*). While I was able to establish the role of representation remapping in behavioral recovery after ischemic injury, the relationship between task-evoked representation remapping and resting-state correlation network plasticity remain unclear. Given the finding in healthy brains that spontaneous correlation occurs between areas that are co-activated during specific tasks, it is likely the case that inter-hemispheric correlation recovery is dependent on remapping. However, the time course of these two phenomenon has not been compared directly. The paradigms established in Chapter 2 offer an approach that can prevent and relocate remapping. This will be valuable for examining the relationship between task-evoked map and spontaneous network plasticity following ischemia, and determining the importance spontaneous network plasticity in

behavioral recovery. In addition, experiments examining task-evoked remapping and functional connectivity plasticity may offer insight into how remapped local circuits integrate with global networks after ischemic injury.

Excitatory neuron mechanisms in cortical functional organization plasticity: a role for Arc

A role for Arc in experience-dependent plasticity has been demonstrated broadly in several settings: Arc-/- mice had attenuated critical period ocular dominance plasticity (*13*); adult Arc-/- mice had attenuated visual orientation learning with repeated orientation presentation (*14*); Arc-/- mice had profound deficits in memory consolidation, and brain slices from Arc-/- mice showed attenuated LTP and LTD (*15*). Importantly, pre-critical period visually-evoked responses were identical in Arc+/+ and Arc-/- mice, demonstrating Arc-mediated effects are specific to experience-dependent plastic change. The experiments performed in this dissertation establish an additional role for Arc in driving functional cortex reorganization after injury and during development.

Several studies have implicated Arc as a key regulator of structural, Hebbian, and homeostatic synaptic plasticity (*16*). More specifically, Arc has been shown to influence dendritic spine dynamics, LTP and LTD durability, as well as whole-neuron synaptic scaling. The best understood mechanism by which Arc influences plasticity concerns its regulation of synaptic strength via control of glutamate receptors. Arc regulates glutamate receptor levels at multiple scales, from individual synapses to the entire neuron (*17-20*). At the individual synapse level, Arc has been shown to target silent dendrites during activation of adjacent dendrites in the same neuron (*19*). Through this mechanism, Arc facilitates the selective removal of silent synapses. In addition, Arc has been shown to translocate to the nucleus and initiate whole-neuron decreases in glutamate receptor production, enabling scaling of synaptic strength throughout the entire neuron (*18, 20*).

Thus, this work establishes Arc-dependent synaptic plasticity as a cellular mechanism required for remapping after ischemia and functional connectivity changes during development. However, the exact components of Arc-dependent mechanisms involved are unclear. Given the complexity

inherent in systems-level organization, it is certainly plausible that several arms of Arc-dependent mechanism participate in these phenomena, but future work will be needed to examine this in detail. It is also worth highlighting that the Arc manipulations performed in this dissertation demonstrate a role for excitatory neuron mechanisms in functional organization plasticity.

Electrically coupled inhibitory interneuron networks modulate cortical functional organization

Visual critical period work has demonstrated an essential role for GABAergic signaling in experience dependent cortical development (*21*). Thus, we expected inhibitory interneuron networks to play an important role in shaping functional organization in the cerebral cortex.

Electrically coupled IIN networks were an attractive candidate for modulating spatial synchrony in spontaneous neural oscillations. It has already been shown that Cx36 gene deletion, which disrupts IIN electrical coupling, attenuated spatial learning and ocular dominance plasticity. Moreover, Cx36 deletion also caused subtle changes in gamma and theta oscillation power that occurs during these plasticity paradigms (*22-26*).

The experiments performed in this dissertation demonstrate that electrically coupled IIN networks play an important role in decoupling spontaneous infra-slow activity synchrony between cortical regions separated by long distances. Thus, IIN networks may be targeted to alter communication between separate brain systems.

It is important to keep in mind that electrical coupling between inhibitory interneurons has a poorly understand influence on inhibitory tone at large. It is also unclear how electrically coupled IIN networks influence relationships over distances thought to be greater than the span of the IIN network. It is likely that neurons project to local IIN networks to achieve long-distance coordination. Future work will take advantage of advanced tools in molecular biology to answer these questions (see below).

Tuning spontaneous activity correlation to the appropriate level

A fascinating component seen both with critical period visual deprivation and Cx36 gene deletion is that disrupting natural processes can increase homotopic functional connectivity. Many studies have utilized functional connectivity as a biomarker, and a correlation between behavioral deficit and functional connectivity has been shown in several neurologic diseases (*11, 27-29*). From a biomarker perspective, this has led to the thinking that higher homotopic correlation in functional connectivity is better. However, this work demonstrates that certain experimental manipulations, which result in neurologic deficits, generate heightened functional connectivity levels.

More specifically, binocular deprivation in wild-type mice results in enhanced visual homotopic correlation, and this did not occur in Arc-/- mice. This suggests that visual experience decreases homotopic correlation to an appropriate level through an Arc-dependent mechanism. In addition, disrupting electrically coupled inhibitory interneuron networks via Cx36 gene deletion resulted in increased homotopic functional connectivity in between specific cortical regions. Cx36-/- mice are known to have various plasticity deficits as well (*23, 26, 30*). In addition to homotopic changes, Arc deletion prevented critical period cross-modal spontaneous correlation changes, and Cx36 deletion altered cross-modal correlation as well. Altogether these findings demonstrate that processes within excitatory and inhibitory neurons play a role in tuning spontaneous correlations to a specific level.

This tuning may be essential for establishing the ideal balance in cross-system independence and integration which must achieved for optimized brain function. Over-synchronization across all systems may limit the ability of each brain system to handle specific tasks independently. One the other hand, complete dyssynchrony may prevent the cross-system communication required for high order tasks.

Plasticizing the adult brain

Critical periods demonstrate a clear plasticity decrease in the adult brain compared to children. In humans, visual and language critical periods are the best demonstration of this (*31, 32*). Of course, it is also clear from human observation and animal model experimentation that adult plasticity, while slower, still occurs (*33*).

In the context of this dissertation, improved adult plasticity is suggested as the answer for reversing chronic disability following neurologic injury. More broadly, the idea of enhanced adult plasticity more broadly comes with the desirable idea of infinite, rapid learning potential throughout life. However, the fact that robust plasticity occurs in limited windows must have some evolutionary advantage, and several potential advantages can be imagined. For example, critical periods may allow specialization in cortical neurons to occur and remain in place without constant exposure—allowing certain “lessons” to be kept. In addition, critical period learning likely comes with extensive energy demands, and a system that learns once is likely much more efficient. This is consistent with PET studies showing brain glucose utilization is highest from 4-10 years of age (*34*).

However, this rigidness is maladaptive in the case of focal ischemia where limited plasticity results in chronic disability. It is promising to see that functional map organization can be modulated with implications for therapeutic gain in a preclinical ischemia model. Indeed, it is exciting to speculate what the clinical potential of this approach might be. Furthermore, my findings that focal manipulations modulate specific cortical regions suggests that we can design strategies to selectively boost plasticity where needed.

Targeted facilitation of cortical plasticity with sensory deprivation

Two separate sensory deprivation paradigms were used in this dissertation: somatosensory deprivation (via whisker trimming) and visual deprivation (via eyelid suture). Given potential concerns with potentiating global plasticity (as mentioned in the previous section), raising

plasticity focally within the perilesional territory may be favorable. In the setting of focal ischemia, the recovery benefits resulting from focal deprivation are especially promising.

However, stroke in human patients occurs in a variety of locations. Currently, it is unclear how many separate systems might offer use deprivation. Most pertinent is the motor system. Will somatosensory deprivation improve motor recovery after infarction involving the motor cortex? Given the intimate interconnection between the sensory and motor system, this may be the case. However, motor cortex infarction may be better treated with perilesional motor deprivation. This could be achieved by limb casting or botulinum toxin A injections targeted to muscle groups with perilesional representations. Given the more recent realization that motor cortex is arranged in coordinated postures, target selection may be more challenging and will have to be addressed in future work.

Stroke, of course, can cause disability in higher level cognition. Language and attention disabilities are particularly devastating. It will be interesting to see if perilesional deprivation offers therapeutic potential for recovery of networks involved in these systems.

Enhancing plasticity with direct cortical manipulation

In addition to manipulating the cortex with interventions applied to the periphery, cortical plasticity will certainly be modifiable with agents that act on the brain directly. Indeed, pharmacologic blockade of GABAergic signaling can alter visual critical period timing and improve behavioral recovery after cortical infarction (*21, 35*). However, increasing cortical plasticity globally may not be favorable as improvements to the injured region may come with unwanted plasticity in uninjured domains.

Invasive and noninvasive transcranial stimulation techniques have been used on stroke patients in an attempt to manipulate excitability on a targeted hemisphere (both the ipsilesional and contralesional hemispheres have been targeted). Unfortunately, the results have been mixed with

larger randomized controlled trials showing no benefit (*36, 37*). This suggests inadequate understanding of how circuits need to be manipulated to improve plasticity.

Improvements in molecular biology have enabled regionally selective manipulation of cortical excitation and inhibition. Prime examples of this include optogenetics and chemogenetics. These tools involve expressing light or chemical sensitive channels in genetically defined neural populations. Using viral gene transfer, these channels can be targeted to specific neuron subtypes in targeted regions. By application of light or chemicals reversible excitation or inhibition to the targeted cell type can be applied (*38, 39*).

In the preclinical setting, this offers a tool kit that dissect the contribution of specific neural circuits in functional cortex organization in health and after injury. For example, instead of applying perilesional sensory deprivation, one could focally block inhibitory interneuron activity in the perilesional cortex. Indeed, applying this to the visual cortex has been shown to extend the visual critical period (*40*). In addition to focal manipulation, these tools can be used to globally manipulate activity in inhibitory interneurons. Compared to gene deletion experiments, this would allow direct examination of how activity from inhibitory interneurons influences functional networks. Further, these manipulations are reversible and avoid off-target development compensation that can result from gene deletion.

In addition to affecting GABAergic neurons broadly, the specific interneuron subtypes can be selectively modulated. This might be especially important as interneuron subtypes, defined by specific protein expression, have distinct circuit arrangements. Subcategories of note include parvalbumin (PV) interneurons, somatostatin (SOM) interneurons, and vasoactive intensitnal polypeptide (VIP) interneurons (*41*).

Although these inhibitory neurons are involved in complex feed-forward and feed-back inhibitory circuits, their broad influences can be generalized: PV and SOM interneurons inhibit pyramidal cells, whereas VIP interneurons inhibit SOM interneurons. PV and SOM interneurons can be

further classified by their synaptic localization with PV neurons synapses on excitatory neuron cell bodies (*42-44*) and SOM neurons synapses on excitatory neuron dendrites (*30, 43, 45*).

This arrangement is generalizable throughout the cortex and appears to be essential for integrating signals across systems. Unsurprisingly, each of these inhibitory interneuron subtypes have been shown to play a role in cortical plasticity (*46*). However, given the non-equivalent relationship of each neuron subtype in generating excitatory-inhibitory balance, understanding individual subtype contributions may be important.

For example, inhibiting PV neuron activity can extend the visual critical period (*40*) whereas enhancing VIP neuron activity can have the same effect (*47*). This dichotomy is not surprising given the known circuitry arrangement of these IIN subtypes. However, it suggests that therapeutic approaches may be more successful if they are more selective in action. In addition, inhibitory activity from each of these interneuron subtypes is likely to contribute distinct features to spontaneous oscillatory neural activity. Future work addressing these questions will be critical in order to understand how specific cellular circuits contribute to functional organization within the cortex, and how specific components of neurocircuitry can be manipulated for therapeutic gain. With current clinical approaches to cortical stimulation after stroke appearing somewhat random (and resulting in no benefits) (*36, 37*), these studies will be especially valuable for rationale cortical stimulation design.

Examining higher frequency content in functional organization relationships

Throughout this dissertation, functional cortex organization was assayed using a hemodynamic contrast. The hemodynamic response is a relatively slow phenomenon, and this creates a serious limitation on the frequencies that can be measured using it. Furthermore, fMRI, which generated the bulk of the foundation of this work, is additionally limited by framerate.

Spontaneous brain oscillations occur over a wide frequency range (<0.01Hz – 600Hz), and hemodynamic contrasts cannot access much of this spectral range (*48*). Although infraslow activity (0.1Hz – 0.01Hz) is clearly important for neurologic function, other components of this broadband activity must be involved. This dissertation, and many cited studies within, argue for infraslow activity's importance in systems-level neurophysiology. However, it may be the case that treating systems-scale neurologic disorders will require understanding the cross-frequency interplay over the entire range at which brain activity occurs.

Emerging technology promises to open up the frequency range that can be examined over large brain volumes. Genetically encoded calcium indicators and genetically encoded voltage sensitive reporters offer faster kinetics and access to high frequency content of the brain's activity. Calcium imaging with GCaMP-expressing mice have already enabled wide-field imaging in the delta frequency range (*49, 50*). These experiments have been especially valuable in revealing wave propagation across the cortex. Voltage sensitive dyes have been used to examine even faster frequency ranges, with limits being set by the imaging frame rate (*51*). Unfortunately, these dyes involve invasive procedures and heavy anesthesia. Improvements in genetically encoded voltage sensitive reporters will be helpful.

Electrophysiological recordings offer sampling rates up to 30KHz (*52*). The limit for these approaches has been placing sufficient numbers of probes to observe systems-level communication. Improvement in probe materials has enabled high density probes that can be placed over large brain volumes. Further, these probes have thicknesses as small as 10 microns, limiting that amount of damage they cause on placement. Current techniques enable thousands of recording sites, and this makes sampling large volumes of brain at up to 30KHz possible.

All of these techniques will be valuable tools for better understanding the brain activity at a systems-level, and improve our model of neurologic function in health and disease in order to improve neurorehabilitation.

Concluding Remarks

Pursuing a better understanding of the mechanisms that generate functional organization within the cerebral cortex, and plasticity of this organization, may dramatically advance neurorehabilitation options for stroke patients with chronic disability. In addition, these pursuits may lead to an improved understanding of how the brain works, and this may have important implications for treating neurological disease at large.

Functional connectivity disruptions, as measured with fMRI, are not unique to ischemic stroke. Disrupted functional connectivity been reported in other types of nervous sytem injury including subarachnoid hemorrhage, spinal cord injury traumatic brain injury, and peripheral nerve injury (*53-55*). In addition several reports have found aberrant functional connectivity in multiple psychiatric diseases.

In schizophrenia and biopolar disorder, reduced functional connectivity between prefrontal, parietal, and temporal cortices has been reported (*56, 57*). This is consistent with additional studies finding generalized functional connectivity decreases between cortical regions in patients diagnosed with schizophrenia (*58, 59*). In addition to cortical abnormalities, there is also evidence Schizophrenia is associated with aberrant functional connectivity between cortical and thalamic regions (*60, 61*).

Autism spectrum disorder offers another example of altered functional connectivity in a psychiatric disorder. fMRI studies on patients diagnosed with autism spectrum disorders have produced discordant findings: some studies have found increased functional connectivity while other have found decreased functional connectivity in inter- and intra- hemispheric relationships (*62-70*). There may be many reasons for these discrepancies including small sample sizes, different analytic approaches, and reliance on a categorical diagnosis for a particularly heterogeneous syndrome. Nonetheless, these studies suggest functional connectivity is perturbed in autism spectrum disorder patients.

These psychiatric diseases are unique because, unlike the other listed examples, there are not known anatomical defects involved. Thus, disrupted communication between brain systems may be the primary defect. If so, techniques that enable adjustments in functional cortex spontaneous activity relationships would be especially valuable for treating psychiatric disease.

Indeed, the neurologic relevance of function connectivity remains elusive. However, it is exciting to speculate that the observed connectivity alterations seen in so many different types of disease are indicative of pathologic communication between brain systems. Hopefully an improved understanding of what this physiology represents, and how it can be modulated, will advance our therapeutic approaches to these complex psychiatric and neurological disorders.

References

1. R. J. Nudo, B. M. Wise, F. SiFuentes, G. W. Milliken, Neural substrates for the effects of rehabilitative training on motor recovery after ischemic infarct. *Science* **272**, 1791-1794 (1996).

2. J. A. Jablonka, K. Burnat, O. W. Witte, M. Kossut, Remapping of the somatosensory cortex after a photothrombotic stroke: dynamics of the compensatory reorganization. *Neuroscience* **165**, 90-100 (2010).

3. C. E. Brown, K. Aminoltejari, H. Erb, I. R. Winship, T. H. Murphy, In vivo voltage-sensitive dye imaging in adult mice reveals that somatosensory maps lost to stroke are replaced over weeks by new structural and functional circuits with prolonged modes of activation within both the peri-infarct zone and distant sites. *J Neurosci* **29**, 1719-1734 (2009).

4. I. R. Winship, T. H. Murphy, In vivo calcium imaging reveals functional rewiring of single somatosensory neurons after stroke. *J Neurosci* **28**, 6592-6606 (2008).

5. R. M. Dijkhuizen *et al.*, Correlation between brain reorganization, ischemic damage, and neurologic status after transient focal cerebral ischemia in rats: a functional magnetic resonance imaging study. *J Neurosci* **23**, 510-517 (2003).

6. R. M. Dijkhuizen *et al.*, Functional magnetic resonance imaging of reorganization in rat brain after stroke. *Proc Natl Acad Sci U S A* **98**, 12766-12771 (2001).

7. C. Weiller, F. Chollet, K. J. Friston, R. J. Wise, R. S. Frackowiak, Functional reorganization of the brain in recovery from striatocapsular infarction in man. *Ann Neurol* **31**, 463-472 (1992).

8. S. C. Cramer *et al.*, A functional MRI study of subjects recovered from hemiparetic stroke. *Stroke* **28**, 2518-2527 (1997).

9. H. Reddy, N. De Stefano, M. Mortilla, A. Federico, P. M. Matthews, Functional reorganization of motor cortex increases with greater axonal injury from CADASIL. *Stroke* **33**, 502-508 (2002).

10. M. P. van Meer *et al.*, Recovery of sensorimotor function after experimental stroke correlates with restoration of resting-state interhemispheric functional connectivity. *J Neurosci* **30**, 3964-3972 (2010).

11. A. R. Carter *et al.*, Resting interhemispheric functional magnetic resonance imaging connectivity predicts performance after stroke. *Ann Neurol* **67**, 365-375 (2010).

12. L. E. Ramsey *et al.*, Normalization of network connectivity in hemispatial neglect recovery. *Ann Neurol* **80**, 127-141 (2016).

13. C. L. McCurry *et al.*, Loss of Arc renders the visual cortex impervious to the effects of sensory experience or deprivation. *Nat Neurosci* **13**, 450-457 (2010).

14. K. H. Wang *et al.*, In vivo two-photon imaging reveals a role of arc in enhancing orientation specificity in visual cortex. *Cell* **126**, 389-402 (2006).

15. N. Plath *et al.*, Arc/Arg3.1 is essential for the consolidation of synaptic plasticity and memories. *Neuron* **52**, 437-444 (2006).

16. E. Korb, S. Finkbeiner, Arc in synaptic plasticity: from gene to behavior. *Trends Neurosci* **34**, 591-598 (2011).

17. S. Chowdhury *et al.*, Arc/Arg3.1 interacts with the endocytic machinery to regulate AMPA receptor trafficking. *Neuron* **52**, 445-459 (2006).

18. J. D. Shepherd *et al.*, Arc/Arg3.1 mediates homeostatic synaptic scaling of AMPA receptors. *Neuron* **52**, 475-484 (2006).

19. H. Okuno *et al.*, Inverse synaptic tagging of inactive synapses via dynamic interaction of Arc/Arg3.1 with CaMKIIbeta. *Cell* **149**, 886-898 (2012).

20. E. Korb, C. L. Wilkinson, R. N. Delgado, K. L. Lovero, S. Finkbeiner, Arc in the nucleus regulates PML-dependent GluA1 transcription and homeostatic plasticity. *Nat Neurosci* **16**, 874-883 (2013).

21. T. K. Hensch, Critical period plasticity in local cortical circuits. *Nat Rev Neurosci* **6**, 877-888 (2005).

22. S. Bissiere *et al.*, Electrical synapses control hippocampal contributions to fear learning and memory. *Science* **331**, 87-91 (2011).

23. F. Postma *et al.*, Electrical synapses formed by connexin36 regulate inhibition- and experience-dependent plasticity. *Proc Natl Acad Sci U S A* **108**, 13770-13775 (2011).

24. D. L. Buhl, K. D. Harris, S. G. Hormuzdi, H. Monyer, G. Buzsaki, Selective impairment of hippocampal gamma oscillations in connexin-36 knock-out mouse in vivo. *J Neurosci* **23**, 1013-1018 (2003).

25. S. G. Hormuzdi *et al.*, Impaired electrical signaling disrupts gamma frequency oscillations in connexin 36-deficient mice. *Neuron* **31**, 487-495 (2001).

26. C. Frisch *et al.*, Stimulus complexity dependent memory impairment and changes in motor performance after deletion of the neuronal gap junction protein connexin36 in mice. *Behav Brain Res* **157**, 177-185 (2005).

27. C. D. Hacker, J. S. Perlmutter, S. R. Criswell, B. M. Ances, A. Z. Snyder, Resting state functional connectivity of the striatum in Parkinson's disease. *Brain* **135**, 3699-3711 (2012).

28. G. Allen *et al.*, Reduced hippocampal functional connectivity in Alzheimer disease. *Arch Neurol* **64**, 1482-1487 (2007).

29. A. Chase, Alzheimer disease: Altered functional connectivity in preclinical dementia. *Nat Rev Neurol* **10**, 609 (2014).

30. E. E. Fanselow, K. A. Richardson, B. W. Connors, Selective, state-dependent activation of somatostatin-expressing inhibitory interneurons in mouse neocortex. *J Neurophysiol* **100**, 2640-2652 (2008).

31. E. L. Newport, *Biological Foundations of Language*. (Wiley, New York, NY, 1967).

32. T. L. Lewis, D. Maurer, Multiple sensitive periods in human visual development: evidence from visually deprived children. *Dev Psychobiol* **46**, 163-183 (2005).

33. Y. Tagawa, P. O. Kanold, M. Majdan, C. J. Shatz, Multiple periods of functional ocular dominance plasticity in mouse visual cortex. *Nat Neurosci* **8**, 380-388 (2005).

34. H. T. Chugani, A critical period of brain development: studies of cerebral glucose utilization with PET. *Prev Med* **27**, 184-188 (1998).

35. A. N. Clarkson, B. S. Huang, S. E. Macisaac, I. Mody, S. T. Carmichael, Reducing excessive GABA-mediated tonic inhibition promotes functional recovery after stroke. *Nature* **468**, 305-309 (2010).

36. J. Seniow *et al.*, Transcranial magnetic stimulation combined with physiotherapy in rehabilitation of poststroke hemiparesis: a randomized, double-blind, placebo-controlled study. *Neurorehabil Neural Repair* **26**, 1072-1079 (2012).

37. R. M. Levy *et al.*, Epidural Electrical Stimulation for Stroke Rehabilitation: Results of the Prospective, Multicenter, Randomized, Single-Blinded Everest Trial. *Neurorehabil Neural Repair* **30**, 107-119 (2016).

38. L. Fenno, O. Yizhar, K. Deisseroth, The development and application of optogenetics. *Annu Rev Neurosci* **34**, 389-412 (2011).

39. S. M. Sternson, B. L. Roth, Chemogenetic tools to interrogate brain functions. *Annu Rev Neurosci* **37**, 387-407 (2014).

40. S. J. Kuhlman *et al.*, A disinhibitory microcircuit initiates critical-period plasticity in the visual cortex. *Nature* **501**, 543-546 (2013).

41. H. Markram *et al.*, Interneurons of the neocortical inhibitory system. *Nat Rev Neurosci* **5**, 793-807 (2004).

42. P. Somogyi, Z. F. Kisvarday, K. A. Martin, D. Whitteridge, Synaptic connections of morphologically identified and physiologically characterized large basket cells in the striate cortex of cat. *Neuroscience* **10**, 261-294 (1983).

43. Y. Kawaguchi, Y. Kubota, Neurochemical features and synaptic connections of large physiologically-identified GABAergic cells in the rat frontal cortex. *Neuroscience* **85**, 677-701 (1998).

44. Y. Kubota, Y. Kawaguchi, Dependence of GABAergic synaptic areas on the interneuron type and target size. *J Neurosci* **20**, 375-386 (2000).

45. Y. Wang *et al.*, Anatomical, physiological and molecular properties of Martinotti cells in the somatosensory cortex of the juvenile rat. *J Physiol* **561**, 65-90 (2004).

46. D. van Versendaal, C. N. Levelt, Inhibitory interneurons in visual cortical plasticity. *Cell Mol Life Sci* **73**, 3677-3691 (2016).

47. Y. Fu, M. Kaneko, Y. Tang, A. Alvarez-Buylla, M. P. Stryker, A cortical disinhibitory circuit for enhancing adult plasticity. *Elife* **4**, e05558 (2015).

48. B. J. He, J. M. Zempel, A. Z. Snyder, M. E. Raichle, The temporal structures and functional significance of scale-free brain activity. *Neuron* **66**, 353-369 (2010).

49. Y. Ma *et al.*, Resting-state hemodynamics are spatiotemporally coupled to synchronized and symmetric neural activity in excitatory neurons. *Proc Natl Acad Sci U S A* **113**, E8463-E8471 (2016).

50. T. Matsui, T. Murakami, K. Ohki, Transient neuronal coactivations embedded in globally propagating waves underlie resting-state functional connectivity. *Proc Natl Acad Sci U S A* **113**, 6556-6561 (2016).

51. A. W. Chan, M. H. Mohajerani, J. M. LeDue, Y. T. Wang, T. H. Murphy, Mesoscale infraslow spontaneous membrane potential fluctuations recapitulate high-frequency activity cortical motifs. *Nat Commun* **6**, 7738 (2015).

52. J. M. Li, W. J. Bentley, L. H. Snyder, Functional connectivity arises from a slow rhythmic mechanism. *Proc Natl Acad Sci U S A* **112**, E2527-2535 (2015).

53. M. C. Stevens *et al.*, Multiple resting state network functional connectivity abnormalities in mild traumatic brain injury. *Brain Imaging Behav* **6**, 293-318 (2012).

54. A. Iraji *et al.*, Resting State Functional Connectivity in Mild Traumatic Brain Injury at the Acute Stage: Independent Component and Seed-Based Analyses. *J Neurotrauma* **32**, 1031-1045 (2015).

55. M. Maher *et al.*, Altered Resting-State Connectivity within Executive Networks after Aneurysmal Subarachnoid Hemorrhage. *PLoS One* **10**, e0130483 (2015).

56. J. T. Baker *et al.*, Disruption of cortical association networks in schizophrenia and psychotic bipolar disorder. *JAMA Psychiatry* **71**, 109-118 (2014).

57. Y. Zhou *et al.*, Functional disintegration in paranoid schizophrenia using resting-state fMRI. *Schizophr Res* **97**, 194-205 (2007).

58. Y. Liu *et al.*, Disrupted small-world networks in schizophrenia. *Brain* **131**, 945-961 (2008).

59. M. Liang *et al.*, Widespread functional disconnectivity in schizophrenia with resting-state functional magnetic resonance imaging. *Neuroreport* **17**, 209-213 (2006).

60. N. D. Woodward, H. Karbasforoushan, S. Heckers, Thalamocortical dysconnectivity in schizophrenia. *Am J Psychiatry* **169**, 1092-1099 (2012).

61. N. D. Woodward, C. J. Cascio, Resting-State Functional Connectivity in Psychiatric Disorders. *JAMA Psychiatry* **72**, 743-744 (2015).

62. M. A. Just, V. L. Cherkassky, T. A. Keller, N. J. Minshew, Cortical activation and synchronization during sentence comprehension in high-functioning autism: evidence of underconnectivity. *Brain* **127**, 1811-1821 (2004).

63. M. K. Belmonte *et al.*, Autism and abnormal development of brain connectivity. *J Neurosci* **24**, 9228-9231 (2004).

64. S. E. Schipul, T. A. Keller, M. A. Just, Inter-regional brain communication and its disturbance in autism. *Front Syst Neurosci* **5**, 10 (2011).

65. I. Dinstein *et al.*, Disrupted neural synchronization in toddlers with autism. *Neuron* **70**, 1218-1225 (2011).

66. J. S. Anderson *et al.*, Decreased interhemispheric functional connectivity in autism. *Cereb Cortex* **21**, 1134-1146 (2011).

67. A. Di Martino *et al.*, The autism brain imaging data exchange: towards a large-scale evaluation of the intrinsic brain architecture in autism. *Mol Psychiatry* **19**, 659-667 (2014).

68. C. L. Keown *et al.*, Local functional overconnectivity in posterior brain regions is associated with symptom severity in autism spectrum disorders. *Cell Rep* **5**, 567-572 (2013).

69. K. Supekar *et al.*, Brain hyperconnectivity in children with autism and its links to social deficits. *Cell Rep* **5**, 738-747 (2013).

70. R. A. Muller *et al.*, Underconnected, but how? A survey of functional connectivity MRI studies in autism spectrum disorders. *Cereb Cortex* **21**, 2233-2243 (2011).